

Aus dem Walter Brendel Zentrum für Experimentelle Medizin
Institut der Ludwig-Maximilians-Universität München
Direktor: Prof.Dr.med. Ulrich Pohl

MST1 kinase is critical for neutrophil transmigration through the vascular basement membrane

DISSERTATION

zum Erwerb des Doctor of Philosophy (Ph.D.)
an der Medizinischen Fakultät der
Ludwig-Maximilians-Universität München

Vorgelegt von
Angela R.M. Kurz
aus
Hallein, Österreich

am

26. Mai 2016



Mit Genehmigung der Medizinischen Fakultät
Der Universität München

Betreuer:	Prof.Dr.med. Markus Sperandio
Zweitgutachter (in):	PD Dr.rer.nat. Markus Moser
	Univ.-Prof.Dr.Dr.med.Oliver Söhnlein
	Prof.Dr.med. Jürgen Bernhagen
Dekan:	Prof.Dr.med.dent. Reinhard Hickel

Tag der mündlichen Prüfung: 13. September 2016

ABSTRACT

Extravasation of neutrophils from postcapillary venules into inflamed tissue is a crucial step during the inflammatory response. Within this process, neutrophils migrate across the endothelium and subsequently need to penetrate the perivascular basement membrane. The precise regulation of both steps is not fully understood, yet. By using multiphoton intravital microscopy and immunofluorescence staining we identified mammalian sterile 20-like kinase 1 (MST1) as a key player for the migration of neutrophils through the perivascular basement membrane. *Mst1* knock out neutrophils (*Mst1*^{-/-}) persist between the endothelium and the basement membrane of inflamed murine cremaster muscle venules and fail to migrate into inflamed tissue. *Mst1*^{-/-} neutrophils also fail to extravasate from gastric submucosal vessels in a murine *Helicobacter pylori* infection model. Mechanistically, impaired extravasation of *Mst1*^{-/-} neutrophils was accompanied by defective translocation of VLA-3, VLA-6, and neutrophil elastase from intracellular vesicles to the neutrophil surface, a requirement for neutrophils to penetrate the basement membrane. Taken together, our findings identify MST1 as a critical regulator of neutrophil transmigration and emphasize the importance of MST1-dependent vesicle trafficking for the recruitment process.

TABLE OF CONTENTS

ABSTRACT	I
TABLE OF CONTENTS	II
TABLE OF FIGURES AND TABLES	V
1 INTRODUCTION.....	1
1.1 NEUTROPHIL RECRUITMENT	1
1.1.1 Luminal interactions between neutrophils and the endothelium.....	2
1.1.2 Neutrophil transmigration	4
1.2 VESICLE TRAFFICKING IN NEUTROPHILS	11
1.2.1 Stimulation of exocytosis.....	12
1.2.2 Vesicle trafficking, docking and fusion in neutrophils	13
1.2.3 Regulation of vesicle trafficking in neutrophils by Rab27a	14
1.3 MAMMALIAN STERILE 20-LIKE KINASE (MST).....	18
1.3.1 Mammalian sterile 20-like kinase 1/2 (MST1/2) subfamily	19
1.3.2 Mammalian sterile 20-like kinase 1 (MST1)	20
1.3.3 Function of MST1 in the immune system	22
1.3.4 Human STK4 deficiency	25
2 AIM OF THE THESIS	27
3 MATERIALS	28
3.1 LABORATORY ANIMALS.....	28
3.1.1 Genotyping	28
3.2 CELL LINES	29
3.3 BUFFERS AND SOLUTIONS	29
3.4 MEDIA.....	31
3.5 SUBSTANCES	32
3.5.1 Antibodies.....	34
3.6 KITS	36
3.7 EQUIPMENT.....	36
3.8 CONSUMABLES.....	37
3.9 SOFTWARE	37
4 METHODS	38

4.1	NEUTROPHIL RECRUITMENT IN VIVO	38
4.1.1	<i>Conventional intravital microscopy of the mouse cremaster muscle</i>	38
4.1.2	<i>Multi-photon intravital microscopy of the mouse cremaster muscle</i>	39
4.1.3	<i>TNF-α induced neutrophil extravasation into the peritoneal cavity</i>	40
4.2	FLOW CHAMBER ASSAYS	40
4.2.1	<i>Murine ex vivo flow chamber system</i>	40
4.2.2	<i>LFA-1 clustering under flow conditions</i>	41
4.2.3	<i>Human flow chamber system</i>	41
4.3	FLUORESCENCE ACTIVATED CELL SORTING (FACS)	42
4.3.1	<i>Neutrophil and monocyte differentiation</i>	42
4.3.2	<i>Surface expression on neutrophils</i>	42
4.3.3	<i>Selectin binding to neutrophils</i>	42
4.3.4	<i>Soluble ICAM-1 binding to neutrophils</i>	43
4.3.5	<i>Phagocytosis</i>	43
4.3.6	<i>Neutrophil viability</i>	43
4.3.7	<i>Number and viability of neutrophils within the cremaster muscle</i>	44
4.4	NEUTROPHIL ISOLATION	44
4.4.1	<i>Murine neutrophil isolation</i>	44
4.4.2	<i>Human neutrophil isolation</i>	44
4.5	IMMUNOFLUORESCENCE	45
4.5.1	<i>Cremaster whole mount staining</i>	45
4.5.2	<i>Mobilization of VLA-3, VLA-6, NE, MST1 and Rab27a in neutrophils</i>	45
4.5.3	<i>In vivo NE activity assay</i>	46
4.6	WESTERN BLOTTING	46
4.7	CELL CULTURE	47
4.7.1	<i>Transwell assays</i>	47
4.7.2	<i>3D Collagen Migration</i>	48
4.8	STATISTICAL ANALYSES	48
5	RESULTS	49
5.1	CHARACTERIZING NEUTROPHILS OF MST1 KNOCK OUT MICE	49
5.1.1	<i>Viability and apoptosis of WT and Mst1^{-/-} neutrophils</i>	50
5.2	MST1 IS DISPENSABLE FOR NEUTROPHIL ROLLING AND ADHESION IN HUMANS AND MICE	51
5.2.1	<i>Neutrophil rolling and adhesion in Mst1^{-/-} mice in vivo</i>	51
5.2.2	<i>Neutrophil adhesion under flow conditions</i>	55
5.2.3	<i>Surface expression and function</i>	56

5.2.4	<i>Neutrophil adhesion in patients with STK4 deficiency</i>	59
5.3	MST1 IS CRITICAL FOR NEUTROPHIL EXTRAVASATION <i>IN VIVO</i>	60
5.3.1	<i>TNF-α induced neutrophil extravasation into the peritoneal cavity</i>	60
5.3.2	<i>Neutrophil extravasation studied by multi-photon laser scanning microscopy</i>	61
5.3.3	<i>Laser injury induced neutrophil swarming</i>	64
5.3.4	<i>Neutrophil penetration through the venular basement membrane</i>	67
5.4	MST1 REGULATES VESICLE TRAFFICKING IN NEUTROPHILS	69
5.4.1	<i>MST1 induced translocation of VLA-3, VLA-6 and NE to the cell surface</i>	69
5.4.2	<i>MST1 and Rab27a in vesicle trafficking</i>	74
6	DISCUSSION	77
6.1	CHARACTERIZING MST1 IN NEUTROPHILS.....	78
6.2	MST1 IS DISPENSABLE FOR LFA-1 ACTIVATION IN NEUTROPHILS	79
6.3	MST1 IS CRITICAL FOR NEUTROPHIL EXTRAVASATION	81
6.3.1	<i>Neutrophil transmigration in a H. pylori mouse infection model</i>	82
6.3.2	<i>Neutrophil penetration through the venular basement membrane</i>	83
6.3.3	<i>MST1 and translocation of VLA-3, VLA-6 and NE to the cell surface</i>	85
6.3.4	<i>MST1 translocation with Rab27a to the plasma membrane</i>	86
6.4	OUTLOOK.....	88
7	REFERENCES	92
8	ABBREVIATION LIST	103
9	ACKNOWLEDGMENTS	106
10	APPENDIX	108
10.1	PUBLICATIONS	108
10.2	MANUSCRIPT	109
	AFFIDAVIT.....	140

TABLE OF FIGURES AND TABLES

FIGURE 1.1 NEUTROPHIL RECRUITMENT CASCADE	2
FIGURE 1.2 LFA1 ACTIVATION IN ROLLING NEUTROPHILS.....	3
FIGURE 1.3 SEQUENTIAL FUNCTIONS OF ADHESION RECEPTORS DURING NEUTROPHIL TRANSENDOTHELIAL MIGRATION.....	7
FIGURE 1.4 SEQUENTIAL PROCESS OF NEUTROPHIL TRANSENDOTHELIAL MIGRATION (TEM)	8
FIGURE 1.5 SIGNALING CASCADE REGULATING NEUTROPHIL DEGRANULATION	12
FIGURE 1.6 VESICLE TRAFFICKING TO THE TARGET MEMBRANE	14
FIGURE 1.7 REGULATION OF VESICULAR DYNAMICS AND EXOCYTOSIS BY GMIP AND SLP1/JFC1	16
FIGURE 1.8 DENDROGRAM OF THE RELATIONSHIP BETWEEN MST KINASES	18
FIGURE 1.9 PHENOTYPES OF HIPPO MUTANTS IN <i>D.MELANOGASTER</i> AND MICE.....	19
FIGURE 1.10 SCHEMATIC REPRESENTATION OF MST1	20
FIGURE 1.11 CANONICAL AND NON-CANONICAL HIPPO PATHWAY.....	21
FIGURE 1.12 MST1/ Rab13 DEPENDENT VESICLE TRAFFICKING AND ACTIVATION OF LFA-1	24
FIGURE 1.13 SCHEMATIC REPRESENTATION OF HUMAN MUTATIONS IN <i>STK4/ MST1</i>	25
FIGURE 5.1 PROTEIN LEVELS OF MST1 AND MST2 IN NEUTROPHILS	49
FIGURE 5.2 DIFFERENTIAL BLOOD COUNTS OF WT AND <i>Mst1</i> ^{-/-} MICE.....	50
FIGURE 5.3 VIABILITY AND APOPTOSIS OF WT AND <i>Mst1</i> ^{-/-} NEUTROPHILS OVER TIME.....	50
FIGURE 5.4 NEUTROPHIL ROLLING AND ADHESION IN THE TRAUMA STIMULATED CREMASTER MUSCLES OF WT AND <i>Mst1</i> ^{-/-} MICE.....	52
FIGURE 5.5 NEUTROPHIL ROLLING AND ADHESION BEFORE AND AFTER CXCL1 INJECTION	53
FIGURE 5.6 NEUTROPHIL ROLLING AND ADHESION IN THE TNF- α INDUCED CREMASTER MUSCLE MODEL IN WT AND <i>Mst1</i> ^{-/-} MICE	54
FIGURE 5.7 NEUTROPHIL ADHESION OF WT AND <i>Mst1</i> ^{-/-} MICE IN AN <i>EX VIVO</i> FLOW CHAMBER	55
FIGURE 5.8 LFA-1 CLUSTERING IN NEUTROPHILS UNDER FLOW CONDITIONS.....	56
FIGURE 5.9 SURFACE EXPRESSION OF ADHESION RELEVANT MOLECULES ON WT AND <i>Mst1</i> ^{-/-} NEUTROPHILS.....	57
FIGURE 5.10 E-SELECTIN AND P-SELECTIN BINDING TO WT AND <i>Mst1</i> ^{-/-} NEUTROPHILS.....	58
FIGURE 5.11 CXCL1 DEPENDENT ICAM-1 BINDING TO WT OR <i>Mst1</i> ^{-/-} NEUTROPHILS	58
FIGURE 5.12 MST1 IS DISPENSABLE FOR NEUTROPHIL ADHESION IN HUMANS.....	59
FIGURE 5.13 TNF- α INDUCED PERITONITIS IN WT AND <i>Mst1</i> ^{-/-} MICE	60
FIGURE 5.14 DIFFERENTIAL BLOOD COUNT FROM <i>Ly22</i> ^{GFP} AND <i>Mst1</i> ^{-/-} X <i>Ly22</i> ^{GFP} MICE	61
FIGURE 5.15 <i>Mst1</i> ^{-/-} NEUTROPHILS FAIL TO TRANSMIGRATE INTO INFLAMED TISSUE.....	62
FIGURE 5.16 3D RECONSTRUCTION OF NEUTROPHIL TRANSMIGRATION IN WT AND <i>Mst1</i> ^{-/-} MICE.....	63
FIGURE 5.17 NUMBER AND VIABILITY OF NEUTROPHILS WITHIN THE CREMASTER MUSCLE	64
FIGURE 5.18 LASER INDUCED INJURY IN THE MOUSE CREMASTER MUSCLE	65
FIGURE 5.19 PHAGOCYTIC CAPACITY OF WT AND <i>Mst1</i> ^{-/-} NEUTROPHILS.....	66

FIGURE 5.20 <i>Mst1</i> ^{-/-} NEUTROPHILS SHOW REDUCED PRENTRATION OF LAMININ OR ENDOTHELIAL CELL COATED, BUT NOT UNCOATED TRANSWELLS.....	68
FIGURE 5.21 MST1 IS REQUIRED FOR THE TRANSLOCATION OF NE, VLA-3 AND VLA-6 TO THE PLASMA MEMBRANE	70
FIGURE 5.22 FLUORESCENCE INTENSITY PROFILE OF VLA-3, VLA6 AND NE IN NEUTROPHILS FROM WT AND <i>Mst1</i> ^{-/-} MICE	71
FIGURE 5.23 LIGANDS RESPONSIBLE FOR VLA-6 AND NE TRANSLOCATION	72
FIGURE 5.24 TOTAL PROTEIN LEVELS OF VLA-3, VLA-6 AND NE.....	72
FIGURE 5.25 NE ACTIVITY IN TNF- α STIMULATED CREMASTER MUSCLE <i>IN VIVO</i>	73
FIGURE 5.26 RAB27A TRANSLOCATION TO THE PLASMA MEMBRANE IN <i>Mst1</i> ^{-/-} NEUTROPHILS	75
FIGURE 5.27 TOTAL PROTEIN LEVELS OF RAB27A.....	75
FIGURE 5.28 TRANSLOCATION OF MST1 TO THE PLASMA MEMBRANE	76
FIGURE 6.1 UPDATED NEUTROPHIL ADHESION CASCADE	84
FIGURE 6.2 CROSSING THE BASEMENT MEMBRANE.....	87
TABLE 1.1 ADHESION MOLECULES INVOLVED IN NEUTROPHIL EXTRAVASATION FROM POSTCAPILLARY VENULES.....	5
TABLE 1.2 CONTENT OF HUMAN NEUTROPHIL GRANULES AND SECRETORY VESICLES	11
TABLE 1.3 TABLE OF THE NOMENCLATURE OF MST KINASES IN DIFFERENT ORGANISMS	18
TABLE 1.4 <i>STK4</i> MUTATIONS REVEALED IN PATIENTS	25
TABLE 3.1 MOUSE STRAINS USED IN THIS THESIS	28
TABLE 3.2 PRIMERS USED FOR GENOTYPING.....	29
TABLE 3.3 RECOMBINANT PROTEINS	32
TABLE 3.4 FLUORESCENT SUBSTANCES	32
TABLE 3.5 OTHER SUBSTANCES.....	32
TABLE 3.6 PRIMARY ANTIBODIES.....	34
TABLE 3.7 SECONDARY ANTIBODIES.....	35
TABLE 5.1 HEMODYNAMIC AND MICROVASCULAR PARAMETERS OF POSTCAPILLARY VENULES IN TRAUMA INDUCED INFLAMMATION	52
TABLE 5.2 HEMODYNAMIC AND MICROVASCULAR PARAMETERS OF POSTCAPILLARY VENULES BEFORE AND AFTER CXCL1 INJECTION.....	53
TABLE 5.3 HEMODYNAMIC AND MICROVASCULAR PARAMETERS OF POSTCAPILLARY VENULES IN TNF- α INDUCED INFLAMMATION	54

1 INTRODUCTION

In humans, neutrophils are the most abundant white blood cells in the circulation, the key cell type of the innate immune system. Neutrophils are the first line of defense; they are the first leukocytes to be recruited to the site of infection and are the major pathogen-fighting immune cells. It is crucial for them to extravasate from the blood vessel to the site of infection. Successfully transmigrated neutrophils recognize, phagocytose and consequently kill pathogens within tissue. They control local infections via various cytotoxic mechanisms, including reactive oxygen species (ROS) production, release of antimicrobial peptides and the release of neutrophil extracellular traps (NETs).

Neutrophil recruitment, activation and function needs to be tightly regulated as malfunction leads to diverse disorders. For example human leukocyte adhesion deficiencies (LAD) are severe immunodeficiencies leading to recurring bacterial and fungal infections due to inherited defects in selectin ligands (LADII), $\beta 2$ integrins (LADI) or Kindlin3 (LADIII) and consequently profound defects in neutrophil recruitment (Schmidt et al., 2013), whereas an extensive or prolonged response results in tissue damage as observed in certain forms of vasculitis and autoimmune disease (Mayadas et al., 2014).

1.1 NEUTROPHIL RECRUITMENT

Recruitment of neutrophils from postcapillary venules to sites of inflammation is a fundamental process during the innate immune response. This process follows a well-defined cascade of events, including neutrophil tethering and rolling, firm adhesion, crawling, extravasation and migration into inflamed tissue (Nourshargh and Alon, 2014) (**Figure 1.1**).

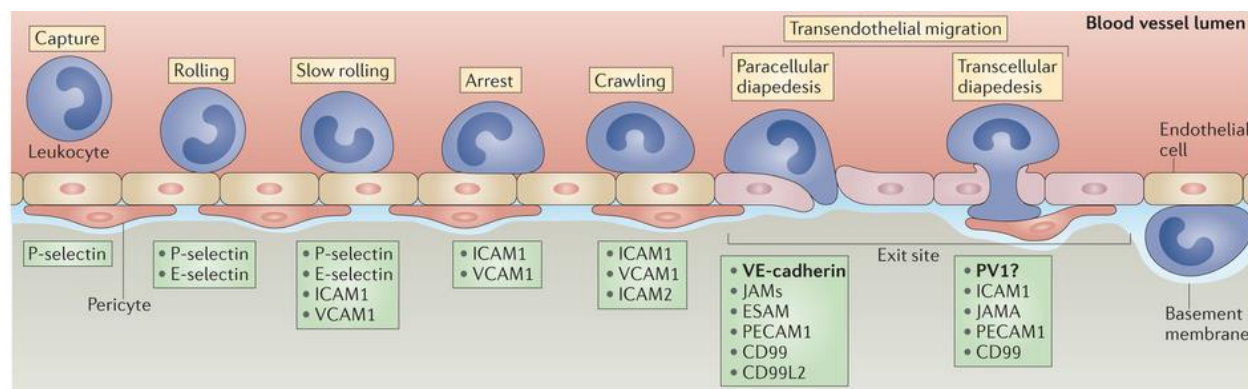


Figure 1.1 Neutrophil recruitment cascade

Schematic representation of the sequential steps of neutrophil recruitment from postcapillary venules into tissue. Neutrophil tethering and rolling, mediated via selectin and selectin ligand interaction, is followed by adhesion and intravascular crawling, which involves the $\beta 2$ integrins LFA1 and Mac1. After finding the appropriate exit point neutrophils migrate through the endothelium via the paracellular or the transcellular route. Following transendothelial migration, neutrophils crawl at the abluminal side of the vessel, interacting with pericytes, and finally extravasate from low expression regions within the basement membrane. Adapted from (Vestweber, 2015)

1.1.1 LUMINAL INTERACTIONS BETWEEN NEUTROPHILS AND THE ENDOTHELIUM

Neutrophil recruitment is initiated by inflammatory mediators which induce changes in the surface expression of adhesion and activation molecules on endothelial cells. Depending on the time and stimulus, P-selectin, prestored in Weibel-Palade bodies, is upregulated within minutes, whereas *de novo* synthesized E-selectin can only be detected in sufficient quantities more than 90 min after stimulation. Circulating neutrophils, expressing P-selectin glycoprotein ligand 1 (PSGL1), E-selectin ligand 1 (ESL1), CD44 and L-selectin, interact with P-selectin and E-selectin on the endothelium initiating capture and rolling. E- and P-selectin bind to PSGL-1 and CD44 inducing talin dependent conformational changes in LFA-1 leading to slow rolling (McEver, 2015). Our group recently discovered a new pathway, where E-selectin binding to PSGL-1 leads to the release of MRP8/14, which in turn binds to TLR4 and induces MyD88- and Rap1-dependent activation of LFA-1 leading to slow rolling of neutrophils across inflamed endothelium (Pruenster et al., 2015). In addition to selectin ligands, chemoattractants on the endothelium induce integrin activation (Kolaczkowska and Kubes, 2013). Crucial chemokines for neutrophil activation are CXCL8 (also known as IL-8) in humans and CXCL1 (also known as Keratinocyte-derived chemokine, Kc and analogue to CXCL8 in humans), CXCL2 and CXCL5 in mice. These chemokines bind to

CXCR2 on neutrophils and activate $\beta 2$ integrins via inside-out signaling. The $\beta 2$ integrins, lymphocyte function-associated antigen 1 (LFA1; CD18/CD11a; $\alpha L\beta 2$) and macrophage-1 antigen (Mac1; CD18/CD11b; $\alpha M\beta 2$), change their conformation and increase their affinity to endothelial expressed intercellular adhesion molecule 1 (ICAM1) and ICAM2 leading to neutrophil adhesion to the endothelium. Upon selectin binding or chemokine stimulation, talin1 interacts with the cytoplasmic tail of $\beta 2$ integrins inducing the intermediate affinity of LFA1 which promotes slow rolling (Lefort and Ley, 2012, Pruenster et al., 2015, McEver, 2015). Binding of both, kindlin3 and talin1, to the cytoplasmic tail of $\beta 2$ lead then to high affinity conformation of LFA1 and firm arrest of neutrophils on the inflamed endothelium (Lefort et al., 2012) (**Figure 1.2**).

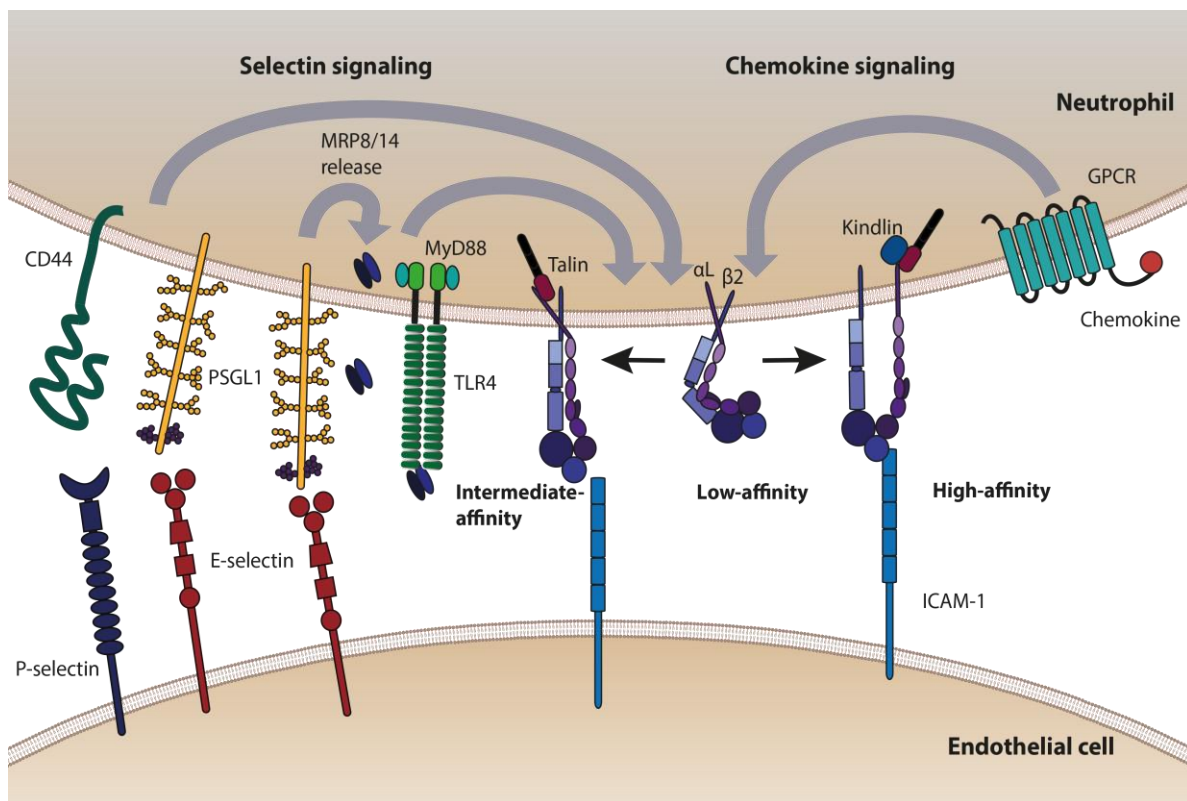


Figure 1.2 LFA1 activation in rolling neutrophils

Both, E- and P-selectin binding to PSGL-1 or CD44; or E-selectin/ PSGL-1 dependent release of MRP14 and binding to TLR4, as well as signals transmitted through chemokine receptors can modulate LFA1 affinity in neutrophils. PSGL-1 or CD44 induce talin1-dependent conformational changes in LFA1 leading to intermediate activity and slow rolling (left). Whereas chemokine receptor stimulation induces a talin1 and kindlin 3 dependent high affinity state (right). Adapted from (Pruenster et al., 2015)

After firm arrest, neutrophils actively crawl along the endothelium scanning for an exit point, a process which is mostly dependent on ICAM1-Mac1 interactions (Phillipson et al., 2006). In addition, blocking ICAM-2 function *in vivo* alters the dynamics of crawling neutrophils to a stop-start profile and prolongs the time neutrophils remain at endothelial cell junctions before initiating transmigration (Halai et al., 2014).

At exit sites, endothelial cells extend ICAM-1 and VCAM-1 enriched membrane structures at their apical surface called 'docking structures' (Barreiro et al., 2002) or 'transmigratory cups' (Carman and Springer, 2004). These pseudopod-like apical membrane extensions surround transmigrating neutrophils. Neutrophil binding to endothelial ICAM-1 stimulates phosphorylation of cortactin, activation of RhoG and ICAM-1 clustering around transmigrating neutrophils (ICAM-1 ring like structures). Blocking RhoG activation inhibits ICAM-1 induced cortactin phosphorylation and neutrophil transendothelial migration (TEM) (Vestweber, 2015).

1.1.2 NEUTROPHIL TRANSMIGRATION

Neutrophils need to leave the vasculature in order to migrate to the site of injury or inflammation. Although most of the recruitment steps have been thoroughly studied in the past (Kolaczkowska and Kubes, 2013), the precise mechanism of neutrophil transmigration across venular walls remains elusive (Hallmann et al., 2015, Muller, 2015, Nourshargh and Alon, 2014, Rowe and Weiss, 2008, Sorokin, 2010, Vestweber, 2015). Neutrophils cross the endothelium within 2- 5 min. This is followed by the penetration of the perivascular basement membrane (BM) and associated incomplete layer of pericytes, which takes 5- 15 min (Kolaczkowska and Kubes, 2013). Transmigration through postcapillary venules can be divided into different steps: Transendothelial migration (TEM), abluminal crawling, followed by penetration through the perivascular BM and migration into the interstitial matrix to the site of inflammation (Nourshargh et al., 2010, Weninger et al., 2014, Nourshargh and Alon, 2014).

Transendothelial Migration

Intravascularly crawling neutrophils search for exit cues, which initiate TEM. Neutrophils breach the endothelial barrier regularly via the paracellular route (between adjacent endothelial cells, ~70-90%) and to a smaller extent via the less efficient transcellular route (through the endothelial cell), which can take 20- 30 min (Kolaczowska and Kubes, 2013) Adhesion molecules involved in neutrophil transmigration are listed in **Table 1.1**.

Table 1.1 Adhesion molecules involved in neutrophil extravasation from postcapillary venules

Adapted from (Kolaczowska and Kubes, 2013, Vestweber, 2015)

Adhesion receptor	Gene family	Neutrophil ligand(s)	Endothelial ligand(s)	Function
E-selectin	Selectin	PSGL-1, CD44, ESL-1	None	Tethering and rolling
P-selectin	Selectin	PSGL-1	None	Tethering and rolling
PSGL-1	Proteoglycan ligand	L-selectin	P-selectin, E-selectin	Tethering and rolling
GlyCAM	Proteoglycan ligand	L-selectin		Tethering and rolling
ICAM-1	Immunoglobulin superfamily	LFA-1, Mac1	None	Slow rolling, adhesion, crawling, triggering VE-cadherin phosphorylation
VCAM-1	Immunoglobulin superfamily	VLA-4	None	Slow rolling, adhesion, crawling, triggering VE-cadherin phosphorylation
ICAM-2	Immunoglobulin superfamily	LFA-1, Mac1	None	Crawling and initiation of TEM
JAM-A	Immunoglobulin superfamily	LFA-1	JAM-A	unknown
JAM-B	Immunoglobulin superfamily	VLA-4	JAM-C, JAM-B	TEM
JAM-C	Immunoglobulin superfamily	Mac-1	JAM-B, JAM-C	Prevents reverse transmigration
ESAM-1	Immunoglobulin superfamily	Unknown	ESAM-1	TEM, supports the induction of increased permeability
PECAM-1	Immunoglobulin superfamily	PECAM-1	PECAM-1	Triggering LBRC recycling in endothelial cells, support disconnection of neutrophils from the endothelial cells and penetration of the BM
CD99	Unique	CD99	CD99	Triggers LBRC recycling in endothelial cells, supports disconnection of neutrophils from the endothelial cells and penetration of the BM
CD99L2	Unique	Unknown	CD99L2	Supports disconnection of neutrophils from the endothelial cells and penetration of the BM
VE-cadherin	Cadherin	None	VE-cadherin	Endothelial cell junction barrier and prevention of TEM

Successful TEM requires interaction of several adhesion molecules and receptors on neutrophils and/or endothelial cells: ICAM-1, ICAM-2, vascular cell adhesion protein 1 (VCAM-1) as well as the junctional proteins, including junctional adhesion molecules [e.g. JAM-A, JAM-B, JAM-C and endothelial cell-selective adhesion molecule 1 (ESAM-1)], platelet endothelial cell adhesion molecule (PECAM-1; also known as CD31), CD99 and CD99 antigen-like protein 2 (CD99L2) and poliovirus receptor (PVR) (Muller, 2015, Vestweber, 2015). These molecules participate in paracellular TEM, but not all of them are involved in transcellular migration. Furthermore, their roles vary between different leukocyte subsets, different organs, venules and inflammatory models (Kolaczkowska and Kubes, 2013, Muller, 2015, Nourshargh and Alon, 2014, Vestweber, 2015) (**Table 1.1**).

Comparing the effects of function blocking antibodies and knockout mice provided evidence for a sequential involvement of these molecules and receptors during neutrophil transmigration. In IL-1 β stimulated murine cremaster muscles, neutrophils lacking JAM-A (genetic depletion) accumulate at endothelial cell junctions. Disruption of PECAM-1 (genetic depletion) arrests neutrophils between endothelial cells and the basement membrane (Woodfin et al., 2007, Bixel et al., 2010). Genetic depletion of ICAM-2 leads to the accumulation of neutrophils at the luminal surface above endothelial cell junctions (Woodfin et al., 2009). Interestingly, JAM-A, PECAM-1 and ICAM-2 display the same cytokine selectivity, as shown in studies where genetic disruption of JAM-A, PECAM-1 or ICAM-2 inhibited neutrophil transmigration in response to IL-1 β , but not TNF- α . In contrast to IL-1 β , TNF- α activates neutrophils, which may lead to TEM that can bypass the requirement for those receptors. Neutrophils lacking TNF-receptors require all three adhesion receptors to transmigrate in TNF- α stimulated postcapillary venules in the murine cremaster muscle (Woodfin et al., 2009). Blocking of CD99 or CD99L2 (functional blocking through specific antibodies) traps migrating neutrophils between endothelial cells and the basement membrane in postcapillary venules of IL-1 β and TNF- α stimulated cremaster muscles, indicating its functional independence from the type of inflammatory stimulus (Bixel et al., 2010).

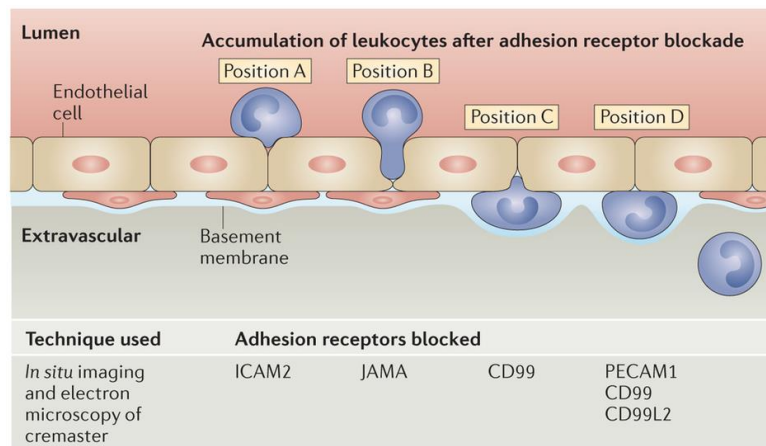


Figure 1.3 Sequential functions of adhesion receptors during neutrophil transendothelial migration

Genetic deletion or function blocking of adhesion receptors leads to the accumulation of extravasating neutrophils at the indicated position. These results are based on 3D analysis by confocal microscopy of stimulated postcapillary venules within the mouse cremaster muscle or skin (Bixel et al., 2010, Watson et al., 2015, Woodfin et al., 2007, Woodfin et al., 2009). Adapted from (Vestweber, 2015).

These studies established that neutrophil TEM is a sequential process, mediated by several cell surface receptors. So far, four positions are characterized: adhesion to the luminal surface above endothelial cell junctions (Position A); engaged between the endothelial junctions (Position B); detaching from the endothelium (Position C); between endothelial cells and the basement membrane (Position D) (Vestweber, 2015) (**Figure 1.3**).

The paracellular transmigration additionally requires the liberation of junctional intercellular protein bonds, such as those formed by vascular endothelial (VE)-cadherin. VE-cadherin is crucial for the stability of endothelial cell junctions. Vascular endothelial protein tyrosine phosphatase (VE-PTP) associates with VE-cadherin and supports its adhesive activity. Neutrophil-endothelial cell interaction and vascular permeability factors trigger the dissociation of VE-PTP from VE-cadherin, which is required for the positive regulation of this exit pathway. This implies that tyrosine phosphorylation of VE-cadherin and/or proteins in close proximity are required (Vestweber, 2015). Neutrophil bound ICAM-1 and VCAM-1 is indeed known to trigger tyrosine phosphorylation in the cytoplasmic domain of VE-cadherin. Dephosphorylation of Y731 of VE-cadherin is required for neutrophil recruitment in TNF- α as well as IL-1 β stimulated cremaster muscle venules, whereas phosphorylation of Y685 is required for increasing the vascular permeability (Wessel et al., 2014, Vestweber, 2015).

TEM of neutrophils may be further supported by the lateral border recycling compartment (LBRC), a multi vesicular compartment inside of endothelial cells containing PECAM-1, CD99 and JAM-A (Mamdouh et al., 2009, Muller, 2015). LBRC vesicles are initially recruited via PECAM-1 to transmigrating neutrophils, followed by a second CD99-dependent wave, helping to accommodate the body of neutrophils within junctions (Mamdouh et al., 2003, Muller, 2015, Watson et al., 2015) (**Figure 1.4**).

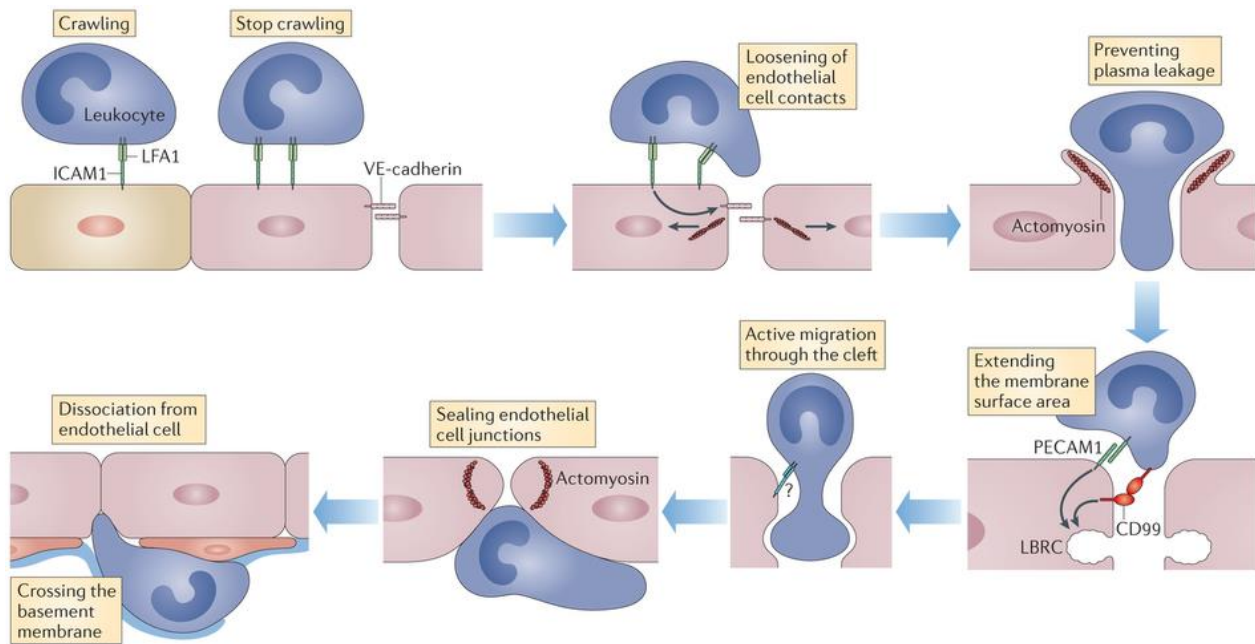


Figure 1.4 Sequential process of neutrophil transendothelial migration (TEM)

TEM is a process mediated by neutrophils and endothelial cells: Stopping at preferential exit points; loosening of endothelial cell contacts; preventing plasma leakage; extending the membrane surface area via LBRCs; migration through the endothelial cleft; sealing of the endothelial cell junction; and dissociation from the endothelial cell. After TEM neutrophils need to transmigrate through the basement membrane. Adapted from (Vestweber, 2015)

Penetration of the basement membrane

Once neutrophils have migrated through the endothelial layer, they need to cross the underlying BM, a dense protein network embedded with pericytes, to enter inflamed tissues.

The perivascular BM consists of a dense (40-70 nm pore size) and heterogeneous network of collagen IV, nidogen1 and 2, perlecan and two specific laminin isoforms (isoform 511 and 411) (Hallmann et al., 2015, Sorokin, 2010, Rowe and Weiss, 2008, Weninger et al., 2014). The BM is crucial for the integrity of the blood vessel wall, and provides a tremendous barrier to transmigrating neutrophils.

Embedded in the BM pericytes reside and form an irregular network of cellular protrusions around the vessel, contributing to the composition of the basement membrane (Sorokin, 2010). Laminin 411 is ubiquitously expressed in perivascular BM of postcapillary venules. In contrast laminin 511 displays a patchy distribution with areas of low or no expression (Sixt et al., 2001, Wu et al., 2009, Voisin et al., 2010) and potentially also low expression of collagen IV (Wang et al., 2006, Proebstl et al., 2012). These 'low expression sites' (LER) localize at the gaps between pericytes (Sorokin, 2010, Voisin et al., 2010) and are the preferential sites for neutrophil extravasation (Wang et al., 2006). Laminin 411 deficient mice demonstrate a ubiquitous expression of laminin 511 in perivascular BM and show reduced neutrophil transmigration, indicating that laminin 511 has inhibitory effects on neutrophil migration (Kenne et al., 2010).

After TEM, neutrophils enter the subendothelial space and crawl along pericytes towards LERs, via pericyte expressed ICAM-1 and neutrophilic Mac-1 and LFA-1 (Proebstl et al., 2012, Ayres-Sander et al., 2013).

The mechanism through which neutrophils breach the perivascular BM is not fully understood yet (Rowe and Weiss, 2008). Neutrophils contain specific proteases, such as matrix metalloproteases (MMPs) and the serine protease, neutrophil elastase (NE), therefore it is tempting to argue that neutrophils 'cut' their way through the basement membrane, but neither genetic nor pharmacologic inhibitors could corroborate this (Kolaczowska and Kubes, 2013). Maintenance of vascular integrity is indeed essential for tissue homeostasis, hence degradation of the basement membrane is unlikely and potentially contentious (Nourshargh and Alon, 2014, Rowe and Weiss, 2008, Hallmann et al., 2015).

Interestingly, neutrophils only penetrate the BM in the presence of an overlying endothelium, indicating that neutrophils are 'educated' by endothelial cells on how to cross the BM (Rowe and Weiss, 2008, Huber and Weiss, 1989). Furthermore, it was reported that LERs are transiently enlarged after neutrophil transmigration, probably through subtle disassembly and physical carriage of neutrophil bound BM-components (e.g. laminins) (Voisin et al., 2010, Wang et al., 2006).

After neutrophils have migrated through the endothelial layer, they are thought to interact with matrix components of the BM such as collagens and laminins via their surface molecules, $\beta 1$ and $\beta 3$ integrins. The use of function blocking antibodies and genetic deletion in *in vivo* studies have implicated several cell adhesion molecules, including the major laminin binding integrins on neutrophils, namely VLA-3 ($\alpha 3\beta 1$, CD49c/CD29) (Hyun et al., 2012) and VLA-6 ($\alpha 6\beta 1$, CD49f/CD29) (Dangerfield et al., 2005) and the junctional molecules ESAM-1, and PECAM-1 and CD99, expressed both by neutrophils and endothelial cells (Vestweber, 2015). These studies suggest that information obtained by migration across the endothelial cell monolayer primes neutrophils for the subsequent penetration of the endothelial BM.

VLA-3 was shown to be necessary for neutrophil extravasation in TNF- α and fMLP-induced transmigration *in vivo* (Hyun et al., 2012). Homophilic interactions between PECAM-1 on neutrophils and on endothelial cells induce the surface expression of VLA-6 on neutrophils enabling them to cross the basement membrane (Dangerfield et al., 2002). Using blocking antibodies suggest a role for VLA-6 in IL-1 β , but not TNF- α dependent neutrophils extravasation (Dangerfield et al., 2005). Migration through the BM was described to be further accompanied by the surface expression of the serine protease NE (Wang et al., 2005), although experiments using NE deficient mice *in vivo* could not confirm a role of NE in the extravasation process (Young et al., 2007). Since VLA-3, VLA-6 and NE are stored in intracellular vesicles (Uriarte et al., 2008, Wang et al., 2005), they need to be translocated to the cell surface during transmigration.

1.2 VESICLE TRAFFICKING IN NEUTROPHILS

Neutrophil immune function strongly depends on the capacity to synthesize and store pre-formed pro-inflammatory mediators in specialized intracellular vesicles (Sheshachalam et al., 2014). Defects result in severe immunodeficiency as seen in patients with neutrophil-specific granule deficiencies (Schaffer and Klein, 2013).

Mature neutrophils from the blood lack any proliferative capacity. Structurally, neutrophils possess a characteristic multi-lobed nucleus, very few mitochondria, a small Golgi apparatus, and a highly granular cytosol, that is packed with vesicles. In contrast to other cells, the protein content of neutrophil granules is not sorted, but sequentially formed during neutrophil differentiation (sequential synthesis model) (Le Cabec et al., 1996). Neutrophils consist of at least four types of granule structures: azurophilic (primary) granules, containing e.g. myeloperoxidases (MPO); specific (secondary) granules, containing e.g. lactoferrin; gelatinase (tertiary) granules, containing e.g. matrix metalloproteinases 9 (MMP9); and secretory vesicles (**Table 1.2**). Azurophilic as well as specific granules can be further subdivided due to their specific protein composition (Borregaard, 2010). Of note, in mature neutrophils secretory vesicles can also be formed *de novo* by the Golgi apparatus (Sheshachalam et al., 2014).

Table 1.2 Content of human neutrophil granules and secretory vesicles

Adapted from (Borregaard and Cowland, 1997)

Azurophilic (primary) granules	Specific (secondary) granules	Gelatinase (tertiary) granules	Secretory vesicles
MPO	Lactoferrin	Acetyltransferase	CD16
Lysozyme	Lysozyme	Lysozyme	CD19
Defensin	MMP9	MMP9	CD14
Cathapsin B/ D/ G	Gelatinase	Gelatinase	C1q-receptor
Neutrophil elastase	Collagenase		Alkaline phosphatase
Proteinase 3	CD11b/CD18	CD11b/CD18	CD11b/CD18
CD63	fMLP-receptor	fMLP-receptor	fMLP-receptor
CD68	Cytochrome b558	Cytochrome b558	Cytochrome b558
VAMP-7	VAMP-2/7	VAMP-2	VAMP-2
	CR3, CR4		CR1
	Laminin-receptor		
	CD66		
	CD67		
	TNF-receptor		
	Vitronectin-receptor		

1.2.1 STIMULATION OF EXOCYTOSIS

In general, secretory vesicles and gelatinase granules can be rapidly transported to the plasma membrane (for example $\beta 2$ integrins) upon moderate activation. A stronger activation of neutrophils is required to release azurophilic and specific granules (Kolaczowska and Kubes, 2013, Mayadas et al., 2014). This hierarchy of granule release corresponds to the different roles of their secreted proteins during adhesion, migration, chemotaxis, phagocytosis and ROS production (Catz, 2014). During TEM, secretory vesicles are exocytosed to 100%, gelatinase granules to 38%, specific granules to 22% and azurophilic granules to only 7% (Rorvig et al., 2009, Sengelov et al., 1995).

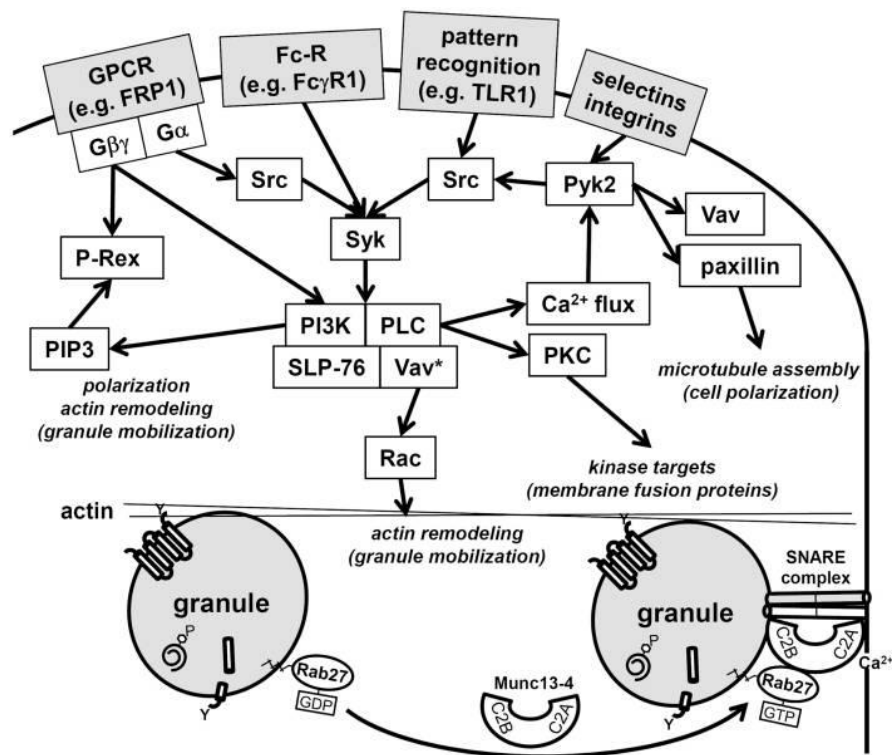


Figure 1.5 Signaling cascade regulating neutrophil degranulation

Both, kinases and the fusion machinery regulate degranulation. Activated surface receptors trigger activation of kinases resulting in cytoskeletal remodeling. Docking of vesicles is regulated by interaction of Rab27 with Munc-13-4, which in turn interacts with SNARE leading to the fusion with the target membrane. Adopted from (Sheshachalam et al., 2014)

Due to high cytotoxicity, release of neutrophilic granules is strongly regulated by binary signals and involves on the one side adhesion-dependent mechanisms ($\beta 2$ -integrin or actin de-polymerization) and on the other ligation and activation of immune receptors (Sengelov et al., 1995). The Src kinases Fgr and Hck mediate both the adhesion-dependent signaling cascade and the immune receptor mediated activation (Mocsai et al., 1999). Current evidence favors the existence of an activation threshold, accomplished by binary signals, which induce degranulation or downstream pathways. This can induce an increase in intracellular Ca^{2+} and subsequently the hierarchical release of neutrophil granules in the order of secretory vesicles > gelatinase granules > specific granules > primary granules (Sengelov et al., 1993) (**Figure 1.5**).

1.2.2 VESICLE TRAFFICKING, DOCKING AND FUSION IN NEUTROPHILS

Granules and vesicles are transported to a target membrane (e.g. plasma membrane or phagosome) via actin remodeling and microtubule assembly through sequential actions of the core fusion machinery (Lacy and Eitzen, 2008, Sheshachalam et al., 2014, Toonen and Verhage, 2003).

Docking and fusion of granules and secretory vesicles to a target membrane are regulated by distinct core fusion proteins, involving the Rab and SNARE (soluble N-ethylmaleimide-sensitive factor attachment protein receptor) protein family. After Rab proteins tie vesicles to the membrane, SNARE proteins catalyze fusion (Lacy and Eitzen, 2008). Vesicle SNAREs (v-SNAREs) pair with target SNAREs (t-SNAREs) resulting in the fusion of vesicles with the target membrane. In neutrophils, vesicle-associated membrane protein 2 (VAMP-2) is mainly localized on secretory vesicles and gelatinase granules, whereas VAMP-7 is predominantly localized to azurophilic granules. Numerous proteins regulate the core fusion machinery and are important for SNARE complex formation (Sheshachalam et al., 2014) (**Figure 1.6**).

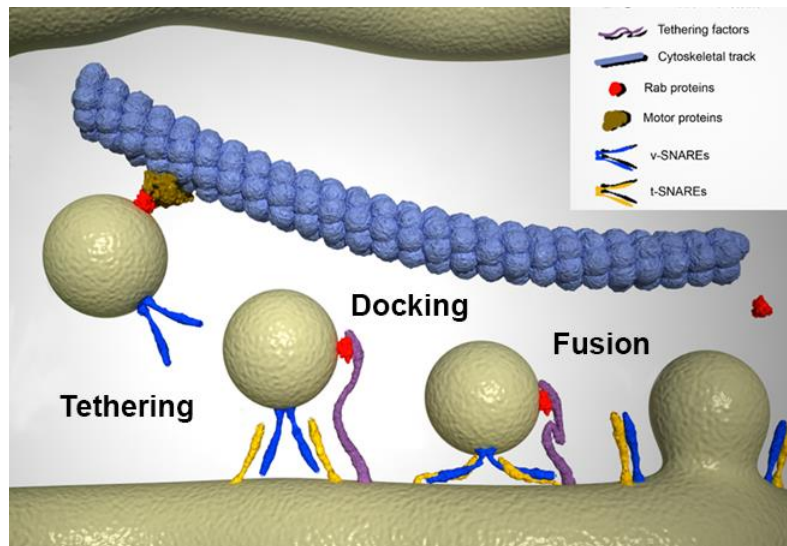


Figure 1.6 Vesicle trafficking to the target membrane

Vesicles are transported along cytoskeletal tracks. Rab-GTP on vesicles associates with motor proteins, directing the movement of the vesicle, and later with Rab effectors (tethering factors), bringing the vesicle in close proximity to the target membrane. Binding of v-SNAREs and t-SNAREs leads to the fusion of vesicles with the target membrane and the release of cargo proteins. Adapted and modified from (Vazquez-Martinez and Malagon, 2011)

1.2.3 REGULATION OF VESICLE TRAFFICKING IN NEUTROPHILS BY RAB27A

The Rab27 GTPases regulate vesicle trafficking in neutrophils. This includes priming, tethering, docking and fusion to target membranes via interaction with multiple cell specific effector molecules. While Rab27 GTPases are expressed in a large variety of cell types and are involved in multiple steps, the expression of their effector proteins is more cell type specific and required to allow sequential interaction with Rab27 (Catz, 2013). Rab27a has emerged as a central regulator of many neutrophil functions, though its ability to regulate vesicle exocytosis (Catz, 2014). So far, two effector molecules, Synaptotagmin-like protein 1 (Slp1/JFC1) and Munc13-4, have been identified to interact with Rab27a in neutrophils (Brzezinska et al., 2008, Johnson et al., 2011b, Munafo et al., 2007, Pivot-Pajot et al., 2008). Rab27b, which is 72% homologous to Rab27a, binds to the same effector molecules as Rab27a and regulates several secretion mechanisms, although studies suggest different roles during azurophilic granules exocytosis in neutrophils (Brzezinska et al., 2008, Johnson et al., 2010).

Interestingly, out of more than 60 Rab GTPases expressed in humans, Rab27a is the only one associated with human disease. Patients with a genetic defect in Rab27a, a

disease called Griscelli syndrome type 2 (GS2), suffer from often fatal viral and bacterial infections, due to a severe immune deficiency, neutropenia, thrombocytopenia and uncontrolled T cell and macrophage activation (Harfi et al., 1992, Klein et al., 1994). Defects in Rab27a cause impaired function of cytotoxic T lymphocytes (CTL), natural killer cells (NK cell) and neutrophils (Munafo et al., 2007, Trambas and Griffiths, 2003).

Rab27a-dependent trafficking of azurophilic granules

Only ~20% of azurophilic granules are able to engage in exocytosis. This coincides with the percentage of azurophilic granules associated with Rab27a (Catz, 2013), but it is unclear whether only Rab27a positive azurophilic granules are mobilized to target membranes. Use of function blocking reagents or genetic deletion of Rab27a leads to impaired azurophilic granule exocytosis and decreased MPO plasma levels (Munafo et al., 2007, Johnson et al., 2010).

The Rab27a effector protein Slp1/JFC1 is expressed in neutrophils and was shown to bind and colocalize with Rab27a on azurophilic granules in close proximity to the plasma membrane (Catz, 2013). The loss of Slp1/JFC1 results in impaired release of azurophilic granules in response to fMLP in neutrophils (Brzezinska et al., 2008, Johnson et al., 2012). In addition, Slp1/JFC1 interacts with Gem-interacting protein (GMIP) regulating RhoA dependent actin remodeling facilitating docking and fusion of vesicles. Furthermore genetic deletion of Slp1/JFC1 or GMIP impairs exocytosis by trapping azurophilic granules within cortical actin, whereas inhibition of RhoA induces exocytosis via increased actin polymerization (Johnson et al., 2012) (**Figure 1.7**).

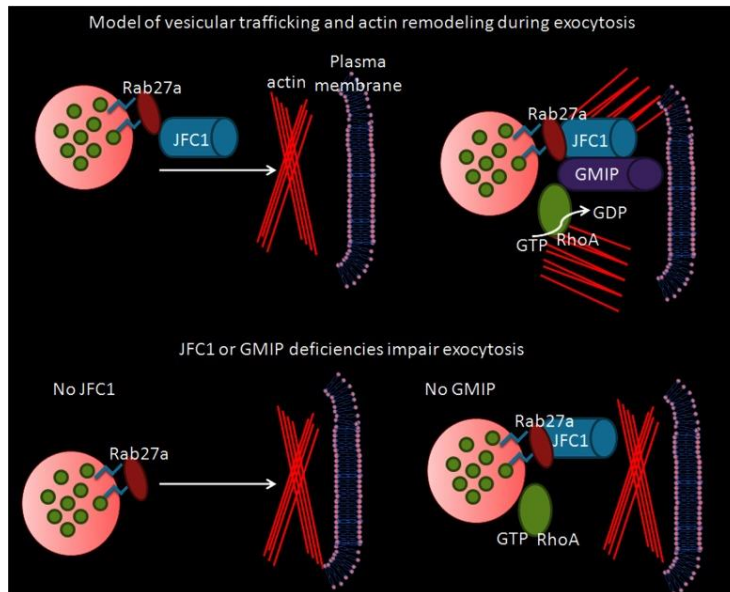


Figure 1.7 Regulation of vesicular dynamics and exocytosis by GMIP and Slp1/JFC1

Rab27a-recruited JFC1 interacts with RhoA and GMIP leading to actin polymerization. Inhibition of Slp1/JFC1 or GMIP impairs exocytosis by trapping granules within the cortical actin network. Adapted from (Catz, 2013)

Another Rab27a effector protein, Munc13-4, also known as UNC13D, was first identified to associate with Rab27a dependent vesicles in platelets and CTLs. Later, it was discovered that Munc13-4 associates with gelatinase and azurophilic granules (colocalizing with MMP9) (Brzezinska et al., 2008, Pivot-Pajot et al., 2008). Function blocking antibodies or genetic deletion of Munc13-4 results in decreased MPO exocytosis and reduced granule docking at the plasma membrane (Johnson et al., 2011b). Munc13-4 links vesicles via two calcium sensitive lipid binding C2 domains (C2A and C2B) to the fusion machinery of SNAREs, regulating the docking of the vesicle to the plasma membrane (Brzezinska et al., 2008) (**Figure 1.5**). Another study recently showed that MST3 (STK24) and cerebral cavernous malformations 3 (CCM3) regulate exocytosis of azurophilic granules. Whereas MST3 inhibited Munc13-4 function, CCM3 antagonized MST3-mediated inhibition, providing additional regulation of degranulation (Zhang et al., 2013). Additionally, Munc13-4 controls phagosomal maturation by regulating the fusion of azurophilic granules and late endosomes to the phagosome, independent of Rab27a (Brzezinska et al., 2008, Johnson et al., 2011b, Monfregola et al., 2012).

Rab27a dependent trafficking of specific and gelatinase granules

In addition to its role in regulating azurophilic granule trafficking, Rab27a is also involved in specific and gelatinase granule trafficking as the blockade of Rab27a leads to impaired MMP9 release (Brzezinska et al., 2008). MMP9 is mostly stored in specific and gelatinase granules. After molecular interference with Rab27a, the upregulation of the specific granule marker CD66b is diminished, supporting the involvement of Rab27a in specific granule trafficking (Herrero-Turrion et al., 2008). Furthermore, it could be demonstrated that the Rab27a effector Munc13-4, but not Slp1/JFC1, is involved in gelatinase granule trafficking (Brzezinska et al., 2008, Pivot-Pajot et al., 2008).

Rab27a dependent trafficking of secretory vesicles

Secretory vesicles contain adhesion molecules, receptor and endocytic cargo proteins (Uriarte et al., 2008) and can be rapidly mobilized, even in response to weak stimulation. Mobilization of secretory vesicles containing Mac-1 or LFA-1, as well as $\alpha 4\beta 1$ and $\alpha 5\beta 1$ is not affected in *Rab27a*^{-/-} or *Munc13-4*^{-/-} neutrophils (Brzezinska et al., 2008, Johnson et al., 2010, Johnson et al., 2011a). In contrast, the surface expression of hyaluronan receptor CD44 is decreased in *Rab27a*^{-/-} neutrophils, impairing neutrophil recruitment to the liver (Johnson et al., 2011a).

1.3 MAMMALIAN STERILE 20-LIKE KINASE (MST)

The Mammalian Sterile 20-like (MST) kinase family (Creasy and Chernoff, 1995), which is related to the Hippo kinase in *Drosophila melanogaster*, consists of five different proteins, which are conserved in all metazoans. These MST kinases can be divided into two subgroups, with the first group containing MST1 (also called STK4 or KRS2) and MST2 (also called STK3), and the second group containing MST3 (also called STK24), MST4 (also called STK26) and YSK1 (Yeast Sps1/Ste20-related kinase 1; also called STK25 or SOK1) (**Figure 1.8** demonstrates the relationship and **Table 1.3** gives an overview on the nomenclature of MST kinases) (Thompson and Sahai, 2015).

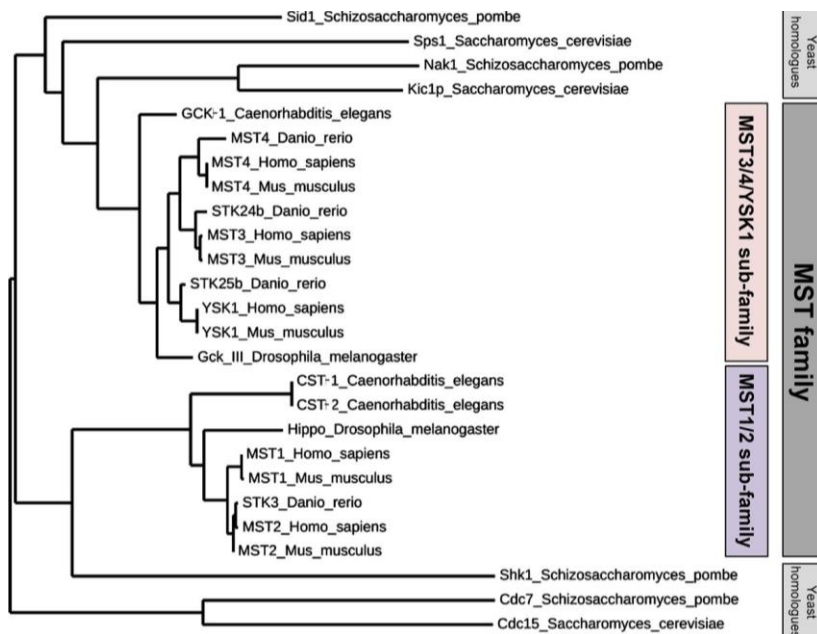


Figure 1.8 Dendrogram of the relationship between MST kinases
Relationships between MST kinases in different organisms. Adapted from (Thompson and Sahai, 2015)

Table 1.3 Table of the nomenclature of MST kinases in different organisms

Adapted from (Thompson and Sahai, 2015)

Organism	MST1/ MST2 sub-family		MST3/ MST4/ YK1 sub-family		
<i>S. cerevisiae</i>	Cdc15		Kic1/ Sps1		
<i>S. pombe</i>	Sid1/ Cdc7/ Shk1		Nak1 (Orb3)/ Pkp11		
<i>D. melanogaster</i>	Hippo		GckIII		
<i>C. elegans</i>	Cst1/2		GckI		
<i>D. rerio</i>	STK3		STK24b	MST4	STK25b
Mammals	MST1/ STK4	MST2/ STK3	MST3/ STK24	MST4/ MASK	MST5/ STK25/ YSK1

Despite millions of years of divergent evolution, MST family kinases exert similar functions across eukaryotes. MST family kinases influence cell proliferation, organ size, cell migration, cell polarity, and cell- and tissue homeostasis (Thompson and Sahai, 2015).

1.3.1 MAMMALIAN STERILE 20-LIKE KINASE 1/2 (MST1/2) SUBFAMILY

Cell division cycle 15 (Cdc15) in *S.cerevisiae* was the first MST kinase characterized (Hartwell et al., 1973, Thompson and Sahai, 2015) and turned out to be crucial for cell proliferation. Later, Hippo (Hpo) was discovered in *D.melanogaster* and identified to control tissue overgrowth by limiting cell proliferation (Halder and Johnson, 2011) (**Figure 1.9**). Both, Cdc15 and Hpo, are homologs of the mammalian MST1 and MST2.

Knockout of *Mst1* and *Mst2* (*Mst1^{-/-}Mst2^{-/-}*) in mice causes embryonic lethality, showing defects in placental development, vascular patterning, primitive hematopoiesis and regulation of cell proliferation and survival (Oh et al., 2009). *Mst1/2* conditional knockouts in the liver lead to tissue overgrowth and tumorigenesis (Lu et al., 2010, Zhou et al., 2009) (**Figure 1.9**). Conditional intestinal *Mst1/2* knockouts cause expansion of stem cell and progenitor cell compartments (Thompson and Sahai, 2015).

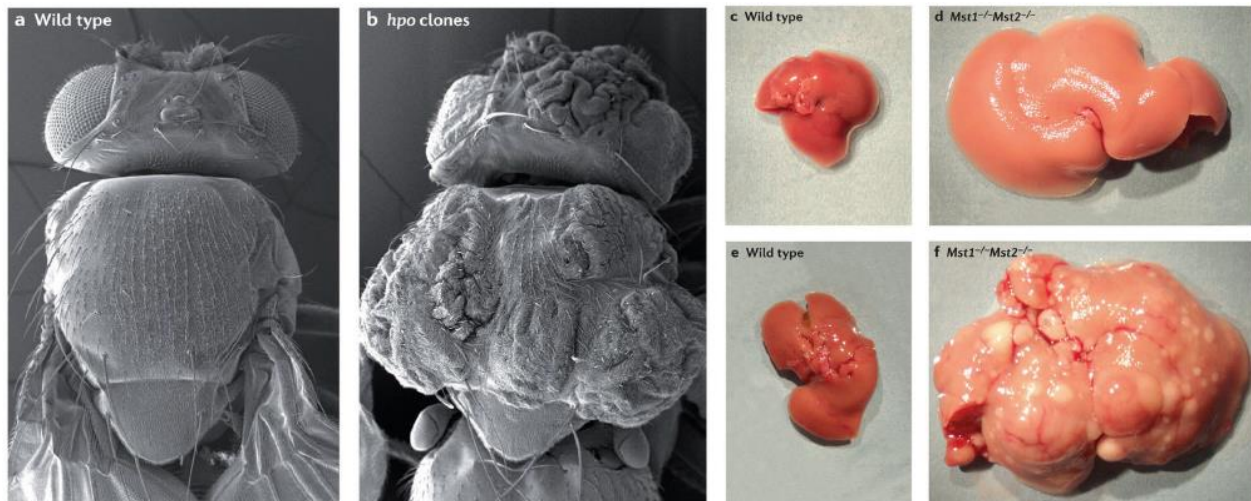


Figure 1.9 Phenotypes of Hippo mutants in *D.melanogaster* and mice

Scanning electron microscopy of WT (a) and *hpo* mutant *D.melanogaster* (b) (Halder and Johnson, 2011). Liver from 2 month old WT (c) and overgrown liver of 2 month old mice, where *Mst1/2* were conditionally deleted in the liver. Liver of 6 month old WT (e) and liver specific *Mst1^{-/-}Mst2^{-/-}* double knockout with overgrowth and foci of hepatocellular carcinoma in the later one (Lu et al., 2010). Adapted from (Johnson and Halder, 2014)

On a cellular level, *hpo* is known to control polarization of the F-actin cytoskeleton and cell migration. These functions are independent of the canonical Hippo pathway, arguing for a dual role of *hpo* and an additional non-canonical Hippo pathway (Lucas et al., 2013). The regulation of MST1/2 kinases is still unclear. Several mechanosensory systems are under discussion to directly or indirectly activate MST1/2 via cell (cytoskeleton) and tissue architecture (tissue forces) (Thompson and Sahai, 2015).

MST1 and MST2 share 88% similarity and 76% identity in amino acid (AA) sequence. Therefore, it is not surprising that *Mst1* and *Mst2* single knockout are viable, revealing that these two kinases act at least in part in a redundant fashion. Although *Mst1*^{-/-} mice are viable and develop normally, they display severe immunophenotypes (see below). In contrast, *Mst2*^{-/-} mice have no obvious phenotype (Oh et al., 2009).

1.3.2 MAMMALIAN STERILE 20-LIKE KINASE 1 (MST1)

MST1 is ubiquitously expressed with particularly high levels in lymphoid organs (Oh et al., 2009). Acting as a serine/threonine kinase MST1 has a N-terminal kinase domain, a coiled coil region, caspase 3 cleavage sites and a C-terminal SARAH domain. The SARAH domain is a highly conserved dimerization domain and important in regulating MST1, as it facilitates trans-autophosphorylation of the activation loop of MST1 through its ability to form antiparallel homodimers. MST1 can be cleaved by caspase 3 at 316 AA and 349 AA in response to apoptotic stimuli, separating the N-terminal kinase domain (37 kDa) and the C-terminal SARAH domain (18 kDa) (Thompson and Sahai, 2015) (**Figure 1.10**).

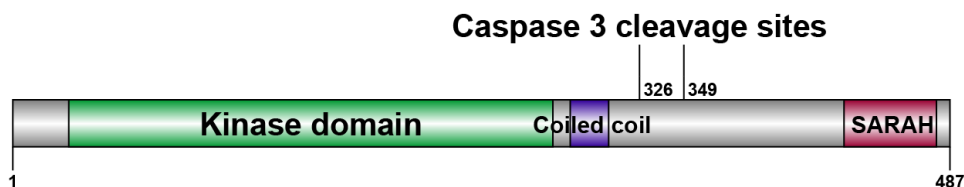


Figure 1.10 Schematic representation of MST1

STK4/ MST1 is a protein of 487 AA with a N-terminal kinase domain (30- 281 AA), a coiled coil region (290- 310 AA), caspase 3 cleavage sites (326, 349 AA) and a C-terminal SARAH domain (432- 480 AA) (Ren et al., 2009)

MST1 signaling can be divided into the canonical and non-canonical Hippo pathway. In the canonical pathway, activated MST1/2 stimulates Large tumor suppressor kinase (LATS) kinases, which phosphorylate and inactivate the transcription factor Yes-associated protein (YAP) and transcriptional co-activator with PDZ-binding motif (TAZ), restricting YAP and TAZ localization to the cytoplasm. Activated YAP and TAZ act as transcription factor and induce the expression of various genes controlling growth. Functions of MST1 other than growth and independent from LATS/ YAP/ TAZ are mediated via the non-canonical Hippo pathway and appear to be cell type specific. For example, genetic deletion of MST1 in T cells as well as activation of MST1 in HeLa or NIH-3T3 cells leads to an adhesion defect (Artemenko and Devreotes, 2013, Johnson and Halder, 2014) (**Figure 1.11**).

MST1/2 is expected to play important roles in cancer, given the importance in controlling cell proliferation. Although some mutations and fusions of MST1/2 have been discovered in some cancer types, those mutations did not appear in high frequency (Miyanaga et al., 2015).

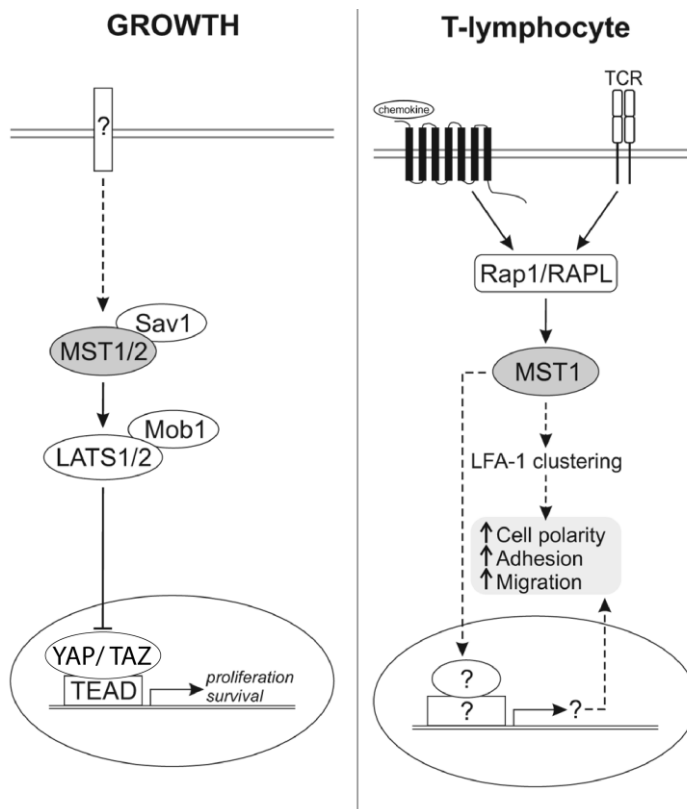


Figure 1.11 Canonical and non-canonical Hippo pathway

On the left side the key steps of the canonical Hippo pathway are depicted, regulating growth. On the right side a simplified version of the non-canonical Hippo pathway in T cells is illustrated. Modified from (Artemenko and Devreotes, 2013).

During development and within the canonical pathway MST1/2 seem to have redundant roles. Interestingly, MST1 and MST2 do not act redundantly in immune cells, possibly reflecting different expression patterns. Loss of MST1 in humans leads to an immunodeficiency syndrome (Abdollahpour et al., 2012, Crequer et al., 2012, Nehme et al., 2012, Dang et al., 2016, Halacli et al., 2015). In addition, single nucleotide polymorphisms (SNPs) in MST1 are associated with colitis and Crohn's disease (Nimmo et al., 2012, Waterman et al., 2011).

1.3.3 FUNCTION OF MST1 IN THE IMMUNE SYSTEM

The expression of murine MST1 is most abundant in lymphoid organs. MST1 is crucial for T cell selection in the thymus, adhesion, migration, growth and apoptosis (Dong et al., 2009, Katagiri et al., 2006, Katagiri et al., 2009, Mou et al., 2012, Zhou et al., 2008, Katagiri et al., 2011). *Mst1*^{-/-} mice display a reduction in splenic white pulp, a decreased number of peripheral CD4⁺ and CD8⁺ T cells, B220⁺ B cells and absence of marginal zone B cells (Qin et al., 2013).

The role of MST1 in T cell development in the thymus

During development and maturation in the thymus, T cells undergo selection processes marked by the surface expression of CD4 and CD8: double negative (DN, CD4⁻CD8⁻) > double positive (DP, CD4⁺CD8⁺) > and single positive (SP, CD4⁺CD8⁻ or CD4⁻CD8⁺). Throughout this selection, immature T cells undergo first a positive followed by a negative selection resulting in mature SP CD4⁺ and CD8⁺ T cells (Du et al., 2015). MST1 and MST2 expression can be detected in DP T cells and increases in SP T cells (Mou et al., 2012). In *Mst1*^{-/-} mice the number of SP T cells in the thymus is increased (Dong et al., 2009, Katagiri et al., 2009), whereas the number of peripheral CD4⁺ and CD8⁺ T cells is strongly reduced (Dong et al., 2009, Katagiri et al., 2009, Zhou et al., 2008, Choi et al., 2009). It was shown that MST1 is important for negative selection, but not positive selection, most likely due to defects in LFA-1/ ICAM-1 mediated adhesion, migration and antigen recognition (Ueda et al., 2012).

Of note, global deletion of *Mst2* did not alter lymphocyte numbers, however additional elimination of *Mst2* in the hematopoietic lineage (*Mst1*^{-/-} *Mst2*^{fl/fl}–*VavCre*

mouse) led to an aggravated phenotype compared to *Mst1*^{-/-} mice, indicating that MST2 can partially compensate for the loss of MST1 (Mou et al., 2012, Du et al., 2014).

MST1 regulates T cell apoptosis and survival

The severe reduction in peripheral T cells in *Mst1*^{-/-} mice is accompanied by a lower percentage of naïve T cells (CD62^{high}CD44^{low}) and a higher percentage of effector/memory T cells (CD62^{low}CD44^{high}) (Zhou et al., 2008, Du et al., 2014). This lymphopenic phenotype is more severe in *Mst1*^{-/-} *Mst2*^{fl/fl}-VavCre double knockout mice (Mou et al., 2012), and reflects the phenotype observed in human *STK4* deficient patients (Abdollahpour et al., 2012, Nehme et al., 2012). The decrease of peripheral T cells is not only due to impaired egress from the thymus, but also due to enhanced cell death (Dong et al., 2009, Katagiri et al., 2009), indicating that MST1 is required for maintaining survival and inhibiting apoptosis, however the exact mechanism is still unclear given that results from different groups vary dramatically and are sometimes contradictory (Du et al., 2015).

MST1 dependent T cell migration and homing

MST1 is critical for lymphocyte trafficking by controlling the proper organization of LFA-1 at the leading edge (Du et al., 2015), a major adhesion molecule involved in T cell trafficking. The study by Katagiri *et al.* provided the first evidence, showing that knockdown of MST1 in T cells affected LFA-1 activation/ clustering, T cell polarization and adhesion in response to chemokine or TCR stimulation (Katagiri et al., 2006) and was later confirmed in *Mst1*^{-/-} T cells (Katagiri et al., 2009, Zhou et al., 2008, Xu et al., 2014). Consistently, *Mst1*^{-/-} mice display defective migration, antigen recognition (Ueda et al., 2012), impaired thymocyte egress (Mou et al., 2012, Dong et al., 2009, Katagiri et al., 2009) and decreased lymphocyte homing (Dong et al., 2009, Katagiri et al., 2009, Zhou et al., 2008).

Functional studies using *Mst1*-deficient mice showed that MST1 is involved in lymphocyte trafficking by controlling exocytosis and localization of lymphocyte function-associated antigen 1 (LFA-1; α L β 2) in the plasma membrane (Nishikimi et al., 2014). After chemokine stimulation, MST1 is activated and associates with the cytoplasmic tail of the α _L subunit via Rap1-RAPL (Katagiri et al., 2006, Katagiri et al., 2003).

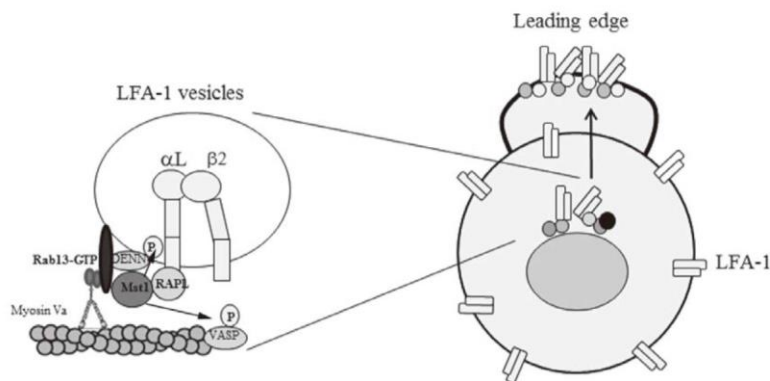


Figure 1.12 MST1/ Rab13 dependent vesicle trafficking and activation of LFA-1
MST1/ RAPL binds to α L chain of LFA-1, activating Rab13 via DENND1C and mobilizing LFA-1 containing vesicles. Adapted from (Nishikimi et al., 2014)

Then, MST1 activates Rab13 by promoting phosphorylation DENND1C, the guanine nucleotide exchange factor (GEF) for Rab13. MST1 together with activated Rab13 leads to the translocation of LFA-1 containing vesicles along actin filaments in a myosin Va-dependent manner (Nishikimi et al., 2014). In addition, MST1 promotes polymerization of F-actin, by phosphorylating VASP, crucial for the Rab13-dependent mobilization of LFA-1 containing vesicles (Nishikimi et al., 2014, Du et al., 2015) (

Figure 1.12). Mou *et al.* further demonstrated that MST1/2 are required for chemokine induced T cell migration and actin polarization by regulating Rho GTPase activation by enhancing Mob1 phosphorylation and its association with Dock8, a Rac1GEF (Mou et al., 2012).

Role of MST1 in B cells

The reduction of peripheral B cells in *Mst1*^{-/-} mice is accompanied by a decreased number of splenic marginal zone B cells, reduced B cells adhesion and trafficking (Dong et al., 2009, Katagiri et al., 2009, Zhou et al., 2008). In contrast to T cells, little is known on the function of MST1 and MST2 in B cells. One study by Salojin *et al.* demonstrated that B cells from *Mst1*^{-/-} mice have decreased responsiveness to B cell mitogen *in vitro* and defective IgE production *in vivo* (Salojin et al., 2014).

Role of MST1 in eosinophils

Both MST1 and MST2 are expressed in eosinophils. However only MST1 gets activated during apoptosis by caspase cleavage, suggesting a role for MST1 in the regulation of eosinophil apoptosis (De Souza et al., 2002). Interestingly, the same study reported no expression of MST1 in neutrophils (De Souza et al., 2002).

1.3.4 HUMAN *STK4* DEFICIENCY

MST1 emerges as a critical regulator of lymphocyte function and autoimmunity. Recently, five independent groups identified mutations in the serine/threonine protein kinase 4 (*STK4*) in human patients causing a novel primary immunodeficiency, called *STK4* deficiency. This disorder is caused by an autosomal recessive nonsense mutation in *STK4*, which encodes for Mst1. So far, three patients form a consanguineous Iranian family (Abdollahpour et al., 2012), six patients form three consanguineous unrelated Turkish families (Halaccli et al., 2015, Nehme et al., 2012), one patient from a consanguineous family of Senegalese origin living in France (Crequer et al., 2012) and three patients of a consanguineous family of unpublished origin (Dang et al., 2016) have been reported. Taken together, so far 16 patients from 6 consanguineous unrelated families were diagnosed with *STK4* deficiency, resulting from 6 different nonsense mutations in *STK4* gene (Abdollahpour et al., 2012, Crequer et al., 2012, Nehme et al., 2012, Dang et al., 2016, Halaccli et al., 2015) (**Table 1.4, Figure 1.13**).

Table 1.4 *STK4* mutations revealed in patients

DNA sequence change	Amino acid change	Commonly used nomenclature	Site of mutation	Type of mutation	Reference
c.58-61delATAG	p.Glu22X	E22X	Exon 2	Nonsense	(Halaccli et al., 2015)
c.C>T	p.Arg115X	R115X	Exon 4	Nonsense	(Crequer et al., 2012)
c.349C>T	p.Arg117X	R117X	Exon 4	Nonsense	(Nehme et al., 2012)
c.442C>T	p.Arg148X	R148X		Nonsense	(Dang et al., 2016)
c.750G>A	p.Trp250X	W250X	Exon 7	Nonsense	(Abdollahpour et al., 2012)
c.1103delT	p.369X	369X		Nonsense	(Nehme et al., 2012)

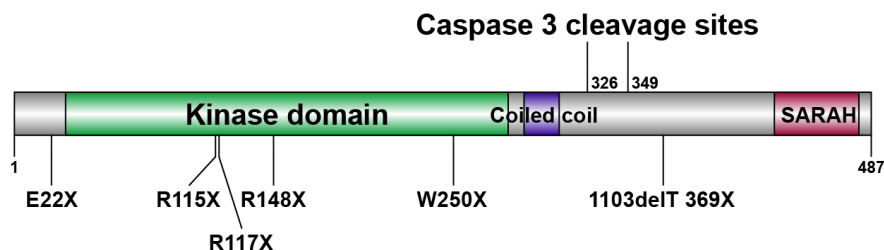


Figure 1.13 Schematic representation of human mutations in *STK4/ MST1*

Patients with *STK4* deficiency suffer from T cell lymphopenia, with a low proportion of naïve T cells and a high proportion of effector T cells, and an impaired T cell response (Nehme et al., 2012). Additional neutropenia and heart malformations could be observed in some patients (Abdollahpour et al., 2012). Patients also display recurring bacterial, viral and fungal infections together with an autoimmune manifestation and their life expectancy is very short unless successfully transplanted. In particular, *STK4* deficient patients frequently suffer from recurrent pulmonary infections, are susceptible to candidiasis, non-regressing cutaneous warts caused by multiple types of human papillomavirus infection and skin abscesses (Abdollahpour et al., 2012, Crequer et al., 2012, Nehme et al., 2012). Furthermore, different autoantibodies are detectable in these patients, indicative for autoimmune diseases (Abdollahpour et al., 2012, Nehme et al., 2012). Finally, T cells as well as neutrophils from *STK4* deficient patients show increased susceptibility to apoptosis (Abdollahpour et al., 2012).

In contrast to *STK4* deficient patients, no increased susceptibility to bacterial, viral and fungal infections have been reported for *Mst1*^{-/-} mice, yet. However, similar to *STK4* deficient patients, *Mst1*^{-/-} mice are prone to autoimmune diseases (Du et al., 2014, Ueda et al., 2012). Several studies suggest, that the major cause of autoimmune disease in *Mst1*^{-/-} mice is the impaired function of regulatory T cells (Tregs) in absence of MST1 (Du et al., 2014, Tomiyama et al., 2013).

While lymphopenia may explain a major part of the clinical manifestation. Impaired responses to acute infections imply an additional defect in myeloid cell function (Abdollahpour et al., 2012, Crequer et al., 2012, Nehme et al., 2012, Dang et al., 2016, Halacli et al., 2015).

2 AIM OF THE THESIS

Children suffering from a novel primary immunodeficiency disorder, caused by nonsense mutations in *STK4*, suffer from lymphopenia, recurring bacterial, viral and fungal infections and their life expectancy is very short unless successfully transplanted. Furthermore, the group of Prof.Dr. Christoph Klein (LMU, München) also reported intermitted neutropenia (Abdollahpour et al., 2012), which together with the impaired response to acute bacterial and fungal infections suggests an additional defect in myeloid cell function.

Until now, little is known about the function of MST1 in myeloid cells, especially in neutrophils. Therefore, in this study the function of MST1 in neutrophils during acute inflammation in humans and mice was elucidated, hypothesizing that the loss of MST1 leads to defective myeloid cell trafficking.

The specific aims of the thesis include:

- to identify potential defects in neutrophil rolling and slow rolling in the absence of MST1
- to uncover any impairment in neutrophil firm adhesion and neutrophil crawling in *Mst1*^{-/-} mice
- to reveal putative neutrophil transmigration defects in the absence of MST1
- to elucidate impaired interstitial migration in *Mst1*^{-/-} mice

3 MATERIALS

3.1 LABORATORY ANIMALS

Mst1^{-/-} mice were generated and provided by Dae Sik Lim, Biomedical Research Center, Korea Advanced Institute of Science and Technology, Daejeon, Korea (Oh et al., 2009). *Lyz2*^{GFP} (Faust et al., 2000) were generously provided by Thomas Graf, Centre for Genomic Regulation, Barcelona, Spain. *Mst1*^{-/-} x *Lyz2*^{GFP} were created by crossbreeding. C57BL/6 wild type (WT) mice were obtained from Janvier Labs (Saint Berthevin, France). All mice were maintained and bred at the Walter Brendel Center for Experimental Medicine, Ludwig Maximilians Universität, Munich, Germany. Animal experiments were approved by Regierung von Oberbayern, Germany, AZ 55.2-1-54-2531-149/10 and AZ 55.2-1-54-2532-34/14.

Table 3.1 Mouse strains used in this thesis

Strain	Background	Genotype	Reference	Source
wild type (WT)	C57Bl/6	Wild type		In-house facility
<i>Lyz2</i> ^{GFP}	C57Bl/6	<i>Lyz2</i> ^{GFP+/+}	Faust et al., 2000	In-house facility
<i>Mst1</i> ^{-/-}	C57Bl/6	<i>Mst1</i> ^{-/-}	Oh et al., 2009	In-house facility
<i>Mst1</i> ^{-/-} x <i>Lyz2</i> ^{GFP}	C57Bl/6	<i>Mst1</i> ^{-/-} x <i>Lyz2</i> ^{GFP}	In-house breeding	In-house facility

3.1.1 GENOTYPING

Detailed PCR protocol for *Lyz2*^{GFP} and *Mst1*^{-/-} mice

Number of cycles	35	
Initial denaturation	95°C	3 min
Denaturation	95°C	15 sec
Annealing	60°C	15 sec
Extension	72°C	15 sec
Final extension	72°C	7 min

Table 3.2 Primers used for genotyping

Primer	Oligoname		5'-3'	Company
MST1	M1 NestF	Fw	GTCCATAAGGTTCTAGCGTG	metabion
MST1	M1 NestR	Rv <i>Mst1</i> ^{-/-}	AGGTGTGGCACAATCGCATG	metabion
MST1	Puro NestR	Rv WT	ATGCTCCAGACTGCCTTGGG	metabion
Lyz2 ^{GFP}	MLYSUP	Fw	AGGCTGTTGGGAAAGGAGGG	metabion
Lyz2 ^{GFP}	MLP1	Rv WT	TCGGCCAGGCTGACTCCATA	metabion
Lyz2 ^{GFP}	EGFPDWN	Rv Lyz2 ^{GFP}	GTCGCCGATGGGGGTGTT	metabion

3.2 CELL LINES

1G11 murine lung endothelial cell line (Dong et al., 1997); generously provided by Annunciata Vecchi, Humanitas Research Hospital, Milan, Italy.

3.3 BUFFERS AND SOLUTIONS

Superfusion buffer

131.89 mM NaCl
 4.68 mM KCl
 2.66 mM CaCl₂
 2.13 mM MgCl₂
 18 mM NaHCO₂

HBSS buffer

1 mM MgCl₂ 0.038 g
 1 mM CaCl₂ 0.044 g
 0.1% Glucose

1 L

HBSS⁺⁺ buffer

HBSS 250 ml
 0.25% BSA 625 mg
 10 mM Hepes 596 mg
 adjust the pH to 7.4

250 ml

Annexin binding buffer	500 ml
10 mM Hepes/NaOH	1.19 g
140 mM NaCl	4.09 g
2.5 mM CaCl ₂	0.14 g
adjust the pH to 7.4	

1.5M Tris-HCl, pH8.8	1 L
Tris base	181.5 g
adjust the pH to 8.8	

0.5M Tris-HCl, pH 6.8	1 L
Tris base	60 g
adjust the pH to 6.8	

TBS buffer (10x)	1 L
Tris base	30.3 g
NaCl	80 g
Adjust to pH 7.5	

TBS-T buffer	1 L
100 ml 10x TBS buffer	
Tween-20	1 ml

SDS Running buffer (10x)	1 L
Tris base	30.3 g
Glycine	144 g
SDS	10 g

Blotting buffer (10x)	1 L
Tris base	30.3 g
Glycine	144 g

To make 1 L of 1x blotting buffer

100 ml	blotting buffer (10x)
25ml	Methanol (fresh)

Add H₂O to a final volume of 1 L

modified RIPA lysis buffer

150 mM	NaCl
1%	Triton X-100
0.5%	sodium deoxycholate
50 mM	Tris-HCl, pH 7.3
2 mM	EDTA
1x	protease inhibitor mixture [Roche]
1x	phosphatase inhibitor cocktail 1+2 [Sigma-Aldrich]

5x Laemmli sample Buffer**50 ml**

	1M Tris-HCl, pH 6.8	15 ml
1%	SDS	5 g
50%	Glycerin	25 ml
	β -Mercaptoethanol	10 ml
	Bromphenol blue	125 mg

store at -20°C

FACS buffer

1%	BSA
----	-----

in PBS

Narcotic Ketamin/Xylazin

125 mg kg ⁻¹	Ketamin
25 mg kg ⁻¹	Rompun 2% (Xylazin)

in NaCl

3.4 MEDIA**Medium for 1G11 murine endothelial cells**

	DMEM (low Glucose)	500 ml
1%	non-essential amino acids	
1 mM	L-Glutamine	
1 mM	Na-pyruvate	
100 µg/ml	Heparin	
20%	FCS	
1 mM	Penicillin/ Streptavidin	

3.5 SUBSTANCES

Table 3.3 Recombinant Proteins

Substance	Company
rmCXCL1 (Kc)	Preprotech
rmICAM-1	R&D Systems
rmTNF- α	R&D Systems
rmE-selectin	R&D Systems
rmPECAM-1	R&D Systems
fMLP	Sigma

Table 3.4 Fluorescent substances

Substance	Company
Streptavidin PE-Cy5	BD
Streptavidin Alexa Fluor 647	Invitrogen
DQ TM Gelatin	Life Technologies
T-MRE	Molecular Probes, Mobitech
TO-PRO3	Invitrogen
Neutrophil Elastase 680 Fast TM	Perkin Elmer

Table 3.5 Other substances

Substance	Company
Acrylamid	
Agarose UltraPure	Invitrogen
Antibody Diluent with Background Reducing Components	Dako
BSA (bovine serum albumin)	PAA Laboratories
Bromophenol Blue sodium salt	Sigma
Chemiluminescent HRP Substrate Immobilon Western	Millipore
Direct PCR Lysis Reagent (Tail)	peQLab
DMEM, low glucose	PAA Laboratories
DMSO	Sigma
DNA Ladder 100bp	peQLab

EDTA	
FCS (fetal calf serum), heat-inactivated	Invitrogen
FACS lysing solution	BD
Flow-Count™ Fluorospere	Beckman Coulter
Fluoromount-G	Biozol/ Southern Biotech
N-Formylmethionyl-leucyl-phenylalanine (fMLP)	Sigma
Gelatine	Sigma
Glutamax	Invitrogen
Glycerin	Roth
Heparin-Natrium-25000	Ratiopharm
Isopropanol/ 2-Propanol	Roth
Ketavet (100mg/ml)	Pharmacia GmbH
NaCl	Fresenius Kabi GmbH
Natural mouse laminin	Life technologies
Liberase™ research grade purified enzyme	Roche
β-Mercaptoethanol	Sigma
Penicillin-Streptomycin, liquid	Invitrogen
Percoll, pH 8.5 – 9.5	Sigma
PermaFluor	Thermo Scientific
Precision Plus Protein Kaleidoscope Standards Western	BioRad
Phorbol 12-myristate 13-acetate (PMA)	Sigma Aldrich
Phosphatase Inhibitor Cocktail 2	Roche
Phosphatase Inhibitor Cocktail 3	Roche
Polymorphoprep	Axi-Shield PoC AS
Protease Inhibitor Cocktail, cOmplete™, mini, EDTA-free	Roche
PermaFluor	Thermoscientific
SDS ultra pure	Roth
Tris base, Tris(hydroxymethyl)-aminomethan	MERCK
Triton X-100	Appli Chem
Türk's solution	MERCK
Tween20	MERCK

3.5.1 ANTIBODIES

Table 3.6 Primary antibodies

h – human, m – mouse

Antibody	Dye	Reactivity	Isotype	Clone	company
CD11a (LFA-1)	-	rat anti m	IgG2a,κ	2D7	BioLegend
CD11a (LFA-1)	Alexa Fluor 546	rat anti m	IgG2a,κ	2D7	BioLegend
CD11a (LFA-1)	APC	rat anti m	IgG2a,κ	M17/4	eBioscience
CD11b (Mac-1)	-	rat anti m	IgG2b,κ	M1/70	BioLegend
CD11b (Mac-1)	PE	rat anti m	IgG2b,κ	M1/70	BioLegend
CD11b (Mac-1)	Brilliant Violet 510	rat anti m	IgG2b,κ	M1/70	BioLegend
CD16/CD32 (mouse Fc-bock)	-	rat anti m	IgGa,λ	93	BioLegend
CD18	FITC	rat anti m	IgG2a,κ	C71/16	Pharmingen
CD31 (PECAM-1)	-	rat anti m	IgG2a,κ	390	BioLegend
CD31 (PECAM-1)	Alexa Fluor 647	rat anti m	IgG2a,κ	390	BioLegend
CD31 (PECAM-1)	Alexa Fluor 488	rat anti m	IgG2a,κ	MEC13.3	BioLegend
CD44	Brilliant Violet 570	rat anti h, m	IgG2b,κ	IM7	BioLegend
CD45	PerCp-Cy5.5	rat anti m	IgG2b,κ	30-F11	BioLegend
CD49c (VLA-3)	-	mouse anti m	IgG1	42/CD49c	BD
CD49f (VLA-6)	Alexa Fluor 647	rat anti h, m	IgG2b	GoH3	BioLegend
CD62E	-	rat anti m	IgG1	9A9	InVivo
CD62L	FITC	rat anti m	IgG2a,κ	MEL-14	BioLegend
CD62P	-	rat anti m	IgG1	RB40.34	InVivo
CD115	APC				
CD162 (PSGL-1)	PE	rat anti m	IgG1	2PH1	Pharmingen
CD182 (CXCR2)	APC	rat anti m	IgG2a	242216	R&D
ESAM-1	-	Rabbit anti m			D.Vestweber
GAPDH	-	Mouse anti	IgG1	6C5	Calbiochem
JFC1/ Slp1		rabbit anti h, m	IgG		Santa Cruz
Laminin alpha 5	-	rat anti m	IgG	4G6	L.Sorokin, Münster
Ly6G	eFluor 405	rat anti m	IgG2a,κ	1A8	BioLegend
Ly6G/Ly6C (Gr-1)	eFluor 405	rat anti m	IgG2b	RB6-8C5	BioLegend
MRP14 (S100A9)	-	rabbit anti m		polyclonal	T.Vogl, Münster
MST1	-	rabbit anti h, m		polyclonal	CellSignaling
MST1	-	rabbit anti h, m	IgG	polyclonal	Upstate

MST2	-	rabbit anti h, m		polyclonal	CellSignaling
Munc13-4	-	rabbit anti h, m	IgG	polyclonal	proteintech
Neutrophil Elastase	-	rabbit anti h, m	IgG	polyclonal	Abcam
Rab27a	-	sheep anti h, m	IgG	polyclonal	R&D
RAPL (Nore1, Rassf5)	-	rabbit anti h, m	IgG	polyclonal	Abcam
Isotype control	FITC	rat anti m	IgG2a,k		eBioscience
Isotype control	PE	rat anti m	IgG1		eBioscience
Isotype control	APC	rat anti m	IgG2a	RTK2758	BioLegend
Isotype control	Brilliant Violett 570	rat anti h, m	IgG2b,k	RTK4530	BioLegend
Isotype control	eFluor 405	rat anti m	IgG2a,k		BioLegend
Isotype control	eFluor 405	Rat anti m	IgG2b		eBioscience

Table 3.7 Secondary antibodies

Antibody	Conjugated	Company
goat anti-human Fcy	Biotin	eBioscience
donkey anti-rabbit	Alexa Fluor® 488	Invitrogen
donkey anti-rat	Alexa Fluor® 488	Invitrogen
goat anti-mouse	Alexa Fluor® 488	Invitrogen
donkey anti-sheep	Alexa Fluor® 488	Invitrogen
goat anti-rat	Alexa Fluor® 555	Invitrogen
goat anti-mouse	Alexa Fluor® 546	Invitrogen
goat anti-rat	Alexa Fluor® 546	Invitrogen
goat anti-rabbit	Alexa Fluor® 546	Invitrogen
donkey anti-goat	Alexa Fluor® 548	Invitrogen
donkey anti-rabbit	Alexa Fluor® 647	Invitrogen
goat anti-rat	Alexa Fluor® 647	Invitrogen
donkey anti-rabbit	Brilliant Violet TM 510	BioLegend
goat anti-mouse IgG (H+L)	HRP	Jackson Immuno
goat anti-rabbit (IgG H+L)	HRP	Jackson Immuno
donkey anti-sheep	HRP	Jackson Immuno

3.6 KITS

Alexa Fluor® 546 antibody labeling Kit	Molecular Probes/ Invitrogen
pHrodo™ E.coli BioParticles® Phagocytosis Kit	Invitrogen
EasySep mouse neutrophil enrichment Kit	STEMCELL Technologies
Mouse MPO ELISA Kit	Hycult biotech

3.7 EQUIPMENT

Intravital BX51WI microscope	Olympus
TrimScope	LaVision Bio Tec,
Confocal microscope SP5	Leica
ProCyt Dx	IDEXX Laboratories
Gallios flow cytometer	Beckman Coulter
Rotina 420R	Hettich
Centrifuge 5427R	Eppendorf
Table centrifuge	Labnet International
pH meter 720	InoLab
Pipetts, Research Plus	Eppendorf
Protein Electrophoresis and Blotting	BioRad
Power Supplies	BioRad
Vortex-Genie 2	Scientific Industries
Rocker 3D basic	IKA
Incubator	Binder
Peq MIX Plus	PeqLab
Thermo Mixer F1.5	Eppendorf
PCR machine T Advanced	Biometra
Compact Multi-Wide	Biometra
Balance AB 104-S-A	Mettler Toledo
Nano Drop 2000	Thermo Scientific
ORCA system	Hamamatsu

3.8 CONSUMABLES

Cell strainer, 40µm Nylon	Falcon, Corning
6-Well plate	Corning
24-Well plate	Corning
96-Well plate	Corning
24-Well transwell plate, 5µm pore size	Corning
Multiscreen filterplate, 3µm pore size	Millipore
Transport receiver plate	Millipore
Flask, 25cm ²	Corning
Flask, 75cm ²	Corning
Flask, 175cm ²	Corning
Syringe, 1, 10ml	Braun
Syringe, 2,5,20ml	BD
Cannulaes	BD
Tube, 5ml	BD Falcon
Tube, 15ml	Greiner
Tube, 50ml	Falcon, Corning
Pipettes, 1, 2, 5, 10, 25ml	Corning
Pasteur Pipetts	Brand

3.9 SOFTWARE

Kaluza 1.3	Beckman Coulter
Prism 6.05	Graphpad
Image J 1.49	National Institute of Health
Inspector Pro	LaVision Biotech
Imaris 7	Bitplane
Adobe Photoshop & Illustrator CS6	Adobe
EndNote X7.4	Thomson Reuter
Wasabi	Hamamatsu

4 METHODS

4.1 NEUTROPHIL RECRUITMENT IN VIVO

4.1.1 CONVENTIONAL INTRAVITAL MICROSCOPY OF THE MOUSE CREMASTER MUSCLE

Anesthetized mice (using 125 mg kg⁻¹ Ketamin and 25 mg kg⁻¹ Xylazin 2%) were intubated (plastic tube inner diameter (ID):0.76 mm; outer diameter (OD): 1.22 mm) and a carotid artery catheter (plastic tube ID:0.28 mm; OD: 0.61 mm) was placed to inject blocking antibodies and collect whole blood for analysis using ProCyt Dx (IDEXX Laboratories). The cremaster muscle was exteriorized and a superfusion buffer - preheated and saturated with 95% N₂ and 5% CO₂ was used to moisturize the tissue and reduce oxygen levels. Venules were recorded for at least 1 min by intravital microscopy (Olympus BX51WI microscope, water immersion objective 40x, 0.80 NA, Olympus; CCD camera, CF8/1, Kappa). Thereafter, rolling flux fraction (rolling cell min⁻¹ divided by all neutrophils passing the vessel min⁻¹), rolling velocity and neutrophil adhesion efficiency (number of adherent neutrophils mm⁻² divided by the systemic neutrophil count) determined, as described before (Pruenster et al., 2015). Postcapillary venules ranged from 20-40 µm in diameter. Blood flow velocity was measured using a dual photodiode connected to a digital on-line temporal intensity cross-correlation program (Circusoft Instrumentation, Hockessin, USA; originally developed by Wayland & Jonson 1967). Microvascular parameters (venular diameter, venular vessel segment length) were determined using Fiji software (Schindelin et al., 2012).

Trauma induced cremaster muscle model and CXCL1 induced adhesion

The trauma induced cremaster muscle model was used to observe leukocyte recruitment under mild inflammatory conditions in WT and *Mst1*^{-/-} mice (Ley et al., 1995). Briefly, the cremaster muscle was exteriorized and superfused for 20 min before recoding venules.

In a second step, a venule was recorded before CXCL1 (Kc) injection, whole blood was collected and 600 ng CXCL1 was injected i.v. through the carotid artery

catheter. One minute after CXCL1 injection the same venule was recorded again for 1 min and the number of adherent neutrophils was compared.

TNF- α induced cremaster muscle model

Leukocyte recruitment in TNF- α stimulated mouse cremaster muscle venules was observed in WT and *Mst1*^{-/-} mice, as previously described (Frommhold et al., 2010). Briefly, 2 h after intrascrotal injection of TNF- α (500 ng mouse⁻¹) the cremaster muscle was exteriorized and rolling flux fraction (rolling cell min⁻¹ divided by all neutrophils passing the vessel min⁻¹), rolling velocity and neutrophil adhesion efficiency (number of adherent cells mm⁻² divided by the systemic neutrophil count) determined by intravital microscopy. Injection of anti-mouse E-selectin (clone 9A9, 30 μ g, i.v.), anti-mouse P-selectin (RB40.34, 30 μ g, i.v.), anti-mouse L-selectin (MEL14, 30 μ g, i.v.), anti-mouse LFA-1 (TIB 217, M17/4.4.11.9, 100 μ g i.p., one hour prior stimulation), anti-mouse Mac1 (TIB 218, M1/70.15.11.5HL, 100 μ g i.p., one hour prior stimulation), and anti-mouse ICAM-1 (YN1/1.7.4, 100 μ g i.p., one hour prior stimulation) were used to alter rolling and adhesive properties.

4.1.2 MULTI-PHOTON INTRAVITAL MICROSCOPY OF THE MOUSE CREMASTER MUSCLE

Extravasation of neutrophils into the inflamed mouse cremaster muscle of *Lyz2*^{GFP} (Faust et al., 2000) and *Lyz2*^{GFP} x *Mst1*^{-/-} mice was investigated by multi photon microscopy (Woodfin et al., 2011). Briefly, TNF- α (500 ng mouse⁻¹) and a rat anti-mouse PECAM-1 antibody labeled with Alexa Fluor 546 (clone 390; labeled 'in house' with monoclonal antibody labeling kit; 3 μ g) were injected into the scrotum of mice. One hour later, the cremaster muscle was prepared for intravital multi photon microscopy. Z-stacks of postcapillary venules between 20-40 μ m in diameter were captured using a TrimScope (LaVision Bio Tec (Rehberg et al., 2011), upgraded with Hamamatsu H7422A-40 high sensitivity GaAsP photomultipliers; Olympus XLUMPlanFI, 20x water immersion objective, 0.95 NA, 810 nm excitation, 390/80 for SHG signal, ultra-sensitive port (USP) 525/50 for GFP, 580/60 for PECAM1-Alexa Fluor 546 detection). Images were acquired by sequential scans at a resolution of 966 x 966 pixels, corresponding to 300 x 300 μ m. Stacks of images with a step size of 4 μ m were acquired at intervals of 30 seconds. After acquisition, sequences of z-stacks were processed and analyzed using

Imaris 7 and Fiji software. Transmigration time was defined from the point neutrophils started to transmigrate (excluding intraluminal crawling) until they completely detached from the abluminal vascular wall.

Laser induced injury using multi-photon intravital microscopy

Neutrophil swarming to the site of injury was observed in *Lyz2^{GFP}* and *Lyz2^{GFP} x Mst1^{-/-}* mice. Four h after intrascrotal injection of TNF- α and one hour after anti-mouse PECAM1 Alexa Fluor 546 antibody intrascrotal injection, a laser injury was induced in the cremaster muscle using high laser power by scanning an area of 50 x 50 μm 121 times in the center of 500 x 500 μm . Images were acquired for 30 min as described above. The GFP intensity, which is proportional to the number of neutrophils at the site of injury, was analyzed using Fiji software.

4.1.3 TNF- α INDUCED NEUTROPHIL EXTRAVASATION INTO THE PERITONEAL CAVITY

WT and *Mst1^{-/-}* mice were intraperitoneally injected with NaCl (control) or TNF- α (rmTNF- α , 1 μg mouse⁻¹). Mice were sacrificed 2 h later and peritoneal lavage performed using 5 ml ice-cold PBS. Cells were collected and stained with a rat anti-mouse Ly6G Pacific Blue antibody (1A8). Number of extravasated neutrophils was measured by using a Beckman Coulter GalliosTM flow cytometer with Flow-CountTM Fluorospheres and analyzed using Kaluza® Flow Analysis Software.

4.2 FLOW CHAMBER ASSAYS

4.2.1 MURINE EX VIVO FLOW CHAMBER SYSTEM

To investigate adhesion under flow conditions we used a previously described flow chamber system (Yang et al., 2012). Glass capillaries (Rect.Boro Capillaries 0.04 x 0.40 mm ID VitroCom, Mountain Lakes, USA) were coated overnight with combinations of E-selectin (CD62E, rmE-selectin Fc chimera, 20 μg ml⁻¹), ICAM-1 (rmICAM-1 Fc chimera, 15 μg ml⁻¹) and CXCL1 (rmCXCL1, 15 μg ml⁻¹). Flow chambers were auto perfused with whole blood from WT or *Mst1^{-/-}* mice via a carotid artery catheter with a shear stress of 2.7 dyne cm⁻². One representative field was recorded (Olympus BX51WI microscope

with a CCD camera CF8/1, Kappa, Germany; water immersion objective x20, 0.95 NA, Olympus). Number of adherent cells was determined using Fiji software.

4.2.2 LFA-1 CLUSTERING UNDER FLOW CONDITIONS

In order to investigate LFA-1 clustering during neutrophil adhesion under flow conditions, flow chambers were perfused ($2 \mu\text{l min}^{-1}$) with whole blood from WT or *Mst1*^{-/-} mice, incubated with rat anti-mouse LFA-1 Alexa Fluor 546 antibody (2D7, labeled 'in house' with monoclonal antibody labeling kit; $2.5 \mu\text{g}$) for 10 min. Adherent cells were imaged using confocal microscopy (Leica System SP5, 63x, 1.4 NA oil objective, xyz-t-series).

4.2.3 HUMAN FLOW CHAMBER SYSTEM

In order to investigate adhesion of human neutrophils under flow conditions we used a previously described flow chamber system (Nussbaum et al., 2013). Glass capillaries (Rect.Boro Capillaries 0.2 x 2 mm ID VitroCom, Mountain Lakes, USA) were coated overnight with combinations of E-selectin (rhCD62E Fc chimera, $5 \mu\text{g ml}^{-1}$), ICAM-1 (rhICAM-1 Fc chimera, $4 \mu\text{g ml}^{-1}$) and CXCL8 (interleukin8, IL-8; rhCXCL8, $5 \mu\text{g ml}^{-1}$). Whole blood was isolated from two patients with *STK4* deficiency and their heterozygous parents in Hannover, Germany and sent to Munich for analysis. Flow chambers were perfused with PolymorphoprepTM purified blood neutrophils ($2 \times 10^5 \text{ ml}^{-1}$) from parents (*STK4*^{+/+}) or *STK4*^{-/-} patients using a high precision pump with a shear rate of 2 dyne cm^{-2} . One representative field of view was recorded (Olympus BX51WI microscope with a CCD camera CF8/1, Kappa, Germany; water immersion objective 20x, 0.95 NA, Olympus). Number of adherent cells was determined. Experiments were approved by the ethical committee, LMU, Germany, AZ 66-14.

4.3 FLUORESCENCE ACTIVATED CELL SORTING (FACS)

4.3.1 NEUTROPHIL AND MONOCYTE DIFFERENTIATION

To differentiate between neutrophils and monocytes, antibodies against CD45 and CD11b were used to gate CD45^{high}, CD11b⁺ myeloid cells. To further differentiate antibodies against CD115 and Gr-1 were used to identify neutrophils (Gr-1^{high}, CD115⁻), inflammatory (Gr-1^{high}, CD115⁺) and non-inflammatory monocytes (Gr-1^{low}, CD115⁺).

4.3.2 SURFACE EXPRESSION ON NEUTROPHILS

Surface expression of α L (LFA-1, CD11a, M17/4), α M (Mac-1, CD11b, M1/70), CXCR2 (CD182, 242216), CD44 (CD44, IM7), PSGL1 (CD162, 2PH1) und L-selectin (CD62L, MEL-14) of bone marrow and blood derived Ly6G⁺ (Ly6G, 1A8) neutrophils from WT and *Mst1*^{-/-} mice was compared using a Beckman Coulter GalliosTM flow cytometer and analyzed using Kaluza® Flow Analysis Software (Beckman Coulter).

4.3.3 SELECTIN BINDING TO NEUTROPHILS

E- and P- selectin binding was performed as described previously (Borsig et al., 2002). Briefly, whole blood was isolated from WT and *Mst1*^{-/-} mice and incubated with an Fc-blocking antibody for 15 min at 4°C. Meanwhile selectin-chimeras were pre-complexed by incubating P- or E-selectin hFc chimera (3.6 µg) with goat anti- human Fc gamma-biotin in 100µl HBSS buffer for 20 min at room temperature. Cells were incubated with pre-complexed selectin-chimera with or without EDTA (10mM) for 50 min at 4°C. EDTA served as a negative control due to its ability to form complexes with Ca²⁺ and Mg²⁺, both cations are required for selectin binding. Cells were fixed (FACS Lysing Solution), stained with streptavidin PE-Cy5 and rat anti-mouse Ly6G-Pacific Blue antibody (1A8) and measured using a Beckman Coulter GalliosTM flow cytometer. For the analysis, Kaluza® Flow Analysis Software was used.

4.3.4 SOLUBLE ICAM-1 BINDING TO NEUTROPHILS

A soluble ICAM-1 binding assay was performed as described previously (Lefort et al., 2012). Briefly, bone marrow neutrophils were isolated from WT and *Mst1*^{-/-} mice using a Percoll gradient. Cells were suspended in complete HBSS⁺⁺ buffer. Cells were stimulated with 100 ng ml⁻¹ CXCL1 or an equal volume of HBSS⁺⁺ buffer, in the presence of ICAM-1 (rmlCAM-1 hFc chimera, 20µg ml⁻¹), goat anti-human Fc gamma-biotin and Streptavidin – PerCP-Cy5.5 for 3 min at 37°C. Cells were fixed, stained with rat anti-mouse Ly6G-Pacific Blue antibody (1A8) and measured using a Beckman Coulter GalliosTM flow cytometer. For the analysis, Kaluza® Flow Analysis Software was used.

4.3.5 PHAGOCYTOSIS

Phagocytic capacity of neutrophils was evaluated using pHrodoTM *E.coli* BioParticles Phagocytosis Kit according to manufacturer. Briefly, whole blood from WT and *Mst1*^{-/-} mice was incubated with pHrodo particles for 15 min at 4°C or 37°C. A rat anti-mouse Gr1-eFluor 405 antibody was used to identify neutrophils (Gr1^{hi}). Using the pHrodoTM dye fluorescence intensity of WT and *Mst1*^{-/-} neutrophils was evaluated by using a Beckman Coulter GalliosTM flow cytometer.

4.3.6 NEUTROPHIL VIABILITY

Viability and apoptosis rate of neutrophils was evaluated using T-MRE (tetramethylrhodamine) and TO-PRO3, respectively. The positively charged dye, T-MRE accumulates in active mitochondria due to their relative negative charge. Depolarized or inactive mitochondria with decreased membrane potential fail to gather T-MRE, making it suitable to indicate live cells (Barteneva et al., 2014). TO-PRO3 is taken up by apoptotic cells via pannexin 1 channels (Poon et al., 2014). Briefly, isolated neutrophils were cultured in HBSS⁺⁺ buffer for 0, 24, 48 and 72 h. Afterwards cells were stained with T-MRE, TO-PRO3 and anti- Ly6G- PB antibody and measured using a Beckman Coulter GalliosTM flow cytometer.

4.3.7 NUMBER AND VIABILITY OF NEUTROPHILS WITHIN THE CREMASTER MUSCLE

In order to evaluate the total number of neutrophils within the whole cremaster muscle, TNF- α (500 ng mouse⁻¹) was injected into the scrotum of WT and *Mst1*^{-/-} mice. Two hours later, the cremaster muscle was exteriorized, dissected and digested with Liberase (0.25 mg ml⁻¹) for 1 h at 37°C. Cells were stained with rat anti-mouse Ly6G PB antibody (1A8), T-MRE and TO-PRO3. The number of neutrophils and the viability was measured by using a Beckman Coulter GalliosTM flow cytometer with Flow-CountTM Fluorospheres and analyzed using Kaluza® Flow Analysis Software.

4.4 NEUTROPHIL ISOLATION

4.4.1 MURINE NEUTROPHIL ISOLATION

For murine neutrophil isolation either percoll density gradient centrifugation was performed or EasySep mouse neutrophil enrichment Kit was used according to the manufacturer (StemCell).

Isolation of murine neutrophils using percoll density gradient centrifugation

The principle of percoll gradient centrifugation was used to separate murine neutrophils. Briefly, two layers of percoll - lower layer with a density of 1.11 g ml⁻¹ and an intermediate layer with a density of 1.08 g ml⁻¹ – are carefully applied. Thereafter, diluted whole blood or bone marrow was applied to the top. After 30 min centrifugation at 1000 g without break, the second interphase containing enriched neutrophils was carefully transferred.

4.4.2 HUMAN NEUTROPHIL ISOLATION

To isolate human neutrophils, venous whole blood was collected using syringes (40 unit heparin ml⁻¹). Whole blood was carefully applied on top of a layer of PolymorphoprepTM. After 30 min centrifugation at 500 g without break, the interphase containing enriched neutrophils was carefully transferred.

4.5 IMMUNOFLUORESCENCE

4.5.1 CREMASTER WHOLE MOUNT STAINING

TNF- α (500 ng mouse⁻¹) was applied to the scrotum of WT and *Mst1*^{-/-} mice. After 2 h the mouse cremaster muscle was dissected and fixed with 4% PFA for 1 h, permeabilized and blocked for 2 h in 0.5% Triton X-100/ 2% ovalbumine /PBS. Thereafter, the cremaster was incubated with rat anti-mouse laminin α 5 antibody 4G6 (Sorokin et al., 1997), rabbit anti-mouse ESAM1 antibody (Wegmann et al., 2006) and goat anti-mouse MRP14 antibody (S100a9) overnight in 2% ovalbumine/ PBS at room temperature (RT). After labeling with secondary antibodies (donkey anti-rat Alexa Fluor 488, donkey anti-goat Alexa Fluor 568, donkey anti-rabbit Alexa Fluor 647) in 1% ovalbumine/ PBS for 5 h at RT, the tissue was embedded on glass slides in PermaFluor Mounting Medium under cover slips. In order to analyze neutrophil extravasation, z-stack images of vessels, with a length of over 150 μ m without branching and an average diameter of 20-40 μ m, were taken using confocal microscope (Zeiss LSM 780, LSM 510). Neutrophils, which appeared within 50 μ m around the vessel segment were counted using Imaris software.

4.5.2 MOBILIZATION OF VLA-3, VLA-6, NE, MST1 AND RAB27A IN NEUTROPHILS

Mobilization of α 3 (VLA-3, CD49c), α 6 (VLA-3, CD49f) and neutrophil elastase (NE) on PECAM-1, ICAM-1 and CXCL1 coated wells was performed as previously described (Wang et al., 2005). Briefly, μ -Slide 8 well chambers were coated with either 2% BSA (control) or a combination of PECAM-1 (2 μ g ml⁻¹), ICAM-1 (8 μ g ml⁻¹) and CXCL1 (10 μ g ml⁻¹) overnight at 4 °C. Bone marrow neutrophils from WT and *Mst1*^{-/-} mice were isolated using a Percoll gradient and incubated on coated wells for 30 min at 37 °C. Cells were fixed with 4% PFA for 15 min at RT, blocked and permeabilized with PBS/ 0.1% Triton X-100/ 2% BSA for 1 h at RT. Cells were incubated with the primary antibodies at 4 °C overnight, in the first set of experiments, cells were incubated with a rabbit anti-mouse NE antibody (polyclonal), a mouse anti-mouse VLA-3 antibody (42/CD49c) and rat anti-mouse VLA-6 Biotin conjugated antibody (GoH3) overnight at 4 °C.

In a second set of experiments, sheep anti-mouse Rab27a antibody, rabbit anti-mouse MST1 antibody (polyclonal) and rat anti-mouse VLA-6 antibody (GoH3) or sheep

anti-mouse Rab27a antibody, a rabbit anti-mouse NE antibody (polyclonal) and a rat anti-mouse VLA-6 antibody (GoH3) was used. Primary antibodies were detected using goat anti-mouse Alexa Fluor® 488, goat anti-rabbit Alexa Fluor® 546, Streptavidin Alexa Fluor® 647, donkey anti-sheep Alexa Fluor® 488 and goat anti-rat Alexa Fluor® 647, respectively. Cells were incubated for 1 h at room temperature. Finally, cells were embedded in PermaFluor and imaged by confocal microscopy (Leica System SP5, 63x, 1.4 NA oil objective) and analyzed using Fiji software.

4.5.3 IN VIVO NE ACTIVITY ASSAY

NE680FAST (4 nmols per mouse) was injected i.v. One h later TNF- α (500 ng mouse⁻¹) was applied to the scrotum of WT and *Mst1*^{-/-} mice. Two h later, the mouse cremaster muscle was dissected and fixed with 4% PFA for 1 h, permeabilized and blocked for 2 h in 0.5% Triton X-100/ 2% ovalbumine /PBS. Thereafter, the cremaster was incubated with rat anti- mouse PECAM-1 antibody labeled with Alexa Fluor 488 (MEC13.3) overnight in 2% BSA/ PBS at room temperature (RT). As a control, only TNF- α (500 ng mouse⁻¹) was applied to the scrotum of WT and *Mst1*^{-/-} mice and stained using rabbit anti-mouse MRP14 antibody (gift of Thomas Vogl, University Münster, Germany). The MRP14 antibody was detected with a goat anti-rabbit Alexa Fluor® 546 antibody (Molecular Probes/ Invitrogen). Afterwards, tissues were embedded on glass slides in PermaFluor under cover slips. Finally, whole cremaster were imaged by confocal microscopy (Leica System SP5, 40x, 1.4 NA oil objective) and analyzed using Fiji and Imaris software.

4.6 WESTERN BLOTTING

Murine neutrophils from WT and *Mst1*^{-/-} mice were isolated from bone marrow using EasySep™ mouse neutrophil enrichment kit. Cells were incubated in lysis buffer, homogenized in Laemmli sample buffer and boiled for 5 min at 95°C. Proteins were resolved by SDS–polyacrylamide gel electrophoresis (SDS–PAGE) gels and then electrophoretically transferred from the gels onto PVDF membranes. Membranes were incubated with rabbit anti-mouse MST1 antibody (Upstate), rabbit anti-mouse MST2

antibody, rabbit anti-mouse NE antibody, mouse anti-mouse VLA-3 antibody (42/CD49c), rabbit anti-mouse VLA-6 antibody, sheep anti-mouse Rab27a or mouse anti-mouse GAPDH antibody and subsequently labeled with goat anti-mouse HRP, goat anti-rabbit HRP or donkey anti-sheep HRP. Bound antibodies were detected using enhanced chemiluminescence using Hamamatsu ORCA system.

4.7 CELL CULTURE

4.7.1 TRANSWELL ASSAYS

Murine neutrophils were isolated from bone marrow using EasySep™ mouse neutrophil enrichment kit. Complete HBSS buffer, 10 ng ml⁻¹ CXCL1 or 100 ng ml⁻¹ CXCL1 was applied to the lower compartments of the transwell system (5 µm pore size). Isolated neutrophils were applied to the upper compartment (5x10⁵ cells per well) and allowed to migrate for 45 min at 37°C. Cells were collected from the lower chamber and stained with a rat anti- mouse Ly6G Pacific Blue antibody (1A8). Number of transmigrated neutrophils was measured by using a Beckman Coulter Gallios™ flow cytometer with Flow-Count™ Fluorospheres and analyzed using Kaluza® Flow Analysis Software.

Transwell assay with filters coated with murine laminin

In a second set of experiments, we performed transmigration assays with additional coating of the membrane as described before (Wang et al., 2005). Briefly, the membrane of the transwell system (3 µm pore size) was coated with laminin 1 (15 µg ml⁻¹) or 2% BSA as a control at 4 °C overnight. Afterwards, laminin was additionally coated with a combination of PECAM-1 (2 µg ml⁻¹) and ICAM-1 (8 µg ml⁻¹) for 2 h at 37 °C. Either complete HBSS buffer alone or with 1 ng ml⁻¹ CXCL1 was added to the lower compartments. Isolated bone-marrow neutrophils (2x10⁵ cells per well) were suspended in complete HBSS buffer, added to the upper compartment and allowed to migrate for 3 h at 37 °C. Cells were collected from the lower chamber and stained with a rat anti-mouse Ly6G Pacific Blue antibody (1A8). Number of transmigrated neutrophils was evaluated by using a Beckman a Coulter Gallios™ flow cytometer with Flow-Count™ Fluorospheres.

Transwell assay with filters coated with murine endothelial cells

In a third set of experiments, murine endothelial 1G11 cells (kindly provided by Annunciata Vecchi) were seeded on transwell inserts (5 μm pore size) coated with 2% gelatin and cultured until a monolayer has formed (on average overnight). Either complete HBSS buffer alone or with 100 ng ml^{-1} CXCL1 was added to the lower compartments. After 30 minutes of equilibration, isolated bone marrow neutrophils (2×10^5 cells per well) were added to the upper compartment and allowed to migrate for 1 h at 37 °C. Numbers of transmigrated cells were evaluated using Ly6G-Pacific blue and Flow-Count™ Fluorospheres with flow cytometry.

4.7.2 3D COLLAGEN MIGRATION

3D Chemotaxis was performed according to the manufacturer's instructions. Briefly, bone marrow neutrophils from WT and *Mst1^{-/-}* mice were isolated using a Percoll gradient and 3×10^5 cells were seeded together with Collagen I into a channel of Ibidi μ -Slides Chemotaxis^{3D}. After 5 min of incubation at 37 °C, the reservoirs were filled with either complete HBSS buffer alone or with CXCL1 (100 ng ml^{-1}) or fMLP (10 μM). Images were acquired every 14 sec for 30 min at 37 °C using an Axiovert 200M microscope. Images were analyzed using Fiji software.

4.8 STATISTICAL ANALYSES

All data were analyzed and plotted using Graph Pad Prism 6 Software. For pairwise comparison of experimental groups a paired t-test, unpaired t-test or Mann-Whitney test was performed. For multiple comparisons, a two way analysis of variance (ANOVA) was used with either Sidak's multiple comparisons test or Tukey's multiple comparisons test (comparison of all experimental groups against each other). A p-value < 0.05 was considered as statistically significant.

5 RESULTS

5.1 CHARACTERIZING NEUTROPHILS OF MST1 KNOCK OUT MICE

In the past, conflicting results on the expression of MST1 in mouse neutrophils were published (De Souza et al., 2002). Therefore, we first confirmed the expression of MST1 in neutrophils from wild type (WT) and the absence of MST1 in *Mst1*^{-/-} neutrophils (**Figure 5.1a**). In addition, the expression of MST2 was tested and no MST2 expression could be detected neither in WT nor *Mst1*^{-/-} neutrophils (**Figure 5.1b**). GAPDH served as a loading control.

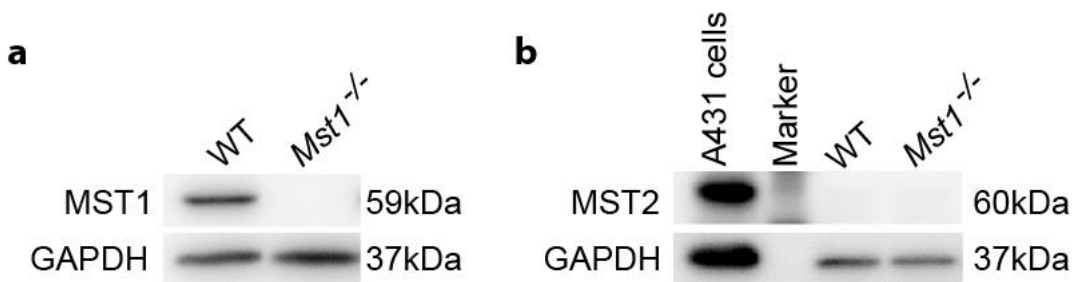


Figure 5.1 Protein levels of MST1 and MST2 in neutrophils

(a) MST1 and (b) MST2 protein levels are shown from neutrophils of WT and *Mst1*^{-/-} mice. GAPDH served as loading control. EGF-stimulated A431 cell lysate was used as control for MST2 expression (n=3).

Next, peripheral blood cell counts were determined and, as previously reported (Choi et al., 2009), a decreased number of lymphocytes found in *Mst1*^{-/-} mice compared to WT mice (**Figure 5.2**). Neutrophil counts were not significantly altered in *Mst1*^{-/-} mice (881 ± 204 neutrophils μl^{-1} , mean \pm SEM) compared to WT mice (669 ± 103 neutrophils μl^{-1} , mean \pm SEM).

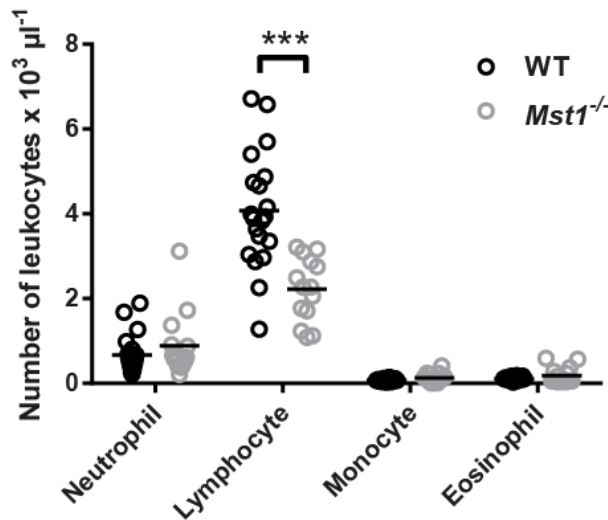


Figure 5.2 Differential blood counts of WT and *Mst1*^{-/-} mice
Differential blood counts of WT (black circles, n= 20) and *Mst1*^{-/-} mice (grey circles, n= 14) (scatter blots with mean, *** p < 0.001, 2way ANOVA, Sidak's multiple comparisons test).

5.1.1 VIABILITY AND APOPTOSIS OF WT AND *MST1*^{-/-} NEUTROPHILS

Numerous publications demonstrated that MST1 regulates apoptosis and proliferation in a cell type specific manner (Johnson and Halder, 2014). To determine whether MST1 has an effect on the survival of neutrophils, isolated bone marrow neutrophils of WT and *Mst1*^{-/-} mice were cultured for 0, 24, 48 and 72 h. Neutrophils were measured by flow cytometry using T-MRE and TO-PRO3 to determine viability and apoptosis, respectively. As illustrated in **Figure 5.3**, the absence of MST1 had no effect on the viability of murine neutrophils *in vitro*.

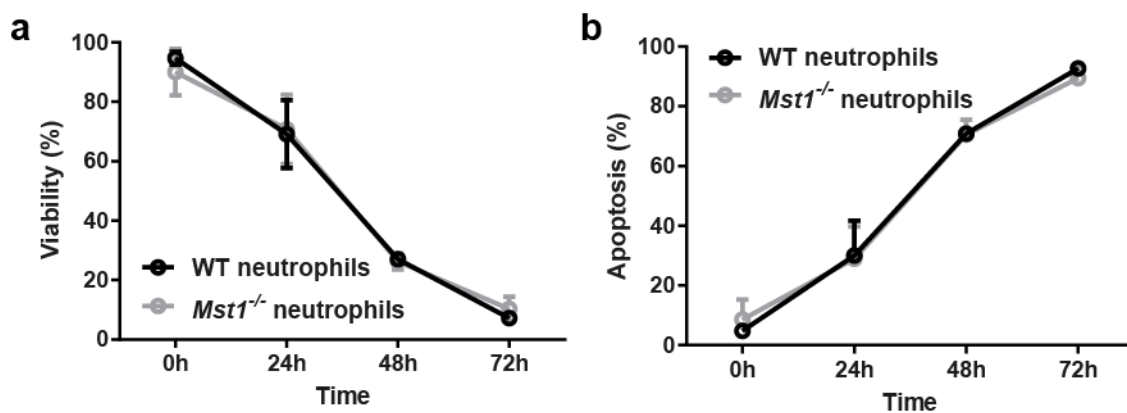


Figure 5.3 Viability and apoptosis of WT and *Mst1*^{-/-} neutrophils over time

Isolated neutrophils from WT (black circles) and *Mst1*^{-/-} mice (grey circles) were cultured for indicated times, stained with Ly6G, T-MRE and TO-PRO3 to quantify (a) viable (TO-PRO3⁻ T-MRE⁺) and (b) apoptotic neutrophils (TO-PRO3⁺ T-MRE⁻) (n=3, mean \pm SEM).

5.2 MST1 IS DISPENSABLE FOR NEUTROPHIL ROLLING AND ADHESION IN HUMANS AND MICE

Previous studies have shown that MST1 is crucial for T-cell adhesion *in vitro* (Katagiri et al., 2006) and *in vivo* (Katagiri et al., 2009) by regulating LFA-1 localization on the T-cell surface (Nishikimi et al., 2014). Therefore, we compared leukocyte rolling and adhesion properties *in vivo* and *in vitro* between WT and *Mst1*^{-/-} mice, both processes are affected by LFA-1 activity.

5.2.1 NEUTROPHIL ROLLING AND ADHESION IN *MST1*^{-/-} MICE IN VIVO

To test whether the absence of MST1 influences neutrophil recruitment *in vivo*, rolling and adhesive properties of neutrophils were compared in trauma and TNF- α stimulated cremaster muscle venules of WT and *Mst1*^{-/-} mice using conventional intravital microscopy.

Trauma induced cremaster muscle model

In this model mild trauma is caused by surgical preparation and exteriorization of the mouse cremaster muscle. Within minutes after exteriorization P-selectin is mobilized from Weibel-Palade bodies within the endothelial cell to the endothelial surface (Ley et al., 1995, Mayadas et al., 1993) leading to P-selectin dependent leukocyte rolling. The model the expression of E-selectin is absent or very low (Ley et al., 1995). Firm leukocyte adhesion is mostly mediated via LFA-1 and Mac-1 interacting with ICAM-1 and RAGE, respectively (Frommhold et al., 2010, Jung and Ley, 1997). Neutrophil rolling (**Figure 5.4a**), rolling velocity (**Figure 5.4b**) and neutrophil adhesion (**Figure 5.4c**) was comparable in trauma stimulated cremaster muscle venules between WT and *Mst1*^{-/-} mice.

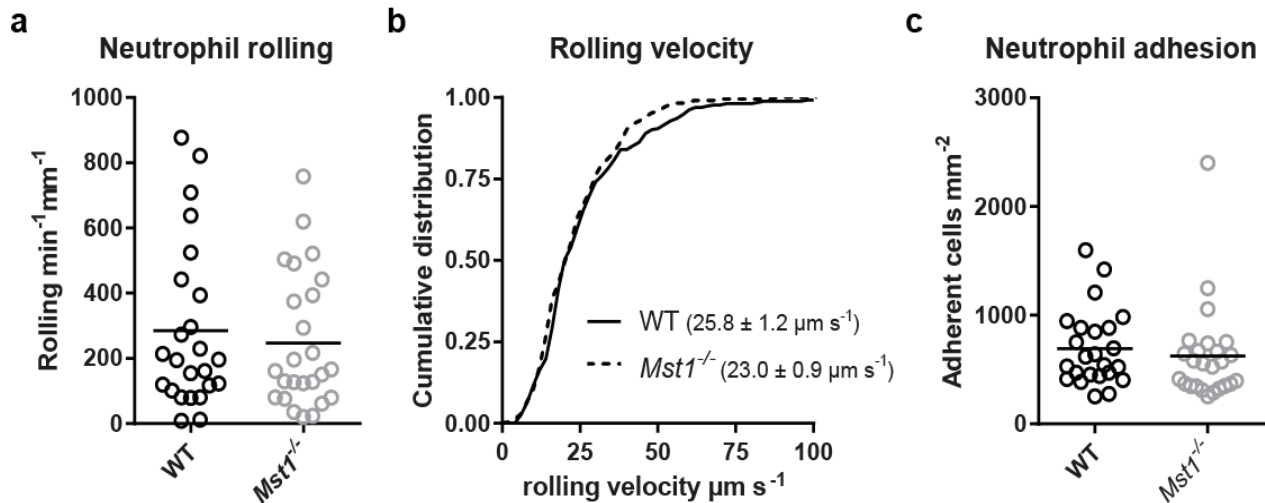


Figure 5.4 Neutrophil rolling and adhesion in the trauma stimulated cremaster muscles of WT and $Mst1^{-/-}$ mice

(a) Neutrophil rolling (rolling neutrophil $\text{min}^{-1} \text{mm}^{-1}$), (b) cumulative distribution of neutrophil rolling velocities and (c) neutrophil adhesion (adherent neutrophil mm^{-2}) in cremaster muscle venules was compared between WT (black circles) and $Mst1^{-/-}$ mice (grey circles) 20 to 40 min after trauma induction (n = 5, scatter blots with mean, n.s., unpaired t-test).

Table 5.1 Hemodynamic and microvascular parameters of postcapillary venules in trauma induced inflammation

Mouse genotype	Mice [n]	Venules [n]	\emptyset [μm]	Blood flow [$\mu\text{m s}^{-1}$]	Shear rate [s^{-1}]	Syst. count [cells μl^{-1}]
WT	5	24	34 ± 2	2100 ± 360	1590 ± 290	6170 ± 690
$Mst1^{-/-}$	5	25	33 ± 2	2640 ± 540	1850 ± 350	3400 ± 260

Next, LFA-1 dependent neutrophil adhesion was investigated by intravenous (i.v.) injection of CXCL1, which in turn activates LFA-1 via integrin inside-out signaling, leading to the arrest of neutrophils (Smith et al., 2004, Frommhold et al., 2008). To do this, one vessel was recorded before and 1 min after i.v. injection of 600 ng CXCL1. Neutrophil rolling (**Figure 5.5a**) and neutrophil adhesion (**Figure 5.5b**) before and after CXCL1 injection was compared between WT and $Mst1^{-/-}$ mice. The reduction in neutrophil rolling and the increase in neutrophil adhesion due to LFA-1 activation after CXCL1 injection was similar in WT and $Mst1^{-/-}$ mice.

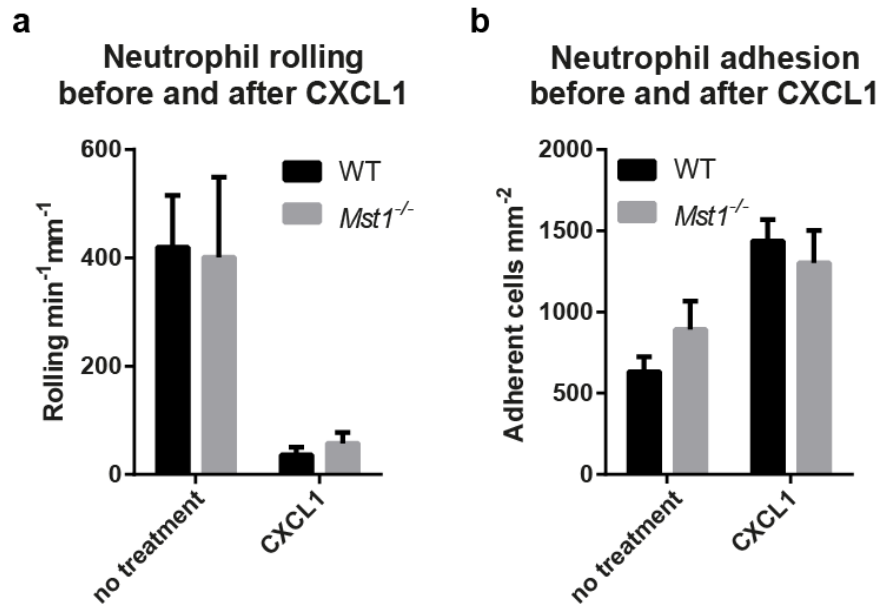


Figure 5.5 Neutrophil rolling and adhesion before and after CXCL1 injection

(a) Neutrophil rolling (rolling neutrophil min⁻¹ mm⁻¹) and **(b)** neutrophil adhesion before and after i.v. injection of 600ng CXCL1 in WT (black bars) and *Mst1*^{-/-} mice (grey bars) (n = 5, mean ± SEM, * p < 0.05, 2way ANOVA, Sidak's multiple comparisons test).

Table 5.2 Hemodynamic and microvascular parameters of postcapillary venules before and after CXCL1 injection

	Mice [n]	Venules [n]	Ø [µm]	Blood flow [µm s ⁻¹]	Shear rate [s ⁻¹]	Syst. count [cells µl ⁻¹]
WT						
untreated	5	5	44±6	2040±510	1090±150	6170±690
CXCL1	5	5	44±6	2180±570	1230±290	
<i>Mst1</i>^{-/-}						
untreated	4	4	40±2	2130±610	1360±460	3420±340
CXCL1	4	4	40±2	2280±610	1210±250	

TNF- α stimulated cremaster muscle model

Next, the TNF- α stimulated cremaster muscle model was used as a model of strong inflammation. TNF- α treatment leads to the expression of P- and E- selectin on the surface of the venular endothelium (Jung and Ley, 1997). This coincides with the induction of slow neutrophil rolling in these microvessels. The expression of ICAM-1 and VCAM-1 is increased, which corresponds to a high number of adherent neutrophils and neutrophil extravasation. No difference could be observed in rolling flux fraction (**Figure 5.6a**), rolling velocity (**Figure 5.6b**) or neutrophil adhesion efficiency between WT and *Mst1*^{-/-} mice (**Figure 5.6c**).

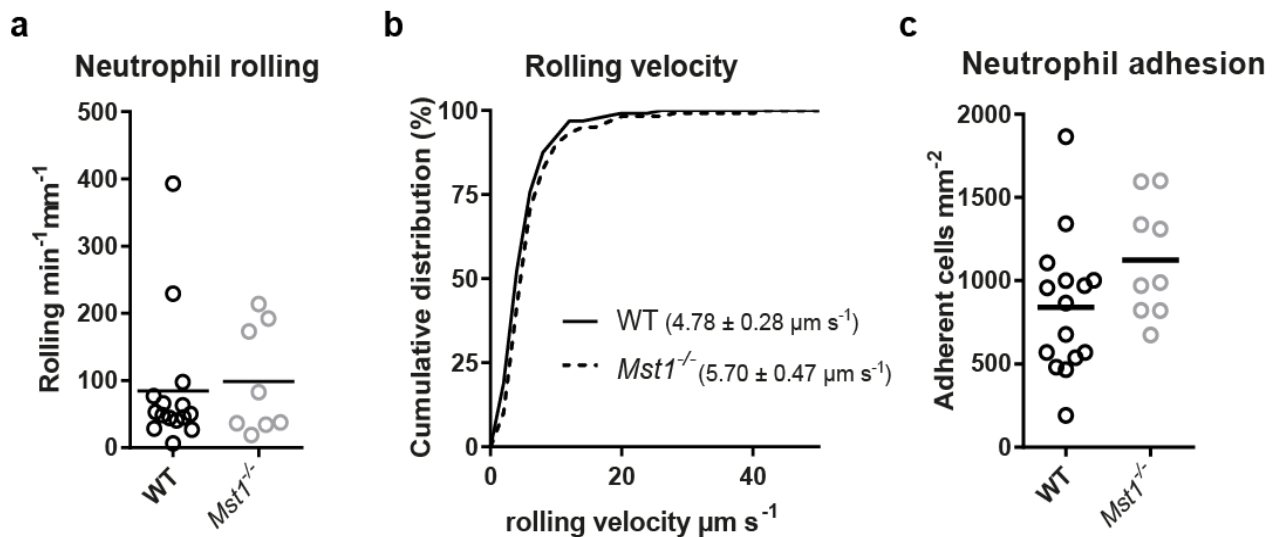


Figure 5.6 Neutrophil rolling and adhesion in the TNF- α induced cremaster muscle model in WT and *Mst1*^{-/-} mice

(a) Neutrophil rolling (rolling neutrophils $\text{min}^{-1} \text{mm}^{-1}$) (b) cumulative distribution of neutrophil rolling velocities and (c) neutrophil adhesion (adherent neutrophils mm^{-2}) in cremaster muscle venules was compared between WT and *Mst1*^{-/-} mice, 2 h after i.s. injection of TNF- α ($n = 5$, scatter blots with mean, n.s., unpaired t-test).

Table 5.3 Hemodynamic and microvascular parameters of postcapillary venules in TNF- α induced inflammation

Mouse genotype	Mice [n]	Venules [n]	\emptyset [μm]	Blood flow [$\mu\text{m s}^{-1}$]	Shear rate [s^{-1}]	Syst. count [cells μl^{-1}]
WT	5	15	32 ± 1	1800 ± 240	1420 ± 200	1240 ± 360
<i>Mst1</i> ^{-/-}	5	9	30 ± 2	2540 ± 360	2300 ± 420	1490 ± 430

5.2.2 NEUTROPHIL ADHESION UNDER FLOW CONDITIONS

To verify the *in vivo* results described above, neutrophil adhesion was investigated under flow conditions *ex vivo* and under static conditions *in vitro*.

In *ex vivo* flow chamber assays, glass capillaries were coated with a combination of E-selectin, ICAM-1 and CXCL1. In flow chambers coated with E-selectin alone or E-selectin/ ICAM-1, a small number of leukocytes became adherent, while coating with E-selectin/ ICAM-1/ CXCL1 induced integrin activation and increased the number of adherent cells FOV⁻¹. For all groups, neutrophil adhesion was similar between WT and *Mst1*^{-/-} mice (**Figure 5.7**).

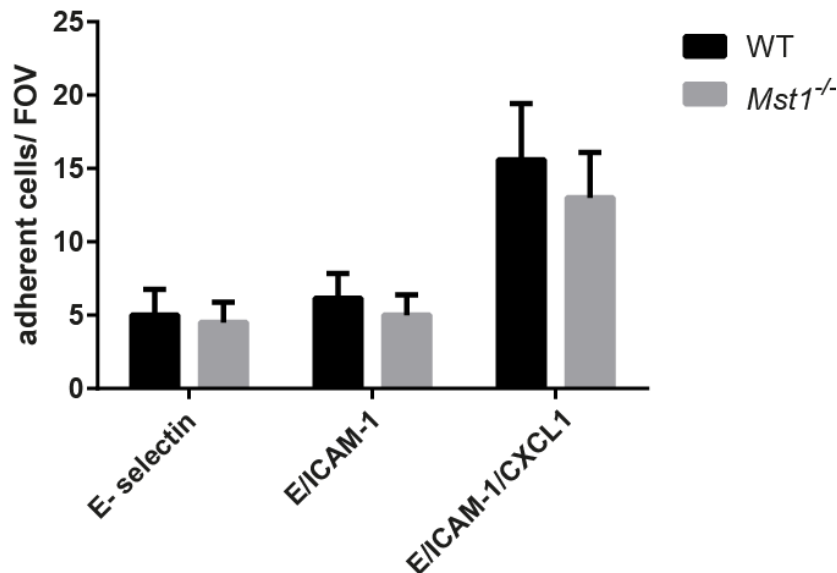


Figure 5.7 Neutrophil adhesion of WT and *Mst1*^{-/-} mice in an *ex vivo* flow chamber

Whole mouse blood from WT or *Mst1*^{-/-} mice was perfused through micro flow chambers coated with E-selectin (E), E/ ICAM-1 or E/ ICAM-1/ CXCL1 and the number of adherent neutrophils per field of view (FOV) assessed (n = 3, mean ± SEM, n.s., 2way ANOVA, Sidak's multiple comparisons test).

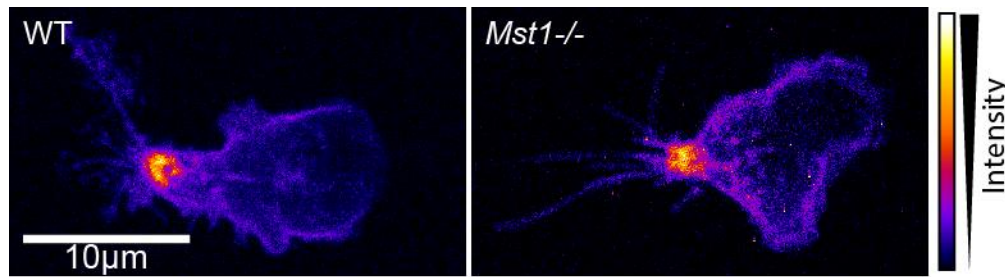


Figure 5.8 LFA-1 clustering in neutrophils under flow conditions

Whole mouse blood from WT or *Mst1*^{-/-} mice labeled with anti LFA-1 antibody (fluorescence intensity scale) was perfused through micro flow chambers coated with E-selectin, ICAM-1 and CXCL1. (n= 3 mice, one representative picture is shown)

To further elucidate, whether MST1 deficiency affected LFA-1 clustering of neutrophils during adhesion in flow chambers, LFA-1 localization was compared in WT and *Mst1*^{-/-} neutrophils. Whole blood was collected and incubated with a non-blocking anti-LFA-1 antibody (clone 2D7) conjugated with Alexa Fluor® 546. Whole blood was perfused through E-selectin/ ICAM-1/ CXCL1 coated glass capillaries. Neutrophils adhering to the coated surfaces were recorded using confocal microscopy. Both, WT as well as *Mst1*^{-/-} neutrophils displayed similar LFA-1 localization under flow, resulting in accumulation of LFA-1 at the uropod of neutrophils (**Figure 5.8**).

5.2.3 SURFACE EXPRESSION AND FUNCTION

The surface expression of the alpha subunit of LFA-1 (CD11a, αL), the alpha subunit of Mac-1 (CD11b, αM), CXCR2, CD44, PSGL1 and L-selectin (CD62L) was investigated, to exclude any effects resulting from differences in the expression levels of those adhesion relevant molecules. Analyzing neutrophils, derived from blood and bone marrow, from WT and *Mst1*^{-/-} mice no difference was found in expression levels of LFA-1, Mac-1, CXCR2, CD44, PSGL-1 and CD62L (**Figure 5.9**).

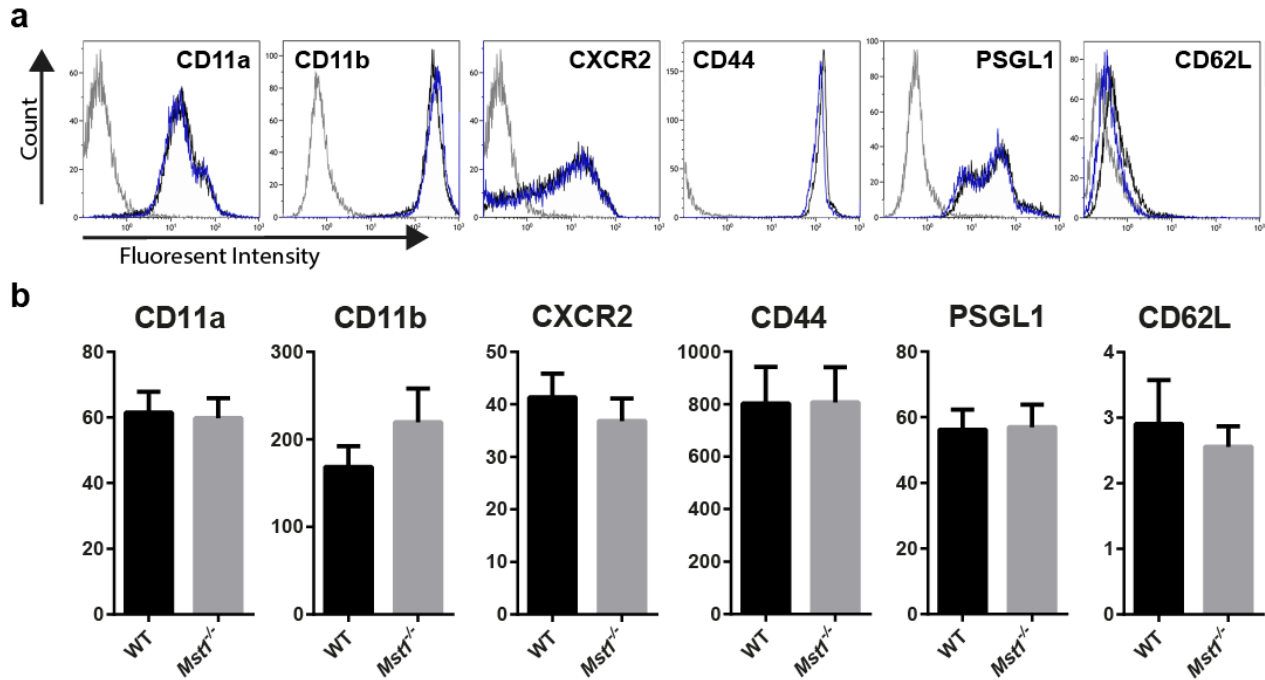


Figure 5.9 Surface expression of adhesion relevant molecules on WT and *Mst1*^{-/-} neutrophils
(a) Representative histograms showing expression of isotype control (grey), WT neutrophils (black) and *Mst1*^{-/-} neutrophils (blue), respectively. **(b)** Mean fluorescence intensity (MFI) ratio (relative to isotype control) of CD11a, CD11b, CXCR2, CD44, PSGL1, CD62L on WT (black) and *Mst1*^{-/-} neutrophils (grey) (n=3, mean ± SEM, p<0.01, unpaired t-test).

E- and P-selectin binding to neutrophils

To investigate the binding capacity of selectins to selectin ligands on neutrophils derived from WT and *Mst1*^{-/-} mice, the binding of soluble selectin chimera was compared between WT and *Mst1*^{-/-} neutrophils. E- or P-selectin hFc-chimeric proteins were incubated with whole blood from WT and *Mst1*^{-/-} mice, with or without EDTA (negative control). The binding of E- or P-selectins were analyzed using flow cytometry. Both, neutrophils from WT and *Mst1*^{-/-} mice, bound E-selectin and P-selectin to the same extent (**Figure 5.10**).

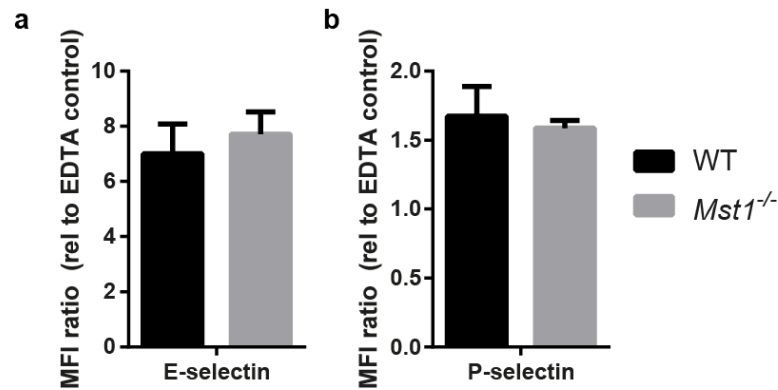


Figure 5.10 E-selectin and P-selectin binding to WT and *Mst1*^{-/-} neutrophils

FACS analysis of (a) E-selectin IgG chimera binding or (b) P-selectin IgG chimera binding, performed with WT (black) or *Mst1*^{-/-} (grey) neutrophils (n=3, n.s., unpaired t-test).

Soluble ICAM-1 binding to neutrophils

Next, the capacity of neutrophils to bind ICAM-1, which is dependent on the integrin activation status of LFA-1, was investigated. To do this, bone marrow derived neutrophils were isolated from WT and *Mst1*^{-/-} mice, unstimulated or stimulated with CXCL1. The capacity of WT or *Mst1*^{-/-} neutrophils to bind soluble ICAM-1 was analyzed using flow cytometry. No difference could be observed in CXCL1-dependent LFA-1 activation between WT and *Mst1*^{-/-} neutrophils (**Figure 5.11a** and **Figure 5.11b**).

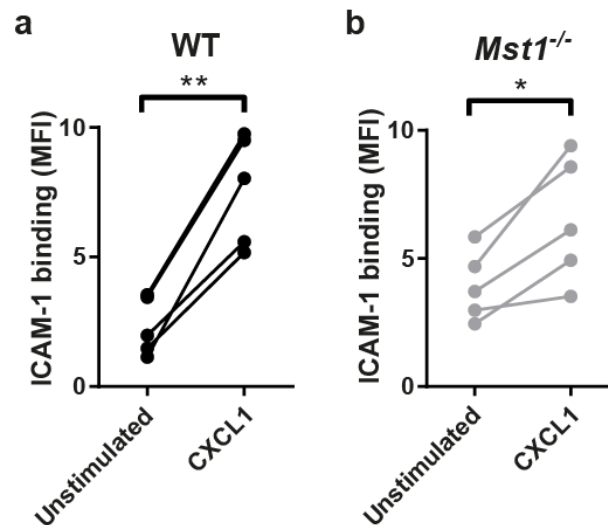


Figure 5.11 CXCL1 dependent ICAM-1 binding to WT or *Mst1*^{-/-} neutrophils

FACS analysis of ICAM-1 binding, with or without CXCL1 stimulation, to (a) WT (black) or (b) *Mst1*^{-/-} (grey) neutrophils (n=5, * p < 0.05, ** p < 0.01 paired t-test).

5.2.4 NEUTROPHIL ADHESION IN PATIENTS WITH *STK4* DEFICIENCY

We had the rare opportunity to investigate the adhesive properties of neutrophils from two patients with *STK4* deficiency and their heterozygote parents (Abdollahpour et al., 2012). These experiments were realized in cooperation with Dr. Claudia Nussbaum and Prof.Dr. Christoph Klein (LMU, München). Human neutrophils were isolated from whole blood. Glass capillaries coated with a combination of E-selectin/ ICAM-1/ IL-8, were then perfused with the isolated neutrophils. The number of adherent leukocytes FOV⁻¹ of *STK4*^{-/-} patients and their heterozygous (*STK4*^{+/-}) parents increased to a similar extent with increased perfusion time (**Figure 5.12**).

Altogether, these *in vitro* and *in vivo* results demonstrate that, in contrast to T cells, MST1 is dispensable for LFA-1 activation and clustering in neutrophils. Hence, neutrophil adhesion is unaffected in *Mst1*^{-/-} mice as well as in patients with *STK4* deficiency.

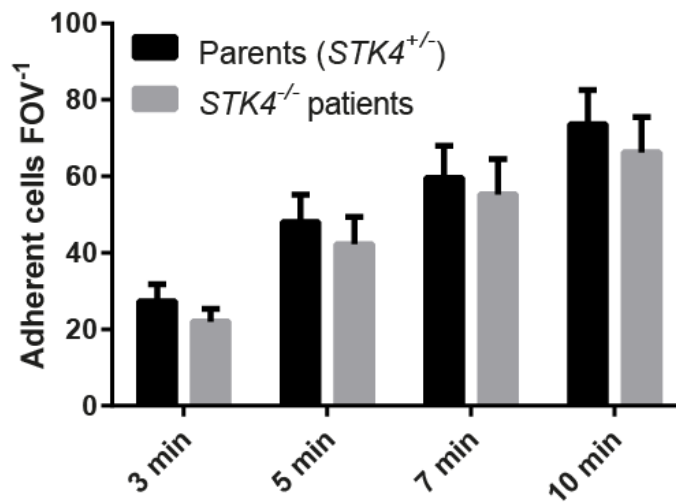


Figure 5.12 MST1 is dispensable for neutrophil adhesion in humans

Number of adherent cells FOV⁻¹ from two patients with *STK4* deficiency and their heterozygous parents was assessed over time in flow chambers coated with E-selectin/ ICAM-1/ CXCL8. (n=2 per group, chambers ≥ 2 per group, mean ± SEM)

5.3 MST1 IS CRITICAL FOR NEUTROPHIL EXTRAVASATION *IN VIVO*

Hence, the last step of the neutrophil adhesion cascade consisting in transmigration through the venular wall and extravasation into the interstitial space was investigated to elucidate the role of MST1 in this process.

5.3.1 TNF- α INDUCED NEUTROPHIL EXTRAVASATION INTO THE PERITONEAL CAVITY

The number of extravasated neutrophils in the TNF- α induced peritonitis model was evaluated. In WT mice, i.p. injection of 1 μ g TNF- α dramatically increased the number of neutrophils in the peritoneum as compared to NaCl control injection. In contrast, neutrophils from *Mst1*^{-/-} mice failed to transmigrate into the peritoneal cavity 2 h after TNF- α stimulation (**Figure 5.13**).

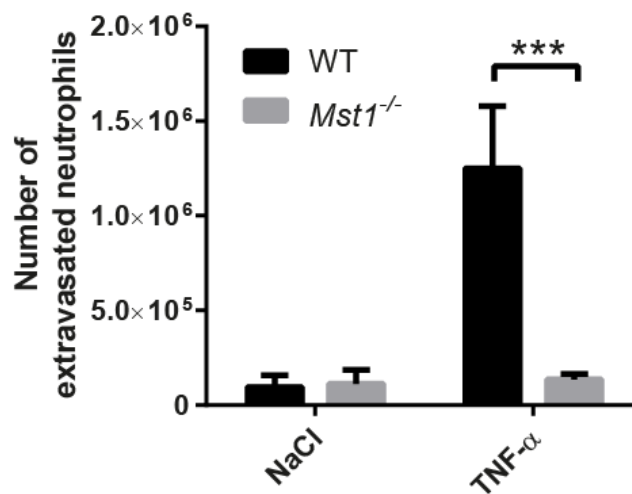


Figure 5.13 TNF- α induced peritonitis in WT and *Mst1*^{-/-} mice

Total number of extravasated neutrophils in the peritoneal lavage was quantified 2 h after i.p. injection of NaCl or 1 μ g TNF- α (n=3, mean \pm SEM, * p < 0.05, 2way ANOVA, Sidak's multiple comparisons test).

5.3.2 NEUTROPHIL EXTRAVASATION STUDIED BY MULTI-PHOTON LASER SCANNING MICROSCOPY

To accurately investigate the exact role of MST1 in neutrophil extravasation *in vivo*, multi-photon laser scanning microscopy of the mouse cremaster muscle was used. To do this, *Lyz2^{GFP}* mice (Faust et al., 2000), in which neutrophils are endogenously labeled with EGFP, were crossed with *Mst1^{-/-}* mice, to generate *Mst1^{-/-} x Lyz2^{GFP}* mice. As in WT and *Mst1^{-/-}* mice (**Figure 5.2**), the number of peripheral lymphocytes was decreased in *Mst1^{-/-} x Lyz2^{GFP}* mice compared with *Lyz2^{GFP}* mice. Neutrophil counts (**Figure 5.14a**) as well as the proportion of EGFP⁺ neutrophils and monocytes (**Figure 5.14b**) were similar between *Lyz2^{GFP}* and *Mst1^{-/-} x Lyz2^{GFP}* mice.

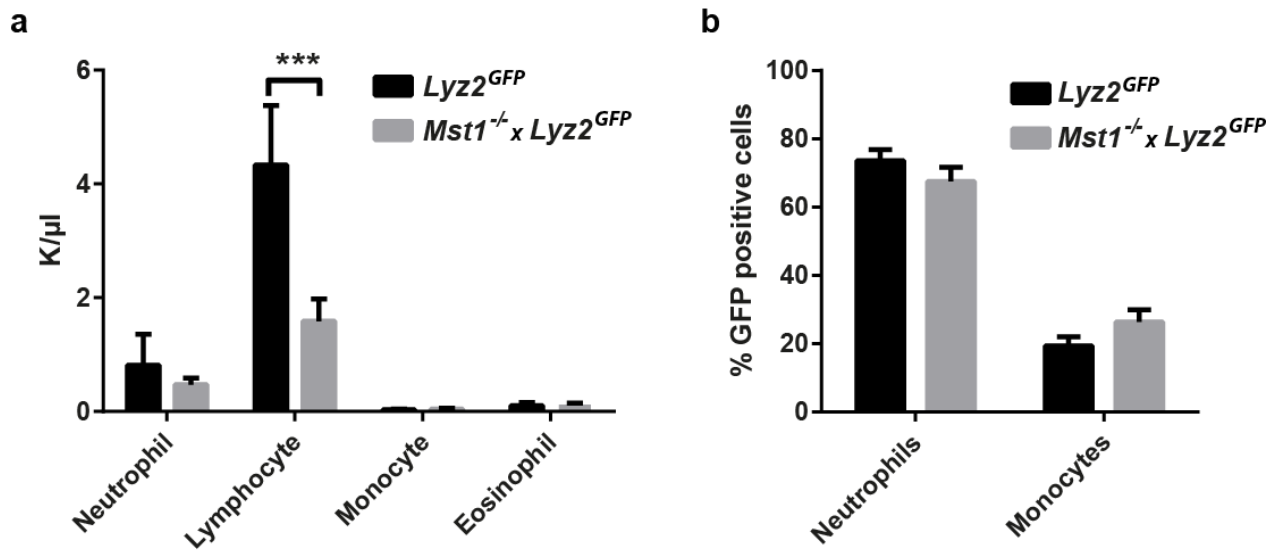


Figure 5.14 Differential blood count from *Lyz2^{GFP}* and *Mst1^{-/-} x Lyz2^{GFP}* mice

Differential blood counts of *Lyz2^{GFP}* (black, n= 5) and *Mst1^{-/-} x Lyz2^{GFP}* mice (grey, n= 4) (mean ± SEM, *** p < 0.001, 2way ANOVA, Sidak's multiple comparisons test). K = 1000

To visualize neutrophil extravasation, TNF-α was injected into the scrotum of *Lyz2^{GFP}* and *Mst1^{-/-} x Lyz2^{GFP}* mice together with a non-blocking antibody against PECAM-1 (clone 390) conjugated with Alexa Fluor 546 to label endothelial cell junctions (Woodfin et al., 2011). Neutrophil crawling and transmigration was investigated between 180 and 240 min after TNF-α injection.

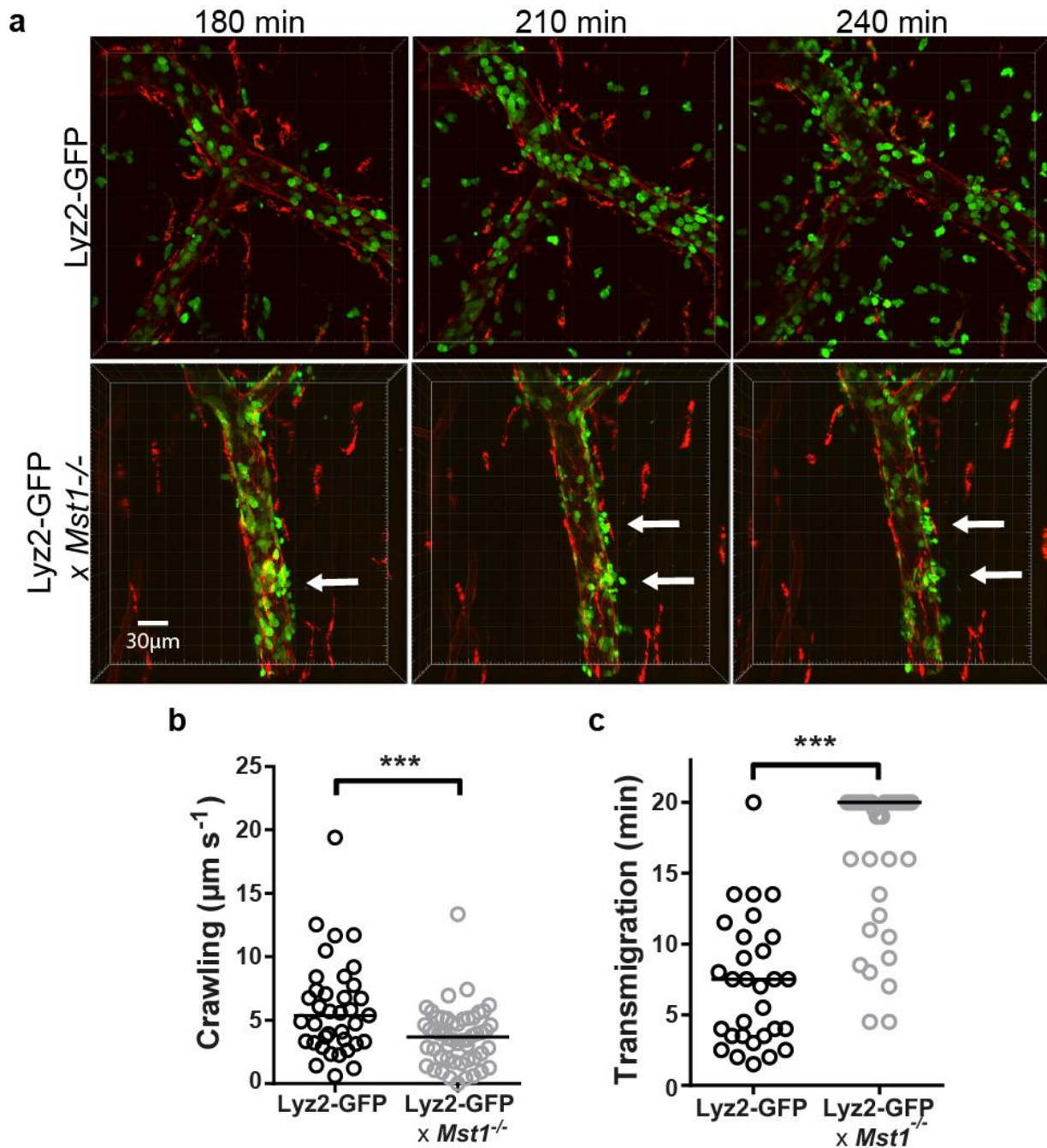


Figure 5.15 *Mst1*^{-/-} neutrophils fail to transmigrate into inflamed tissue

Neutrophils (green) and the microvasculature (PECAM-1, red) of TNF- α stimulated mouse cremaster muscle. **(a)** Neutrophil transmigration in Lyz2^{GFP} and the accumulation of neutrophils in Lyz2^{GFP} x *Mst1*^{-/-} mice (with arrow) at 180 min, 210 min and 240 min after i.s. injection of TNF- α . Images were obtained using intravital multi photon microscopy (n = 3). **(b)** Intravascular crawling velocity of neutrophils in Lyz2^{GFP} and Lyz2^{GFP} x *Mst1*^{-/-} mice (n = 3 mice, scatter blot with median of > 30 analyzed cells per group, *** p < 0.001, unpaired t test). **(c)** Transmigration time of Lyz2^{GFP} and Lyz2^{GFP} x *Mst1*^{-/-} neutrophils. Cut off was set at 20 min (n = 3 mice, scatter blot with median of > 30 analyzed transmigration events per group, *** p < 0.001, Mann Whitney test).

During the time of observation, an increasing number of GFP⁺ neutrophils crossed the venule and migrated into the inflamed tissue in *Lyz2^{GFP}* mice (**Figure 5.15a**, upper panel). In contrast, most neutrophils in *Mst1^{-/-}* x *Lyz2^{GFP}* mice remained closely associated with the abluminal side of the vessel (**Figure 5.15a**, lower panel, white arrow) and were unable to migrate further into the inflamed tissue. In addition, intravascular crawling velocity of neutrophils was reduced in *Mst1^{-/-}* x *Lyz2^{GFP}* mice compared to *Lyz2^{GFP}* mice (**Figure 5.15b**). Furthermore, neutrophil transmigration of postcapillary venules in *Lyz2^{GFP}* mice required 7.5 ± 0.8 min (median \pm SEM), which was similar to the time reported by others (Woodfin et al., 2011). In contrast, most neutrophils in *Mst1^{-/-}* x *Lyz2^{GFP}* mice failed to transmigrate from the vessels within a 20 min observation period (20 ± 0.8 min, median \pm SEM) (**Figure 5.15c**). Instead, *Mst1^{-/-}* x *Lyz2^{GFP}* neutrophils accumulated at the abluminal side of postcapillary venules where they remained for the whole time of observation (**Figure 5.16**, lower panel, white circle).

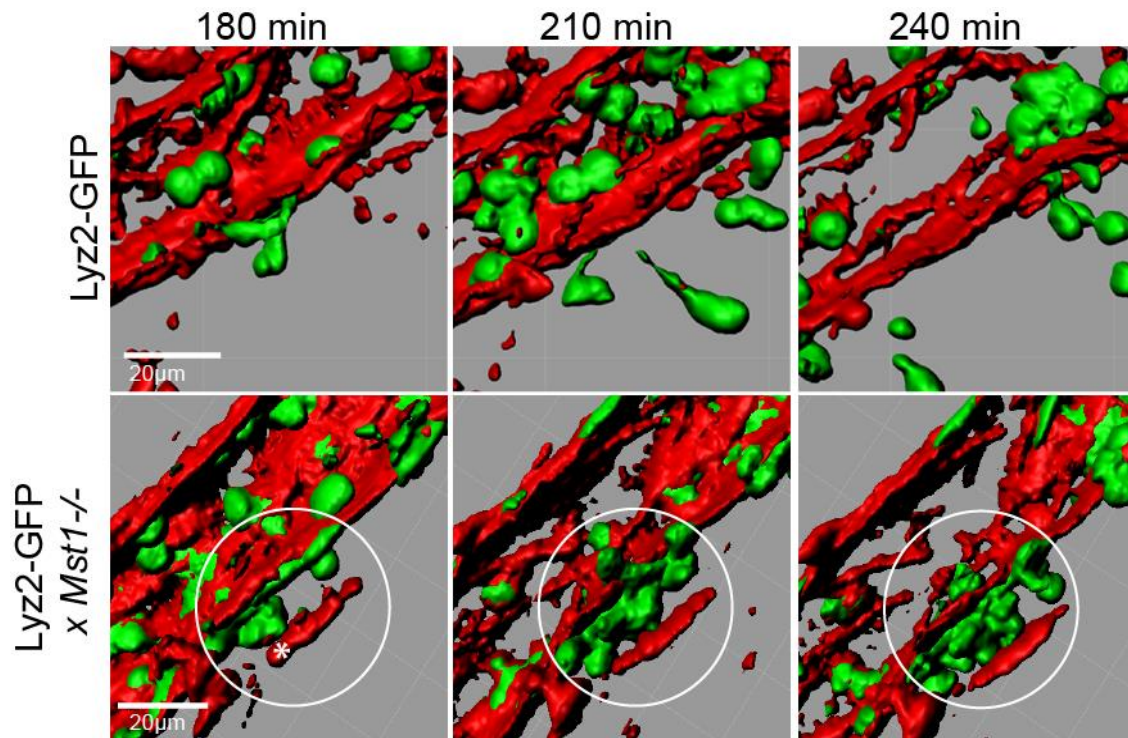


Figure 5.16 3D reconstruction of neutrophil transmigration in WT and *Mst1^{-/-}* mice

Lyz2^{GFP} neutrophils transmigrating from postcapillary venules (upper panel) and the accumulation of neutrophils in *Mst1^{-/-}* x *Lyz2^{GFP}* mice (white circle). * indicates nonspecific labeling of extravascular cells (Woodfin et al., 2011).

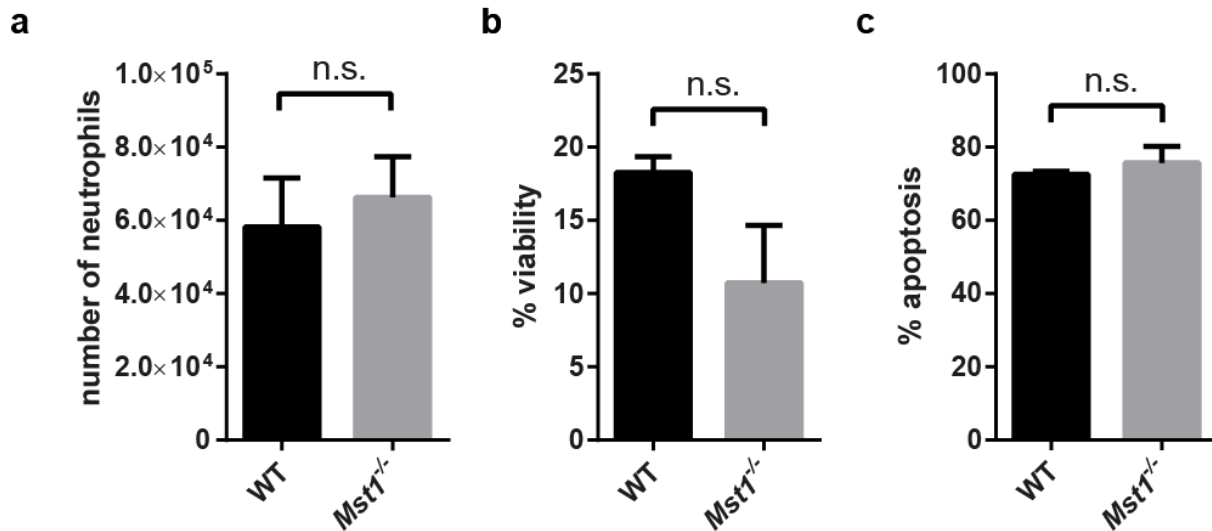


Figure 5.17 Number and viability of neutrophils within the cremaster muscle

(a) Total number of neutrophils, (b) viability (TO-PRO3⁺ T-MRE⁺) and (c) apoptosis rate (TO-PRO3⁺ T-MRE⁻) of neutrophils within the whole cremaster muscle of WT and *Mst1*^{-/-} mice 2 h after TNF-α injection (n = 5, paired t test).

Interestingly, the total number of neutrophils within the cremaster muscle was similar between WT and *Mst1*^{-/-} mice, 2 h after TNF-α injection (**Figure 5.17a**). Furthermore the viability (**Figure 5.17b**) and apoptosis rate of isolated neutrophils (**Figure 5.17c**) was similar between WT and *Mst1*^{-/-} mice.

5.3.3 LASER INJURY INDUCED NEUTROPHIL SWARMING

To test, whether further stimulation could induce migration into the interstitial space, a laser injury near postcapillary venules was induced 3 h after TNF-α stimulation. Neutrophils of Lyz2^{GFP} mice swarmed and accumulated at the site of laser injury within 30 min, as described by Lämmermann et al. (Lämmermann et al., 2013). Interestingly, neutrophils deficient in MST1 remained at the abluminal site of venules and were unable to migrate to the site of laser injury (**Figure 5.18a**), suggesting that they could not overcome the vessel wall. The green fluorescence intensity at the site of laser injury (white square) was measured over time, as a read out for the accumulation of EGFP⁺ neutrophils. In Lyz2^{GFP} mice a continuous increase of green fluorescence intensity could be observed over time, which was completely absent in *Mst1*^{-/-} x Lyz2^{GFP} mice (**Figure 5.18b**).

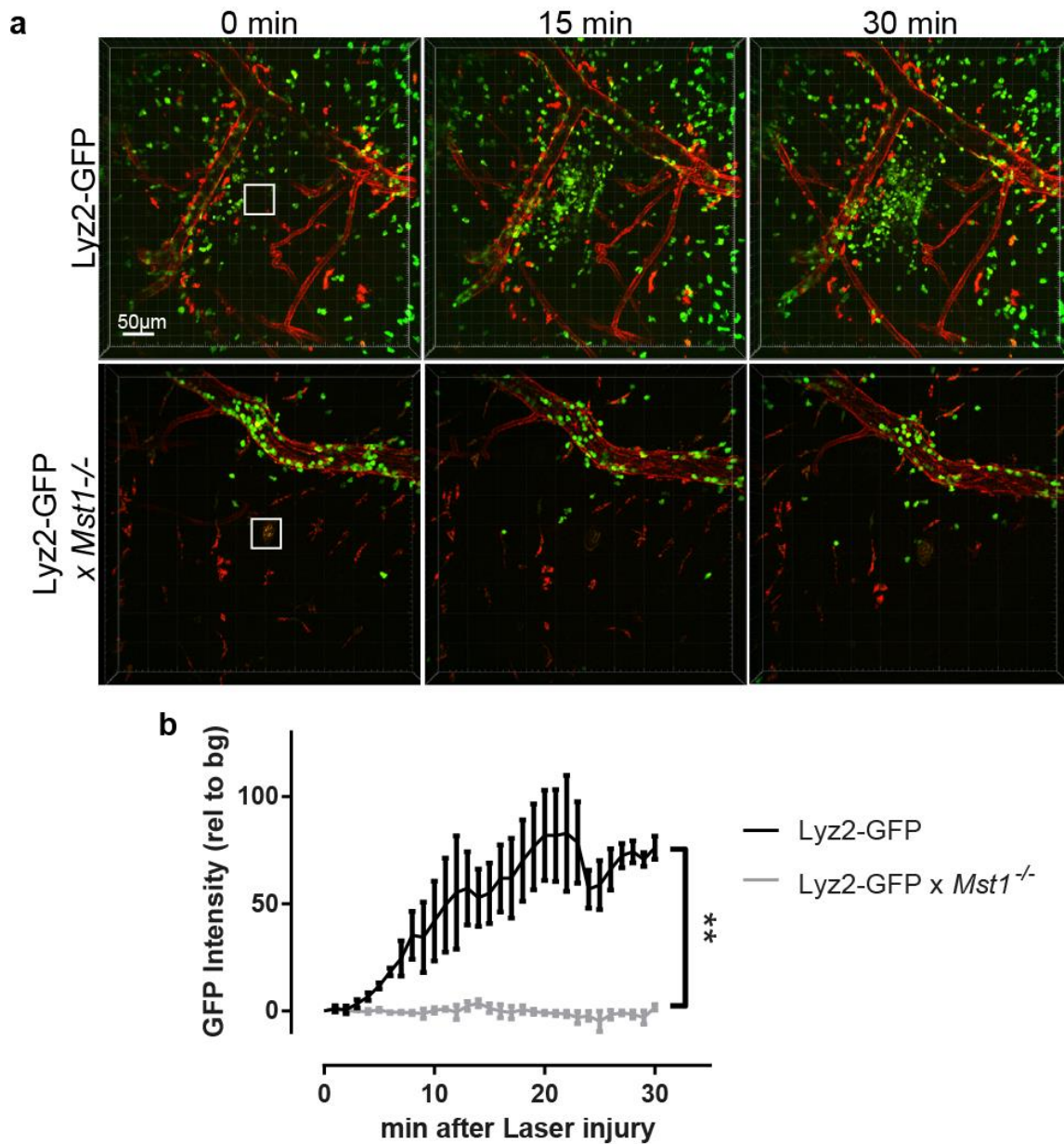


Figure 5.18 Laser induced injury in the mouse cremaster muscle

(a) Representative images of swarming neutrophils (green) and the microvasculature (PECAM-1, red) in the mouse cremaster muscle of Lyz2^{GFP} and Lyz2^{GFP} x *Mst1*^{-/-} mice after induction of a laser injury (white square). (b) Intensity profile of the GFP signal in Lyz2^{GFP} and Lyz2^{GFP} x *Mst1*^{-/-} mice at the site of laser injury (n=3, mean ± SEM, p<0.05 after 12 min, ** p<0.01, 2way ANOVA, Sidak's multiple comparisons test).

To exclude migration defects within the interstitial matrix, a process which can occur in an integrin independent fashion (Wolf et al., 2009, Lammermann et al., 2008), migration in 3D collagen gels (integrin independent migration assay) was compared between WT and *Mst1*^{-/-} neutrophils in cooperation with Babara Walzog. The absence of MST1 did not affect migration in 3D collagen gels (see **Appendix/ Manuscript/ Supplemental Figure 2**).

Furthermore, the phagocytic capacity within the first 15 min of WT and *Mst1*^{-/-} neutrophils was similar (**Figure 5.19**), although others showed impaired phagocytosis of conditional *Mst1*^{-/-} *Mst2*^{-/-} double knockout neutrophils after 50min of injection (Geng et al., 2015).

Taken together, these results suggest that neutrophils from *Mst1*^{-/-} mice fail to completely extravasate from postcapillary venules, but are functionally capable of migrating in the interstitial matrix and phagocytosing pathogens.

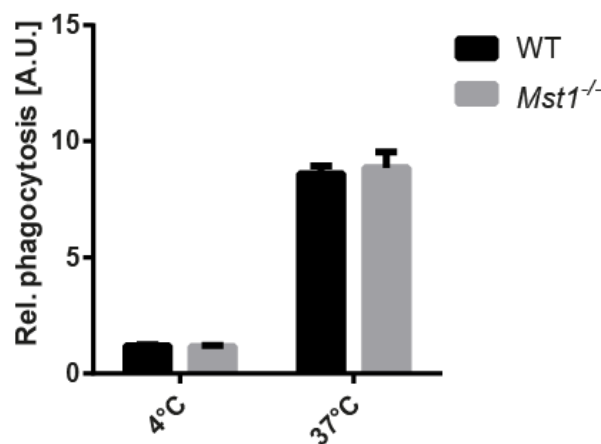


Figure 5.19 Phagocytic capacity of WT and *Mst1*^{-/-} neutrophils

Flow cytometry of WT and *Mst1*^{-/-} neutrophils infected with pHrodo™ *E.coli* BioParticles for 15 min at 4°C (no phagocytosis) and 37°C (n= 3 mice, mean ± SEM, n.s., 2way ANOVA, Sidak's multiple comparisons test).

5.3.4 NEUTROPHIL PENETRATION THROUGH THE VENULAR BASEMENT MEMBRANE

To better define at which step during transmigration neutrophils from *Mst1*^{-/-} mice were inhibited, we cooperated with Dietmar Vestweber to investigate the capacity of neutrophils to migrate through the endothelium and penetrate the perivascular basement membrane (BM) in more detail. Using confocal microscopy of TNF- α stimulated cremaster muscles whole mount, we discovered that neutrophils of *Mst1*^{-/-} mice accumulated between the endothelium and the BM, compared to WT mice (Bixel et al., 2010) (**see Appendix/ Manuscript/ Figure 4A-C**).

To verify these results *in vitro*, transmigration assays using CXCL1 as a chemoattractant were performed. First, transwell filters were coated with BSA (control), laminin, a key component of the BM (Yousif et al., 2013), or laminin combination with PECAM-1 and ICAM-1. Laminin alone did not allow transmigration of unstimulated WT or *Mst1*^{-/-} neutrophils. The number of transmigrated WT or *Mst1*^{-/-} neutrophils through laminin-coated filters in response to CXCL1 increased and was comparable to transmigration through BSA-coated filters in the absence of a chemoattractant.

However, additional coating with PECAM-1 and ICAM-1 of laminin coated filters efficiently induced neutrophil transmigration along a CXCL1 gradient in WT neutrophils (**Figure 5.20a**). These findings are in line with previously published data (Wang et al., 2005). Conversely the number of transmigrated *Mst1*^{-/-} neutrophils did not increase when laminin coated filters were additionally coated with PECAM-1 and ICAM-1 (**Figure 5.20a**).

In line with this finding, *Mst1*^{-/-} neutrophils failed to transmigrate as efficiently as WT neutrophils in response to CXCL1 through filters containing a monolayer of mouse endothelial 1G11 cells, which forms its own extracellular matrix (**Figure 5.20b**). Importantly, we did not find differences in transmigrated WT and *Mst1*^{-/-} neutrophils in transwell assays without coating (**Figure 5.20c**).

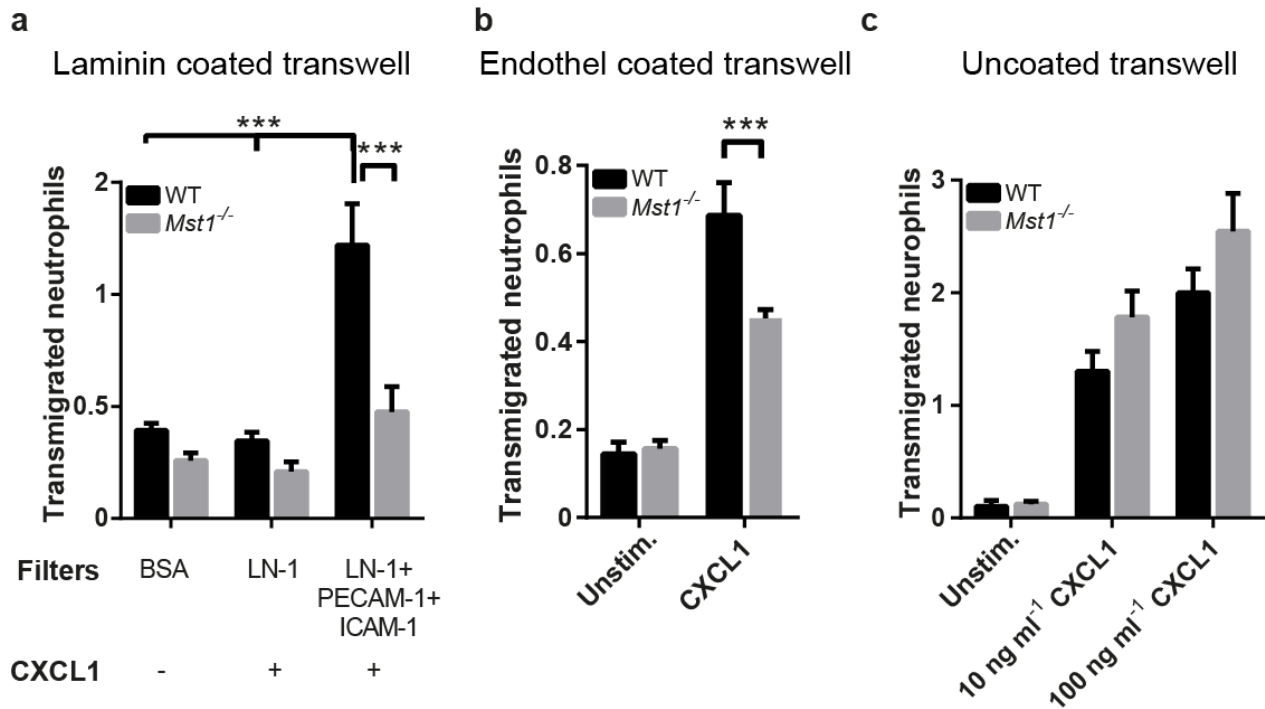


Figure 5.20 *Mst1*^{-/-} neutrophils show reduced pretration of laminin or endothelial cell coated, but not uncoated transwells

Transmigration of neutrophils in transwell assays **(a)** with or without CXCL1 stimulation through BSA (control), laminin-1 (LN-1) and LN-1, PECAM-1 and ICAM-1 coated filters (n= 3 mice, mean \pm SEM, *** p < 0.001, ** p < 0.01, 2way ANOVA, Sidak's multiple comparisons test), **(b)** with or without CXCL1 stimulation through an endothelial monolayer of 1G11 cells (n= 3 mice, mean \pm SEM, *** p < 0.001, 2way ANOVA, Sidak's multiple comparisons test), **(c)** to HBSS, 10ng ml⁻¹ and 100ng ml⁻¹ CXCL1 (n= 3 mice, mean \pm SEM., 2way ANOVA, Sidak's multiple comparisons test).

These results demonstrate that MST1 is essential for neutrophils to penetrate the BM *in vivo* and *in vitro*.

5.4 MST1 REGULATES VESICLE TRAFFICKING IN NEUTROPHILS

5.4.1 MST1 INDUCED TRANSLOCATION OF VLA-3, VLA-6 AND NE TO THE CELL SURFACE

It was shown previously, that the mobilization of VLA-3 (CD49c, $\alpha 3\beta 1$ integrin), VLA-6 (CD49f, $\alpha 6\beta 1$ integrin) and NE (neutrophil elastase) from intracellular stores to the plasma membrane is a crucial step for successful neutrophil transmigration (Hyun et al., 2012, Lerman et al., 2014, Wang et al., 2005). In addition, it was reported that MST1 regulates vesicle trafficking in T cells (Nishikimi et al., 2014). In order to evaluate the putative role of MST1 in the mobilization of VLA-3, VLA-6 and NE, neutrophils from WT or *Mst1*^{-/-} mice were seeded on slides coated with BSA or PECAM-1/ ICAM-1/ CXCL1. After 30 min, cells were fixed, permeabilized and immunostained with antibodies against VLA-3, VLA-6 or NE. By means of confocal microscopy WT as well as *Mst1*^{-/-} neutrophils seeded on BSA displayed all three molecules - VLA-3, VLA-6 and NE (**Figure 5.21a, c, e**) - within intracellular stores. PECAM-1/ ICAM-1/ CXCL1 coating induced the translocation of VLA-3, VLA-6 and NE to the surface of interacting WT neutrophils, leading to a ring-like expression at the cell boarder (**Figure 5.21a, c, e**). Ring formation of VLA-3, VLA-6 and NE could be observed in $94.3 \pm 4.3\%$, $80.9 \pm 9.8\%$ and $93.8 \pm 3.6\%$ of all analyzed WT neutrophils, respectively (**Figure 5.21b, d, f**). In contrast, neutrophils derived from *Mst1*^{-/-} mice failed to efficiently mobilize any of these three proteins to the cell surface (**Figure 5.21a-i**). Only $46.7 \pm 7.6\%$ of all analyzed *Mst1*^{-/-} neutrophils showed a ring formation for VLA-3, $17.4 \pm 2.4\%$ for VLA-6 and $22.5 \pm 4.0\%$ for NE. These values were similar to the values found for WT ($31.6 \pm 9.4\%$ for VLA-3, $20.1 \pm 8.9\%$ for VLA-6, $23.4 \pm 3.7\%$ for NE) and *Mst1*^{-/-} ($31.2 \pm 6.6\%$ for VLA-3, $4.8 \pm 0.6\%$ for VLA-6, $24.7 \pm 4.4\%$ for NE) neutrophils seeded on BSA (**Figure 5.21b, d, f**).

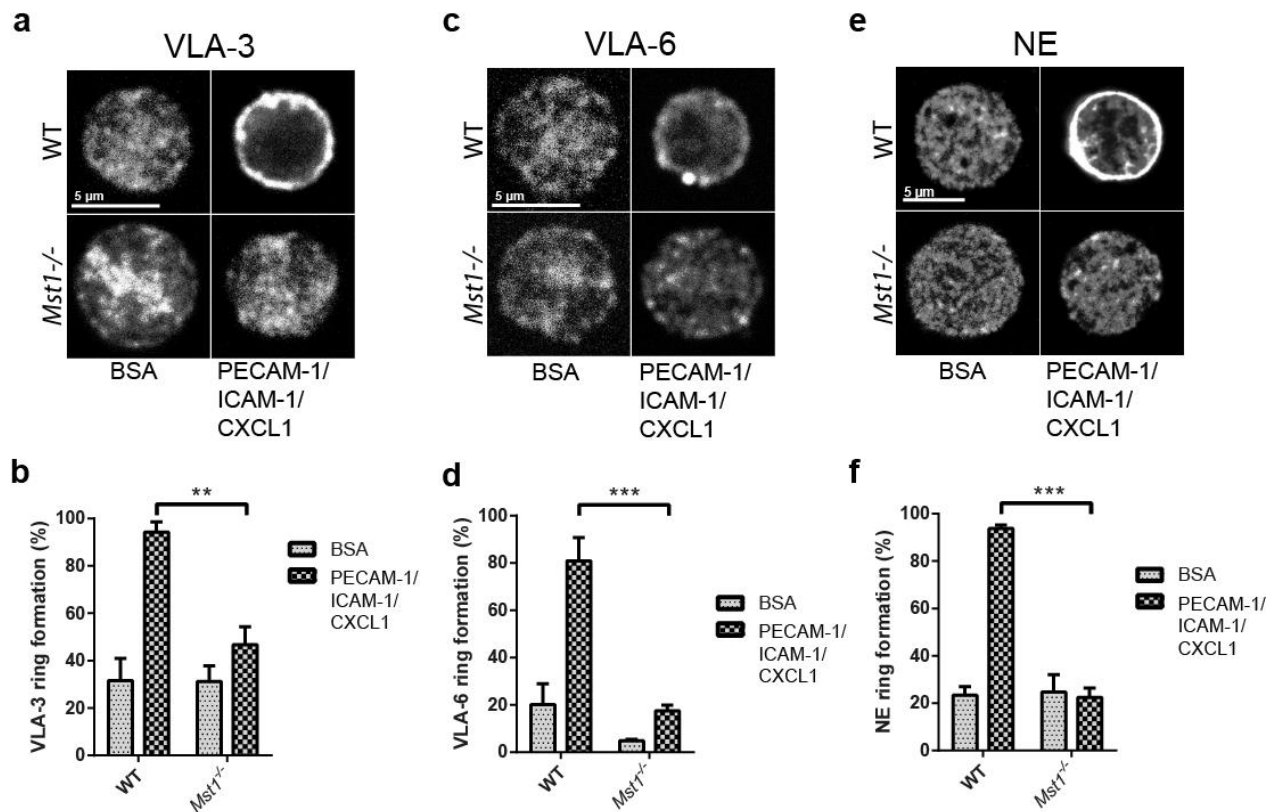


Figure 5.21 MST1 is required for the translocation of NE, VLA-3 and VLA-6 to the plasma membrane

Immunostaining of representative WT and *Mst1*^{-/-} neutrophil on BSA or PECAM-1/ ICAM-1/ CXCL1 coated slides for (a) VLA-3, (c) VLA-6 and (e) NE. Quantification of ring like expression of (b) VLA-3, (d) VLA-6 and (f) NE (n= 3 mice, mean ± SEM of >50 analyzed neutrophils, *** p < 0.001, ** p < 0.01, 2way ANOVA, Sidak's multiple comparisons test or Tukey's multiple comparisons test).

Ring formation was further evaluated by measuring the fluorescence intensity profiles along a line through the center of the cell (**Figure 5.22a**). Fluorescence intensity profile of VLA-3, VLA-6 and NE were similar between WT or *Mst1*^{-/-} cells seeded on BSA (**Figure 5.22b, c, d**). Translocation of VLA-3, VLA-6 and NE to the plasma membrane of WT neutrophils increased the fluorescence signal at the cell borders (**Figure 5.22e, f, g**, black line). In contrast, the accumulation of the fluorescence signal at the cell surface was absent for VLA-3, VLA-6 and NE in *Mst1*^{-/-} neutrophils (**Figure 5.22e, f, g**, grey line).

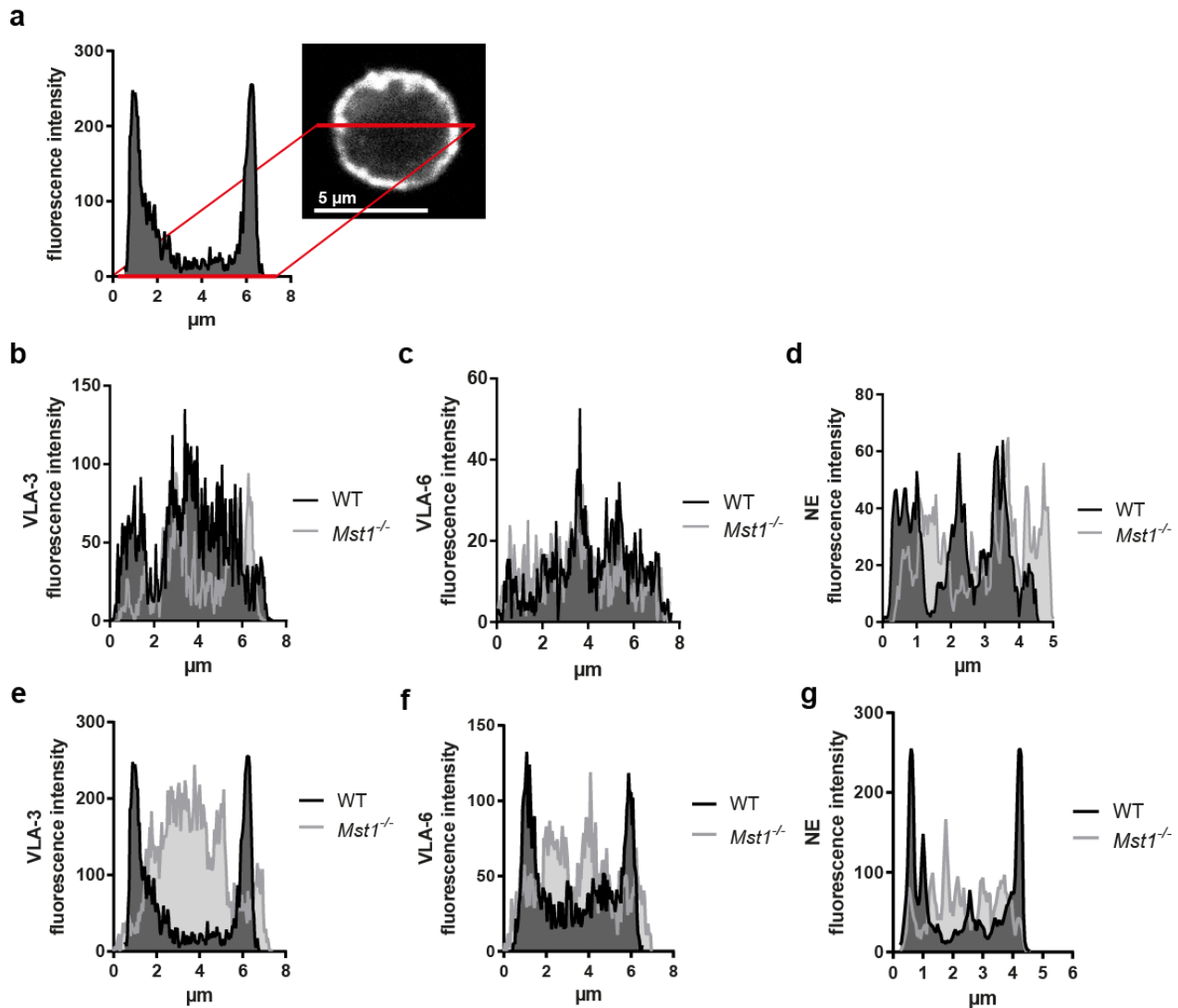


Figure 5.22 Fluorescence intensity profile of VLA-3, VLA-6 and NE in neutrophils from WT and *Mst1*^{-/-} mice

(a) Fluorescence intensity profiles along a line through the cell center (red thick line) for (b) VLA-3, (c) VLA-6 and (d) NE seeded on BSA and for (e) VLA-3, (f) VLA-6 and (g) NE seeded on PECAM-1/ ICAM-1/ CXCL1 of a representative WT (black line) and *Mst1*^{-/-} neutrophil (grey line).

To unravel the ligand responsible for the translocation of VLA-3, VLA-6 and NE, WT neutrophils were either seeded on BSA, PECAM-1, ICAM-1/ CXCL1, or PECAM-1/ ICAM-1/ CXCL1. WT neutrophils seeded on PECAM-1 coated coverslips alone induced the translocation of VLA-6 ($63.0 \pm 2.4\%$), but not NE ($10.0 \pm 5.0\%$). Whereas WT neutrophils seeded on ICAM-1/ CXCL1 coated coverslips translocated NE ($63.1 \pm 10.7\%$), but not VLA-6 ($39.2 \pm 7.5\%$) (**Figure 5.23a and b**). The results for VLA-3 were not conclusive.

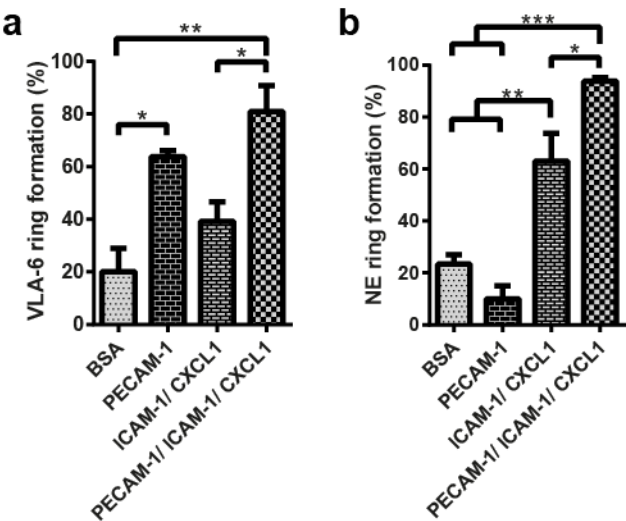


Figure 5.23 Ligands responsible for VLA-6 and NE translocation
Quantification of ring like expression of (a) VLA-6 and (b) NE in WT neutrophil on BSA, PECAM-1, ICAM-1/ CXCL1 or PECAM-1/ ICAM-1/ CXCL1 coating (n= 3 mice, mean \pm SEM of >50 analyzed neutrophils, *** p < 0.001, ** p < 0.01, one way ANOVA, Tukey's multiple comparisons test).

Importantly, western blot analysis showed no difference in the total protein levels of VLA-3, VLA-6 and NE between WT and *Mst1*^{-/-} neutrophils (Figure 5.24).

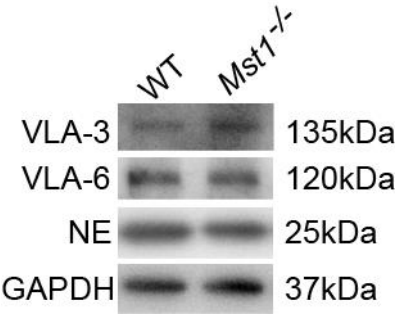


Figure 5.24 Total Protein levels of VLA-3, VLA-6 and NE
Total protein levels of VLA-3, VLA-6 and NE from neutrophils of WT and *Mst1*^{-/-} mice. GAPDH served as loading control (n=3 mice).

In order to verify MST1 dependent mobilization *in vivo*, NE activity was investigated with an NE-fluorescent activatable substrate (NE680FAST) in postcapillary venules of unstimulated and TNF- α stimulated cremaster muscle whole mounts from WT and *Mst1*^{-/-} mice.

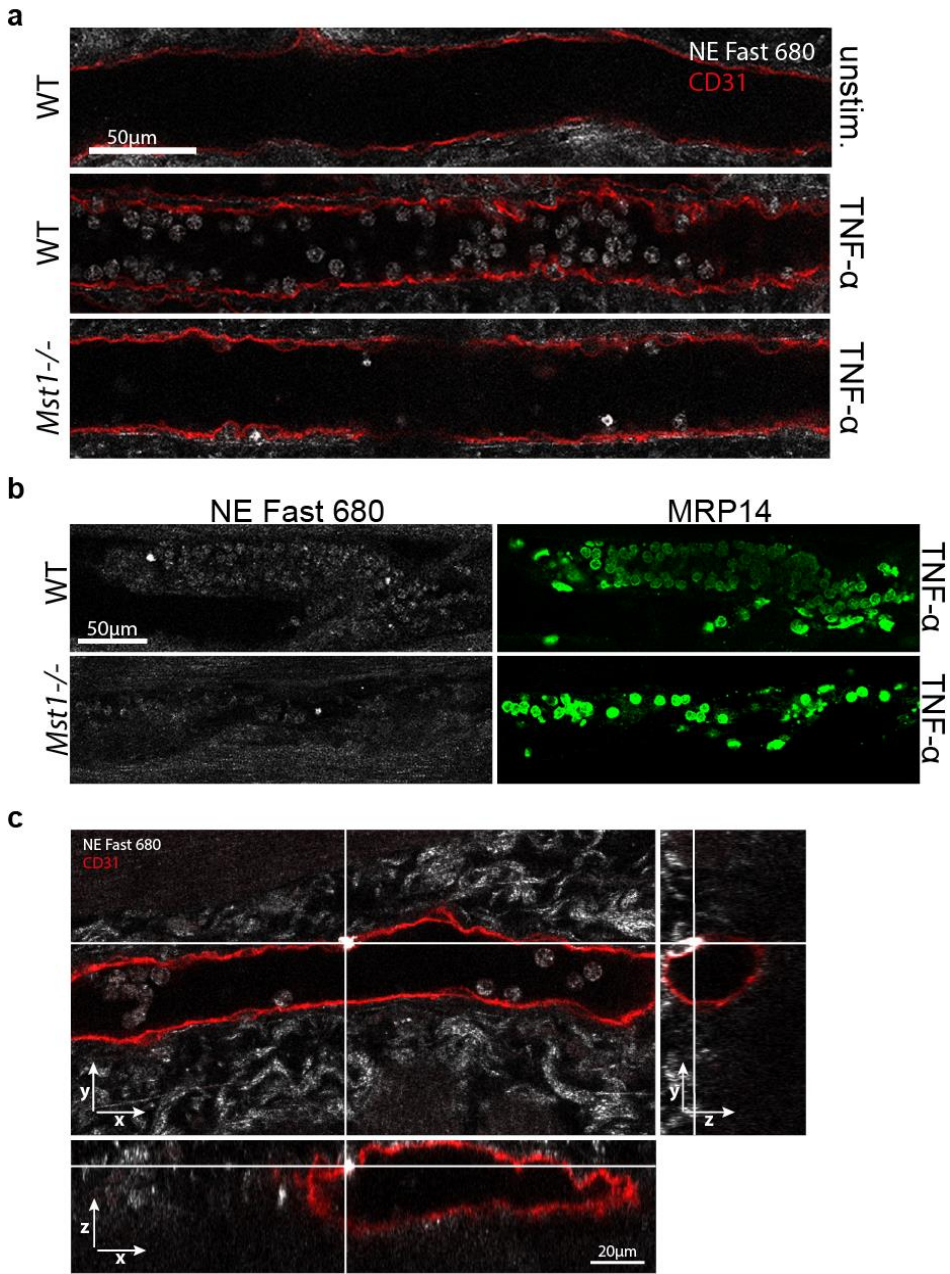


Figure 5.25 NE activity in TNF- α stimulated cremaster muscle *in vivo*
Confocal images of unstimulated and TNF- α stimulated cremaster muscle whole mounts from WT and *Mst1*^{-/-} mice showing NE activity (white) within venules labels with PECAM-1 (red). (n=3)

In unstimulated venules of WT mice NE activity could not be detected, while 2h after TNF- α stimulation NE activity could be observed (**Figure 5.25a**). TNF- α stimulated venules from *Mst1*^{-/-} mice showed decreased NE activity as compared to WT mice (**Figure 5.25a**). Importantly, the number of adherent cells was similar in WT and *Mst1*^{-/-} mice (**Figure 5.25b**). Furthermore occasionally high NE activity close to the vessel could be observed. Using 3D reconstruction, a ring like NE activity close to the abluminal site of the vessel could be detected, although only very few events were noted (**Figure 5.25c**).

Taken together, these *in vitro* and *in vivo* results demonstrate that MST1 is indispensable for efficient translocation of VLA-3, VLA-6 and NE to the surface of neutrophils.

5.4.2 MST1 AND RAB27A IN VESICLE TRAFFICKING

Rab27a is a central regulator of vesicle trafficking in neutrophils (Catz, 2014, Sheshachalam et al., 2014). Therefore, Rab27a translocation to the plasma membrane in response to PECAM-1/ ICAM-1/ CXCL1-stimulation was investigated. Rab27a displayed an intracellular localization in WT and *Mst1*^{-/-} neutrophils when seeded on BSA (**Figure 5.26a** and **b**). Rab27a showed a granular distribution in WT neutrophils, while the distribution was more homogenous in *Mst1*^{-/-} neutrophils. Furthermore, in WT neutrophils, PECAM-1/ ICAM-1/ CXCL1-coating induced the translocation of Rab27a to the plasma membrane (**Figure 5.26a**, upper, right panel). Again, the translocation of Rab27a to the plasma membrane of WT neutrophils transferred the main fluorescence to the cell border (**Figure 5.26c**, black line). Ring formation of Rab27a was observed in $78.0 \pm 6.5\%$ of all analyzed WT neutrophils, compared to $11.7 \pm 3.7\%$ of WT neutrophils seeded on BSA (**Figure 5.26d**). In contrast, neutrophils derived from *Mst1*^{-/-} mice displayed a reduced translocation rate of Rab27a to the plasma membrane in response to PECAM-1/ ICAM-1/ CXCL1 stimulation (**Figure 5.26a**, lower panel). Only $1.7 \pm 1.7\%$ of all analyzed *Mst1*^{-/-} neutrophils showed a ring formation for Rab27a and $17.7 \pm 7.5\%$ of *Mst1*^{-/-} neutrophils seeded on BSA (**Figure 5.26d**). Hence, *Mst1*^{-/-} neutrophils display a defect in Rab27a mobilization upon stimulation with ICAM-1/ PECAM-1/ CXCL1.

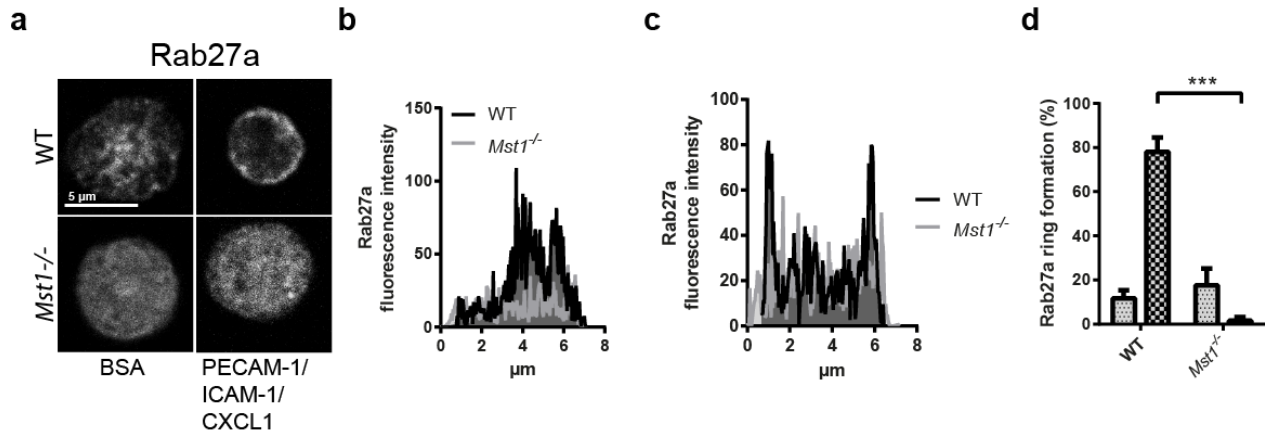


Figure 5.26 Rab27a translocation to the plasma membrane in *Mst1*^{-/-} neutrophils

(a) Immunostaining of WT and *Mst1*^{-/-} neutrophils seeded on BSA or PECAM-1/ ICAM-1/ CXCL1 coated wells for Rab27a. (b, c) Fluorescence intensity profiles along a line through the cell center for Rab27a of representative WT (black line) and *Mst1*^{-/-} neutrophil (grey line) seeded on (b) BSA or (c) PECAM-1/ ICAM-1/ CXCL1 coated wells. (d) Quantification of ring like expression of Rab27a (n= 3 mice, mean ± SEM of >50 analyzed neutrophils, *** p < 0.001, unpaired t-test).

Interestingly, total protein levels of Rab27 were similar between WT and *Mst1*^{-/-} neutrophils (Figure 5.27).

Next, the translocation of MST1 itself to the plasma membrane upon PECAM-1/ ICAM-1/ CXCL1 stimulation was investigated. MST1 displayed an intracellular localization in WT neutrophils seeded on BSA (Figure 5.28a, upper panel and Figure 5.28b, grey line). In response to PECAM-1/ ICAM-1/ CXCL1 stimulation, MST1 localized together with Rab27a and VLA-6 to the plasma membrane (Figure 5.28a, lower panel and Figure 5.28b, black line). Only 11.8 ± 7.2% of analyzed WT neutrophils seeded on BSA showed a ring formation for MST1, seeding neutrophils on PECAM-1/ ICAM-1/ CXCL1 resulted in a ring formation of MST1 in 93.2 ± 1.6% of analyzed WT neutrophils (Figure 5.28c).

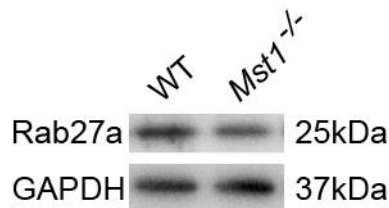


Figure 5.27 Total protein levels of Rab27a

Total protein levels of Rab27a from neutrophils of WT and *Mst1*^{-/-} mice. GAPDH served as loading control (n=3 mice).

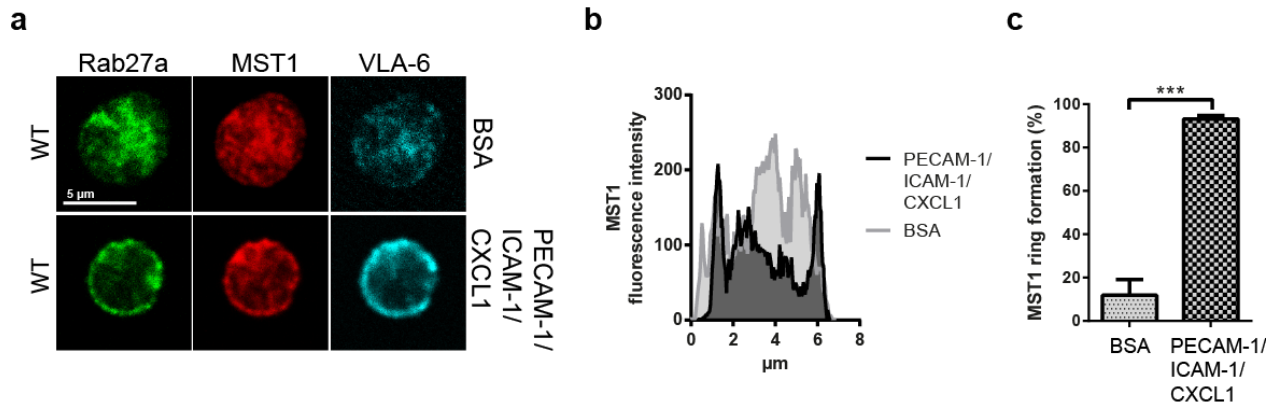


Figure 5.28 Translocation of MST1 to the plasma membrane

(a) Immunostaining of WT and *Mst1*^{-/-} neutrophils seeded on BSA or PECAM-1/ ICAM-1/ CXCL1 coated wells for Rab27a (green), MST1 (red) and VLA-6 (cyan). (b) Fluorescence intensity profiles along a line through the cell center for MST1 of a representative WT neutrophil seeded on BSA (grey line) or PECAM-1/ ICAM-1/ CXCL1 (black line) coated wells. (c) Quantification of ring like expression of MST1 in response to BSA or PECAM-1/ ICAM-1/ CXCL1 stimulation (n=3 mice, mean \pm SEM of >50 analyzed neutrophils, *** p < 0.001, 2way ANOVA, Sidak's multiple comparisons test).

These results demonstrate that Rab27a and MST1 translocate to the cellular membrane upon ICAM-1/ PECAM-1/ CXCL1 stimulation. Hence, we hypothesize, that MST-1 is involved in Rap27a dependent vesicle transport.

6 DISCUSSION

Originally, MST1 (mammalian homolog of the *Drosophila* Hippo protein) was identified in *Drosophila* as the central constituent and negative regulator of the Hippo pathway, controlling organ size and proliferation. Recently, MST1 has attracted more attention due to its role in cancer development (Kodaka and Hata, 2015) and the discovery that mutations in human *STK4* (Mst1) lead to a primary immune deficiency. Patients with a deficiency in *STK4* present with recurring bacterial, fungal and viral infections, they display lymphopenia and intermittent neutropenia, and their life expectancy is very short unless successfully transplanted (Abdollahpour et al., 2012, Crequer et al., 2012, Nehme et al., 2012, Dang et al., 2016, Halacli et al., 2015). Together with neutropenia, their impaired response to acute bacterial and fungal infections suggests an additional defect in myeloid cell function.

Until now, little is known about the function of MST1 in myeloid cells. One study suggested a role for MST1 in human eosinophil apoptosis, but not neutrophil apoptosis (De Souza et al., 2002). In contrast, neutrophils from patients with *STK4* deficiency exhibit an increased susceptibility to apoptosis (Abdollahpour et al., 2012). A recent study linked MST1 and MST2 in phagocytes (macrophages and neutrophils) to the recruitment of mitochondria to the phagosome. The fusion of mitochondria with the phagosome leads to increased ROS production and consequently promotes effective killing of bacteria (Geng et al., 2015). The aim of this thesis was to investigate how MST1 deficiency affects neutrophil recruitment *in vivo*.

The experimental work presented here, discovered that MST1 deficiency does not affect neutrophil rolling and adhesion, but extravasation of neutrophils. In contrast to T cells (Katagiri et al., 2006, Katagiri et al., 2009), MST1 is dispensable for activation of LFA-1 in neutrophils, identified as the first signaling molecule indispensable for neutrophil transmigration, in particular the penetration of neutrophils through the perivascular basement membrane. Mechanistically, *Mst1*^{-/-} neutrophils fail to translocate VLA-3, VLA-6 and neutrophil elastase from intracellular vesicles to the neutrophil surface, a putative requirement for neutrophils to successfully penetrate the basement membrane.

6.1 CHARACTERIZING MST1 IN NEUTROPHILS

First, the expression of MST1 and MST2 in murine neutrophils was evaluated, due to conflicting results in the past. De Souza and colleges investigated the expression of MST1 and MST2 in neutrophils and eosinophils and could only detect expression of MST1 and MST2 in eosinophils, but not in neutrophils (De Souza et al., 2002). In contrast, here it is demonstrated that murine neutrophils from WT mice express MST1, but not MST2. In addition, the absence of MST1 in neutrophils from *Mst1*^{-/-} mice could be confirmed. As MST1 is rapidly cleaved in neutrophil lysates into the 37kDa N-terminal fragment, which cannot be detected by all of the available antibodies, the absence of MST1 in De Souza's work may be explained by the use of antibodies unable to recognize the fragment. Here, the expression of MST1 was verified with antibodies against MST1 from two different companies. One antibody is specific for the C-terminal fragments for MST1 (Upstate; 276-487aa) and the other antibody recognizes the N-terminal region of MST1 (Cell Signaling). In accordance with data published by De Souza et al., we also could not detect the expression of MST2 in neutrophils, neither in WT nor *Mst1*^{-/-} neutrophils. Next, peripheral blood counts in WT and *Mst1*^{-/-} mice were compared. As reported by others (Oh et al., 2009, Mou et al., 2012), white blood cell counts were significantly decreased due to a decreased number of peripheral lymphocytes. This was also discovered in patients with *STK4* deficiency (Abdollahpour et al., 2012, Crequer et al., 2012, Nehme et al., 2012, Dang et al., 2016, Halacli et al., 2015). However, in contrast to human patients (Abdollahpour et al., 2012), the number of peripheral neutrophils was similar between WT and *Mst1*^{-/-} mice. In addition, the absence of MST1 in murine neutrophils did not increase susceptibility to apoptosis in contrast to neutrophils from patients with *STK4* deficiency (Abdollahpour et al., 2012). Differences in neutrophil counts between the human and the murine system could also be observed for other genes causing congenital neutropenia (CN) or severe congenital neutropenia (SCN) (Klein, 2011). The two most common genetic etiologies of SCN, *HAX1* and *ELA2* deficiency lead to SCN only in humans, but *Hax1*^{-/-} and *Ela2*^{-/-} mice do not display neutropenia (Belaaouaj et al., 1998, Chao et al., 2008, Dale et al., 2000, Horwitz et al., 1999, Horwitz et al., 2007, Klein et al., 2007), indicating a different regulation of neutrophil apoptosis between humans and mice.

6.2 MST1 IS DISPENSABLE FOR LFA-1 ACTIVATION IN NEUTROPHILS

The canonical Hippo (MST1/2) pathway is known for controlling proliferation and apoptosis, tissue growth, organ size and tumorigenesis. However, there is emerging evidence that various non-canonical Hippo pathways regulate other biological processes, often in a cell type specific manner. Recent studies have revealed that MST1 is involved in T cell development, function, survival, trafficking, homing and autoimmunity (Du et al., 2015).

MST1 was shown to be required for LFA-1 dependent T cell trafficking (Dong et al., 2009, Ueda et al., 2012, Katagiri et al., 2009), by regulating the transport and distribution of LFA-1 containing vesicles to the plasma membrane and by subsequently influencing LFA-1 activation, clustering and adhesion of T cells (Katagiri et al., 2006). Furthermore, Nishikimi et al. showed that MST1 associates via Rap1-RAPL to the cytoplasmic tail of the α_L subunit (Katagiri et al., 2006, Katagiri et al., 2003). This in turn is followed by phosphorylation of DENND1C, a Rab guanyl-nucleotide exchange factor, which results in Rab13-dependent LFA-1-containing vesicle transport (Nishikimi et al., 2014).

In contrast to T cells (Katagiri et al., 2006, Katagiri et al., 2009), it could be demonstrated that *Mst1*^{-/-} neutrophils have no defect in LFA-1-dependent slow rolling and adhesion implying that MST1 is dispensable for LFA-1 activation in neutrophils. The absence of MST1 did not influence the number of rolling neutrophils or rolling velocities in postcapillary venules of trauma stimulated or TNF- α stimulated cremaster muscles *in vivo*. Under inflammatory conditions, E-selectin and P-selectin induce talin dependent conformational changes in LFA-1 which leads to intermediate activity and slow rolling of neutrophils in post postcapillary venules (McEver, 2015). Both, neutrophils from WT and *Mst1*^{-/-} mice, bound E-selectin and P-selectin to the same extent and no difference in the surface expression of rolling and adhesion relevant molecules could be observed between WT and *Mst1*^{-/-} neutrophils.

Additional activation, for example by chemokine stimulation, results in the binding of both, kindlin3 and talin1, to the cytoplasmic tail of the β subunit of LFA-1, leading to the high affinity conformation of LFA1 (Lefort et al., 2012). High affinity conformation of

LFA-1 increases the affinity to endothelial expressed ICAM1 and ICAM2 leading to firm arrest of neutrophils (Lefort and Ley, 2012). Consistent with the hypothesis that MST1 does not regulate LFA-1 activity in neutrophils, no difference in adhesive properties of neutrophils in postcapillary venules of trauma and TNF- α stimulated cremaster muscle of WT and *Mst1*^{-/-} mice was observed. Also LFA-1 dependent neutrophil adhesion induced by i.v. injection of CXCL1 *in vivo*, activating LFA-1 via integrin inside-out signaling, showed no difference between WT and *Mst1*^{-/-} mice.

To exclude compensatory effects from the endothelium, *ex vivo* flow chambers coated with a combination of E-selectin, ICAM-1 and CXCL1 were used to confirm *in vivo* findings. Neutrophils from WT and *Mst1*^{-/-} mice adhered to a similar extent to E-selectin, E-selectin/ ICAM-1 and E-selectin/ ICAM-1/ CXCL1 coated flow chambers.

In addition, LFA-1 clustering under flow conditions, as well as LFA-1 activation, measured using a soluble ICAM-1 binding assay, and the surface expression of LFA-1 and Mac-1 was not altered in *Mst1*^{-/-} neutrophils compared to WT neutrophils.

Finally, we were able to investigate the adhesive properties of neutrophils from patients with *STK4* deficiency and their heterozygous parents with the help from Dr. Claudia Nussbaum and Prof.Dr. Christoph Klein (Dr. von Hauner Children's hospital, LMU, Munich). Using flow chambers coated with E-selectin/ ICAM-1/ CXCL8, we could demonstrate that MST1 was also dispensable for neutrophil adhesion in the human system.

These results suggest that different mechanisms of LFA-1 regulation/ activation exist between lymphocytes and neutrophils. This hypothesis is supported by data from Fabbri et al., reporting that Rab11, but not Rab13 (as in T cells), is required for the trafficking of LFA-1 containing vesicles in neutrophils (Fabbri et al., 2005).

6.3 MST1 IS CRITICAL FOR NEUTROPHIL EXTRAVASATION

Although *Mst1*^{-/-} neutrophils showed no defective rolling or adhesion, they failed to extravasate into the peritoneal cavity 2h after TNF-α stimulation.

To accurately investigate the exact role of MST1 in neutrophil extravasation *in vivo*, an imaging platform using multi-photon laser scanning microscopy in the mouse cremaster muscle was established. To this end, *Mst1*^{-/-} mice were crossed with *Ly22*^{GFP} mice, in which neutrophils are endogenously labeled with EGFP. *Mst1*^{-/-} x *Ly22*^{GFP} mice displayed a decreased number of peripheral lymphocytes compared to *Ly22*^{GFP} mice. Importantly, the numbers of neutrophils as well as the proportion of EGFP⁺ neutrophils and monocytes were similar between *Ly22*^{GFP} and *Mst1*^{-/-} x *Ly22*^{GFP} mice. Neutrophil transmigration was then observed in postcapillary venules of TNF-α stimulated cremaster muscles with endothelial cells stained with Alexa Fluor 546 conjugated anti-PECAM-1 antibody (Christofidou-Solomidou et al., 1997, Woodfin et al., 2011). *Mst1*^{-/-} neutrophils failed to properly extravasate from postcapillary venules to the site of inflammation. Instead, neutrophils remained in close contact with the abluminal side of the vessel. Interestingly, the total number of neutrophils within the cremaster muscle was similar between WT and *Mst1*^{-/-} mice. Even after additional stimulation by inducing a laser injury next to the vessel 4 h after TNF-α stimulation, *Mst1*^{-/-} neutrophils persisted at the vessel wall and failed to migrate to the site of injury. Effects due to decreased viability could be excluded as neutrophils isolated from the TNF-α stimulated cremaster muscle showed no difference in viability.

Interstitial matrix migration can be integrin independent (Wolf et al., 2009, Lammermann et al., 2008). In order to exclude a general migration defect of *Mst1*^{-/-} neutrophils, migration of WT and *Mst1*^{-/-} neutrophils was investigated in 3D collagen gels by the group of Prof. Barbara Walzog, Walter-Brendel-Center of Experimental Medicine, LMU, Munich. They tested migration of bone marrow-derived neutrophils within 3D collagen gels in response to fMLP or CXCL1. The absence of MST1 did not alter the 3D migration capacity of neutrophils (**see Appendix/ Manuscript/ Supplemental Figure 2**), indicating that MST1 does not affect migration in 3D collagen gels.

Additionally, the imaging approach using multi-photon laser scanning microscopy of the mouse cremaster muscle allowed us to investigate neutrophil crawling on the luminal side of postcapillary venules *in vivo*. *Mst1*^{-/-} x *Lyz2*^{GFP} neutrophils showed a decreased crawling velocity compared to *Lyz2*^{GFP} neutrophils, suggesting that MST1 regulates neutrophil crawling *in vivo*.

6.3.1 NEUTROPHIL TRANSMIGRATION IN A *H. PYLORI* MOUSE INFECTION MODEL

In order to evaluate the impact of MST1 deficiency in neutrophils during a clinically relevant infection, the group of Prof. Rainer Haas, Max von Pettenkofer-Institute, LMU, Munich evaluated the role of MST1 in a murine *Helicobacter pylori* (*H. pylori*) infection model. More than 50% of the human population suffers from chronic *H. pylori* infection, which makes this gram-negative bacterium one of the most successful human bacterial pathogens. While most infected people are asymptomatic, about 15-20% develop chronic gastritis, duodenal ulcers, or even adenocarcinoma or mucosa-associated lymphoid tissue (MALT) lymphoma. Previous work has shown that neutrophils play an important role in the pathogenesis of *H. pylori* (Kusters et al., 2006). The bacterium induces a strong inflammatory response in the gastric mucosa, which is dependent on *H. pylori* neutrophil-activating protein (HP-NAP). Furthermore, pro-inflammatory cytokines like CXCL8 (IL-8) are secreted during the inflammatory process, recruiting additional neutrophils and monocytes to the site of inflammation (Montecucco and Rappuoli, 2001).

WT and *Mst1*^{-/-} mice were orogastrically infected with *H. pylori* and sacrificed 3 months later, when a chronic gastric infection was established. Tissue sections of the gastric epithelium from the antrum and corpus of the stomach were immunostained with DAPI and anti-mouse Ly6G antibodies, to identify neutrophils. The antrum is known to be the major site of *H. pylori* infection (Sachs et al., 2003). Indeed, the majority of infiltrated neutrophils were found in the antrum and not in the corpus in WT mice (**see Appendix/ Manuscript/ Figure 3A**, upper panel). In contrast, only a very small number of neutrophils could be detected in the gastric epithelium of the antrum in *Mst1*^{-/-} mice (**see Appendix/ Manuscript/ Figure 3A**, lower panel). The number of extravasated neutrophils in the antrum was significantly reduced in *Mst1*^{-/-} mice compared to WT mice (**see Appendix/ Manuscript/ Figure 3B**). In line with the reduced number of

extravasated neutrophils in *Mst1*^{-/-} mice, the number of the colony forming units (cfu) of *H. pylori* in the antrum showed a significant increase in *Mst1*^{-/-} mice compared to WT mice (**see Appendix/ Manuscript/ Figure 3C**), indicating a more successful colonization.

To distinguish if the increased colonization in the antrum of *Mst1*^{-/-} mice results from defects in transmigration and/ or defects in the phagocytosis, the phagocytic capacity of *Mst1*^{-/-} neutrophils was evaluated. The phagocytic capacity of neutrophils was not impaired within the first 15 min in absence of MST1. This is line with another study (Geng et al., 2015). However, they reported impaired phagocytosis of conditional *Mst1*^{-/-} *Mst2*^{-/-} double knockout neutrophils after 50 min (Geng et al., 2015). Within this study later time points were not investigated, therefore it cannot be excluded that *Mst1*^{-/-} single knockout neutrophils display defects after 50 min.

These results suggest that the increase in colonization in *Mst1*^{-/-} mice is due to the inability of neutrophils to migrate to the site of inflammation, although an additional role of MST1 in phagocytosing the pathogens cannot be completely exclude.

6.3.2 NEUTROPHIL PENETRATION THROUGH THE VENULAR BASEMENT MEMBRANE

To better define at which step during transmigration neutrophils from *Mst1*^{-/-} mice were inhibited (**Figure 6.1**), Prof.Dr. Dietmar Vestweber, Max-Planck-Institute for Molecular Biomedicine, Münster and his groups investigated in collaboration with our group the capacity of neutrophils to migrate through the endothelium and penetrate the perivascular basement membrane (BM) in more detail. To do this, whole mount immune stainings of TNF- α stimulated cremaster muscles were performed using antibodies against laminin $\alpha 5$ (LN $\alpha 5$) and the endothelial cell-specific adhesion molecule 1 (ESAM1) to visualize the BM and endothelial cell contacts, respectively. An antibody against MRP14 was used to identify neutrophils (**see Appendix/ Manuscript/ Figure 4A**). By means of confocal microscopy, neutrophils were classified into three groups according to their position during the extravasation from postcapillary venules. Neutrophils, embedded within the endothelial layer belonged to position I. Position II represents neutrophils located between the endothelium and BM

and fully transmigrated neutrophils were classified as position III (Bixel et al., 2010) (**see Appendix/ Manuscript/ Figure 4B**). $49.0 \pm 3.9\%$ of WT neutrophils were in intimate contact with the endothelium (position I), $16.4 \pm 2.3\%$ were found between the endothelium and the BM (position II) and $34.6 \pm 3.8\%$ were fully transmigrated (position III) 2h after TNF- α stimulation. Neutrophils of *Mst1*^{-/-} mice were present at similar percentages embedded within the endothelium (position I, $43.0 \pm 2.8\%$). However, almost the same amount of cells was located between the endothelium and the BM (position II, $41.8 \pm 2.0\%$). Only $15.1 \pm 2.2\%$ of the *Mst1*^{-/-} neutrophils were fully transmigrated (position III) (**see Appendix/ Manuscript/ Figure 4C**).

These data indicate that MST1 is crucial for neutrophils to overcome the basement membrane. This could not only be demonstrated in postcapillary venules of TNF- α stimulated cremaster muscles, but also in the submucosal vasculature and tissue of the *H. pylori* infected murine stomach of WT and *Mst1*^{-/-} mice (**see Appendix/ Manuscript/ Figure 3D-F**).

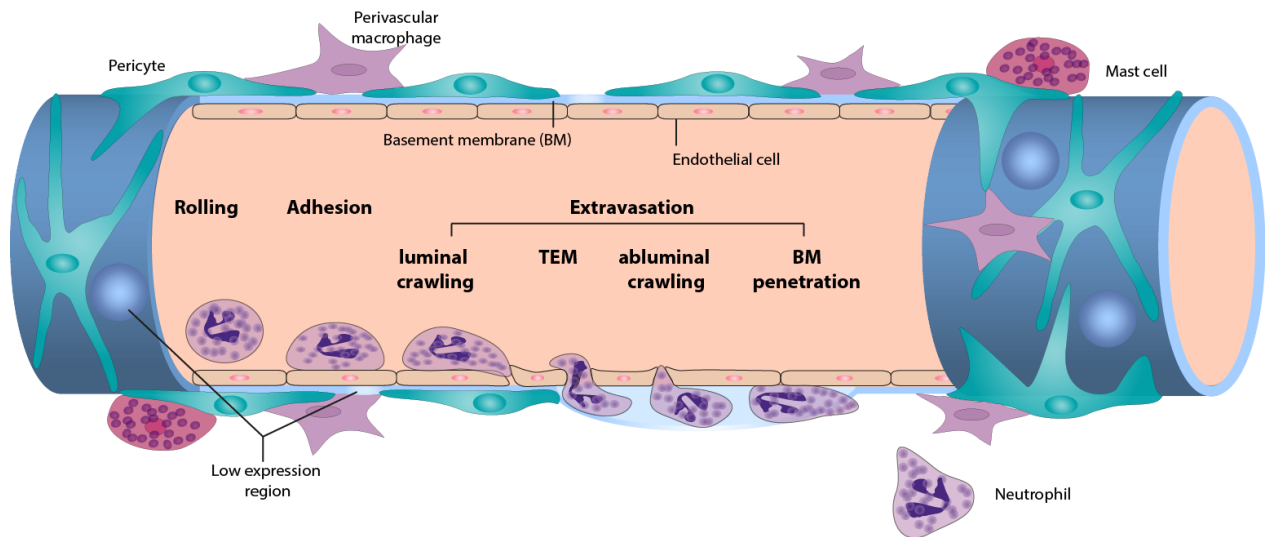


Figure 6.1 Updated neutrophil adhesion cascade

Depicted are the sequential steps of neutrophil recruitment from the vasculature to the tissue.

6.3.3 MST1 AND TRANSLOCATION OF VLA-3, VLA-6 AND NE TO THE CELL SURFACE

After crossing the endothelial cell layer, neutrophils have to penetrate the underlying BM (Proebstl et al., 2012, Wang et al., 2006). The BM of postcapillary venules is mainly composed of laminin 411 ($\alpha 4\beta 1\gamma 1$ laminin subunit), laminin 511 ($\alpha 5\beta 1\gamma 1$ laminin subunit) and type IV collagen (Sorokin, 2010). Although many studies have been performed on leukocyte adhesion and TEM, the mechanisms by which neutrophils penetrate the BM are still poorly understood.

Previous studies showed that genetic, antibody or inhibitor-mediated blockade of PECAM-1 (Wang et al., 2005), VLA-3 (Hyun et al., 2012), VLA-6 (Dangerfield et al., 2002, Dangerfield et al., 2005, Wang et al., 2005) or NE (Wang et al., 2005) in the mouse cremaster muscle leads to an arrest of infiltrating neutrophils between the endothelial layer and the underlying BM. Extravasating neutrophils need to interact with ICAM-1 and PECAM-1 to induce the mobilization of vesicles containing VLA-6 and NE. This mobilization translocates VLA-6 and NE to the cellular surface, a prerequisite to pass the BM.

To proof this hypothesis, an *in vitro* transmigration assay was established where filters were coated with laminin, mimicking the basement membrane. Interestingly, WT as well as *Mst1*^{-/-} neutrophils were unable to pass filters coated only with laminin. However, additional coating with PECAM-1 and ICAM-1 of laminin coated filters efficiently induced neutrophil transmigration along a CXCL1 gradient in WT neutrophils. These findings are in line with previously published data (Wang et al., 2005). Furthermore, in contrast to WT neutrophils, neutrophils from *Mst1*^{-/-} mice failed to pass through PECAM-1, ICAM-1 and laminin-coated transwell filters. Similar to this finding, *Mst1*^{-/-} neutrophils failed to transmigrate as efficiently as WT neutrophils through filters containing a monolayer of mouse endothelial 1G11 cells in response to CXCL1. Importantly, we did not find differences in the number of transmigrated WT and *Mst1*^{-/-} neutrophils in transwell assays without coating.

Next, the mobilization of VLA-3, VLA-6 and NE from intracellular stores to the plasma membrane in the absence of MST1 was investigated. It was discovered that MST1 is essential for the exocytosis of VLA-3, VLA-6 and NE as neutrophils from *Mst1*^{-/-} mice fail to translocate these proteins to the cell surface upon stimulation with PECAM-1, ICAM-1 and CXCL1. Further, it was demonstrated that ICAM-1 and CXCL1 coating are

responsible for the translocation of NE, whereas PECAM-1 lead to the mobilization of VLA-6. The results for VLA-3 were not conclusive.

Taken together, neutrophils deficient in MST1 fail to efficiently penetrate the basement membrane. This is accompanied by their inability to mobilize VLA-3, VLA-6 and/or NE from intracellular vesicles in response to interactions with endothelial CXCL-1, ICAM-1 and PECAM-1 (**Figure 6.2**).

6.3.4 MST1 TRANSLOCATION WITH RAB27A TO THE PLASMA MEMBRANE

As MST1 influences LFA-1 clustering in T cells by regulating LFA-1 containing vesicle trafficking via Rab13 (Nishikimi et al., 2014), we hypothesized, that MST1 is similarly involved in the mobilization of the vesicles containing VLA-3, VLA-6 and NE to the plasma membrane in neutrophils. The GTPase Rab27a is a central regulator of vesicle exocytosis, thus regulating a variety of neutrophil functions (Catz, 2014). Several studies indicate that Rab27a and its effectors JFC1 (synaptotagmin-like protein 1) and Munc13-4 regulate the secretion of several granules and vesicles, for example azurophilic granules containing e.g. NE (Brzezinska et al., 2008, Munafo et al., 2007). Rab27a and MST1 itself were discovered to translocate to the plasma membrane in response to PECAM-1/ ICAM-1/ CXCL1. However, translocation of Rab27a is defective in *Mst1*^{-/-} neutrophils indicating that MST1 is involved in Rab27a dependent vesicle trafficking. Further studies may elucidate, whether Rab27a regulates only NE secretion or is additionally involved in VLA-3 and VLA-6 translocation.

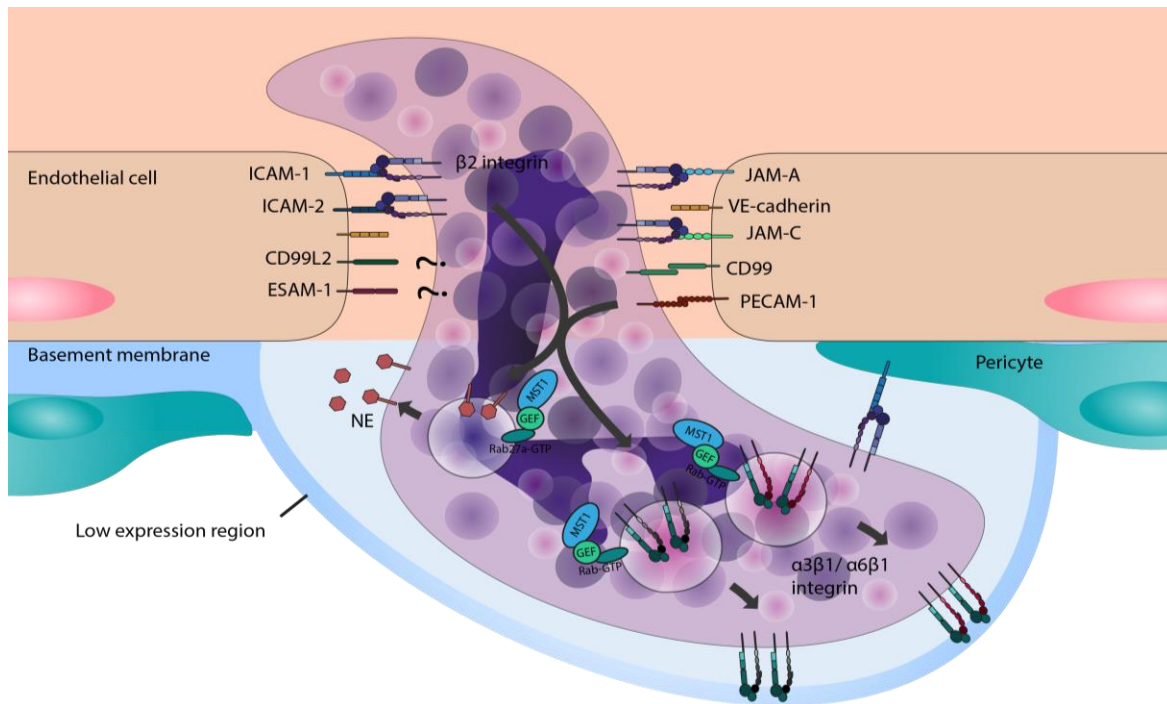


Figure 6.2 Crossing the basement membrane

During transendothelial migration, neutrophils interact with endothelial cells. Interactions with CXCL1, ICAM-1 and PECAM-1 lead to the mobilization of VLA-3, VLA-6 and NE in a MST1- and Rab27a-dependent manner.

6.4 OUTLOOK

The results of the work presented expand our understanding of the underlying mechanisms by which endothelial cell interactions ‘educate’ neutrophils to penetrate the basement membrane. Huber et al. demonstrated that neutrophils only penetrate the BM in the presence of an overlying endothelium (Huber and Weiss, 1989). Furthermore, it was shown that interactions with endothelial PECAM-1, ICAM-1 and CXCL1 are required to overcome the BM (Wang et al., 2005). So far, no signaling molecules could be associated with this step. In this study, the serine/threonine kinase MST1 was identified as the first signaling molecule indispensable for neutrophil BM penetration into inflamed tissue. Furthermore, interactions of endothelial ICAM-1 and CXCL1 with $\beta 2$ integrins on neutrophils could be associated with the exocytosis of NE, whereas interactions with endothelial PECAM-1 are important for the exocytosis of VLA-6. Whether ICAM-1/CXCL1 and/or PECAM-1 lead to the exocytosis of VLA-3 is not clear yet. In addition, the exact cooperation of the laminin-binding integrins VLA-3 and VLA-6 and the protease NE on neutrophils to penetrate the BM is also still unclear.

Since the basement membrane is essential for maintaining vascular integrity, significant degradation of the basement membrane is unlikely. Enormous numbers of neutrophils penetrate the BM, but leave the BM morphologically intact (Nourshargh and Alon, 2014, Rowe and Weiss, 2008, Hallmann et al., 2015). One of the hypothesis is that during transmigration, endothelial cell traction forces and/or surface-associated enzymatic activity might promote local reversible disassembly of the BM network and consequently increase local pore size to permit transmigration via a proteinase-independent process (Rowe and Weiss, 2008). This hypothesis is supported by Wang et al who showed that neutrophils seek for LER sites and that these sites are enlarged after IL-1 β induced neutrophil transmigration (Wang et al., 2006). Only in rare cases, using an NE-fluorescent activatable substrate (NE680FAST), a high NE activity could be detected close to the abluminal site of postcapillary venules in TNF- α stimulated cremaster muscles. In addition, it could be demonstrated that a couple of transmigrated neutrophils were positive for laminin alpha 5 in TNF- α stimulated cremaster muscles. This is in line with results from other groups showing laminin alpha 5 positive

transmigrated neutrophils in IL-1 β stimulated cremaster muscles (Wang et al., 2006). Furthermore, neutrophils extravasate from so called 'hot spots' (Colom et al., 2015, Voisin et al., 2009, Weninger et al., 2014). Keeping that in mind, one could hypothesize that the first line of neutrophils penetrating the basement membrane enlarges LERs and drag some laminin fibers along with them.

Using an NE-fluorescent activatable substrate (NE680FAST) revealed a mild activity of NE on the surface of neutrophils interacting with the luminal site of venular endothelial cells in TNF- α stimulated cremaster muscles. This activity of NE is decreased in *Mst1*^{-/-} mice, although the number of rolling and adherent neutrophils is similar. Release of granules is regulated by a binary signal, one being adhesion dependent and the other involves the ligation and activation of immune receptors (Sengelov et al., 1995). As TNF- α activates neutrophils themselves in addition to the interaction between β 2 integrins and endothelial ICAM-1, it is not surprising that at least a mild release of NE is triggered in these rolling and adherent neutrophils. Moreover, it was demonstrated that interactions with endothelial ICAM-1 and CXCL1 are sufficient to mobilize NE to the surface of neutrophils, a process dependent on MST1. A recent study by Colom et al. showed that neutrophil derived NE, mobilized to the cell surface in response to LTB₄, bound to neutrophilic Mac-1 and was responsible for cleavage of JAM-C. This LTB₄-NE-Mac-1 axis promotes neutrophil reverse TEM (Colom et al., 2015). It is tempting to speculate that NE promotes efficient TEM of neutrophils from postcapillary venules to the site of inflammation.

After neutrophils migrate through the endothelial layer, they are hypothesized to interact with matrix components of the BM via laminin binding β 1 integrins, like VLA-3 and VLA-6, and β 3 integrins. Extravasating neutrophils need to interact with ICAM-1 and PECAM-1 to induce the mobilization of vesicles containing laminin binding β 1 integrins. This vesicle mobilization translocates laminin binding β 1 integrins to the cellular surface, a prerequisite to pass the BM (Dangerfield et al., 2002, Wang et al., 2005). The result of this thesis demonstrate that MST1 is essential for the exocytosis of VLA-3 and VLA-6 as neutrophils from *Mst1*^{-/-} mice failed to translocate these proteins to the cell surface upon stimulation with PECAM-1/ ICAM-1/ CXCL1.

VLA-3 and VLA-6 seem to be regulated by cytokine dependent mechanisms. VLA-3 was shown to be necessary for neutrophil extravasation in TNF- α and fMLP-induced transmigration *in vivo* (Hyun et al., 2012). Using blocking antibodies suggest a role for VLA-6 in IL-1 β , but not TNF- α dependent neutrophils extravasation (Dangerfield et al., 2005). Interestingly, when using neutrophils deficient in the TNF receptor, blocking of PECAM-1 traps neutrophil between the endothelial layer and the BM (Woodfin et al., 2009). This suggest different mechanisms to penetrate the basement membrane, dependent on the stimulus, which is either activating the endothelium only (e.g. IL-1 β) or both the endothelium and the neutrophil (e.g. TNF- α).

Nevertheless, these results show that VLA-3, VLA-6 and NE are stored in distinct vesicles and are differently regulated. MST1 regulates the mobilization of all three, VLA-3, VLA-6 and NE, in response to PECAM-1, ICAM-1 and CXCL1 stimulation. Additionally, the distribution and translocation of Rab27a was disrupted in *Mst1*^{-/-} neutrophils. From these experiments we cannot conclude whether Rab27a is responsible for the mobilization of only one or all vesicles, containing VLA-3, VLA-6 and NE. It is very likely that Rab27a at least controls the translocation of NE containing vesicles, as demonstrated by the group of Sergio Catz (Catz, 2013). Further studies are required to define the exact involvement of Rab27a during the translocation of VLA-3, VLA-6 and NE during vesicle trafficking. Moreover, it would be intriguing to discover the specific function of Rab27a-controlled vesicle trafficking for neutrophil function *in vivo*. Rab27a is the only Rab associated with a human disease, called Griscelli syndrome type 2 (GS2), where patients suffer from often fatal viral and bacterial infections, due to severe immunodeficiency including neutropenia.

Rab GTPases are controlled by Rab effector proteins. So far, two Rab27a effector proteins, Slp1/JFC1 and Munc13-4, could be associated with impaired release of granules in neutrophils. It would be exciting to explore if Slp1/JFC1 and/or Munc13-4 regulate the translocation of VLA-3, VLA-6 and NE. As MST1 influences LFA-1 containing vesicle trafficking in T cells by regulating the Rab13 effector DENND1C (Nishikimi et al., 2014), it is tempting to speculate that MST1 is involved in the vesicle transport of neutrophils by controlling the activity of the Rab27a effector proteins,

Slp1/JFC1 and Munc13-4. Further experiments are necessary to explore these possibilities.

Defining the exact function of MST1 will contribute to a better understanding of the underlying defects in patients suffering from *STK4* deficiency. Recently, Lerman et al. reported that VLA-3 is upregulated in neutrophils in human septic patients and in septic mice (Lerman et al., 2014). Neutrophils with an increased expression of VLA-3 displayed a hyperinflammatory phenotype and blocking VLA-3 on neutrophils in septic mice improved their survival (Lerman et al., 2014). It would be interesting to outline the involvement of MST1 and reveal if MST1 could modulate the inflammatory phenotype during sepsis.

Taken together, we demonstrate that the serine/threonine-kinase MST1 is indispensable for neutrophil penetration of the basement membrane by regulating the mobilization of VLA-3, VLA-6 and NE from intracellular vesicles to the plasma membrane. These findings emphasize the importance of MST1 for early innate immune responses and also helps to understand the phenotype of recurring infections found in patients suffering from *STK4* immune deficiency.

7 REFERENCES

- ABDOLLAHPOUR, H., APPASWAMY, G., KOTLARZ, D., DIESTELHORST, J., BEIER, R., SCHAFFER, A. A., GERTZ, E. M., SCHAMBACH, A., KREIPE, H. H., PFEIFER, D., ENGELHARDT, K. R., REZAEI, N., GRIMBACHER, B., LOHRMANN, S., SHERKAT, R. & KLEIN, C. 2012. The phenotype of human STK4 deficiency. *Blood*, 119, 3450-7.
- ARTEMENKO, Y. & DEVREOTES, P. N. 2013. Hippo on the move: tumor suppressor regulates adhesion and migration. *Cell Cycle*, 12, 535-6.
- AYRES-SANDER, C. E., LAURIDSEN, H., MAIER, C. L., SAVA, P., POBER, J. S. & GONZALEZ, A. L. 2013. Transendothelial migration enables subsequent transmigration of neutrophils through underlying pericytes. *PLoS One*, 8, e60025.
- BARREIRO, O., YANEZ-MO, M., SERRADOR, J. M., MONTOYA, M. C., VICENTE-MANZANARES, M., TEJEDOR, R., FURTHMAYR, H. & SANCHEZ-MADRID, F. 2002. Dynamic interaction of VCAM-1 and ICAM-1 with moesin and ezrin in a novel endothelial docking structure for adherent leukocytes. *J Cell Biol*, 157, 1233-45.
- BARTENEVA, N. S., PONOMAREV, E. D., TSYTSYKOVA, A., ARMANT, M. & VOROBYEV, I. A. 2014. Mitochondrial staining allows robust elimination of apoptotic and damaged cells during cell sorting. *J Histochem Cytochem*, 62, 265-75.
- BELAAOUAJ, A., MCCARTHY, R., BAUMANN, M., GAO, Z., LEY, T. J., ABRAHAM, S. N. & SHAPIRO, S. D. 1998. Mice lacking neutrophil elastase reveal impaired host defense against gram negative bacterial sepsis. *Nat Med*, 4, 615-8.
- BIXEL, M. G., LI, H., PETRI, B., KHANDOGA, A. G., KHANDOGA, A., ZARBOCK, A., WOLBURG-BUCHHOLZ, K., WOLBURG, H., SOROKIN, L., ZEUSCHNER, D., MAERZ, S., BUTZ, S., KROMBACH, F. & VESTWEBER, D. 2010. CD99 and CD99L2 act at the same site as, but independently of, PECAM-1 during leukocyte diapedesis. *Blood*, 116, 1172-84.
- BORREGAARD, N. 2010. Neutrophils, from marrow to microbes. *Immunity*, 33, 657-70.
- BORREGAARD, N. & COWLAND, J. B. 1997. Granules of the human neutrophilic polymorphonuclear leukocyte. *Blood*, 89, 3503-21.
- BORSIG, L., WONG, R., HYNES, R. O., VARKI, N. M. & VARKI, A. 2002. Synergistic effects of L- and P-selectin in facilitating tumor metastasis can involve non-mucin ligands and implicate leukocytes as enhancers of metastasis. *Proc Natl Acad Sci U S A*, 99, 2193-8.
- BRZEZINSKA, A. A., JOHNSON, J. L., MUNAFO, D. B., CROZAT, K., BEUTLER, B., KIOSSES, W. B., ELLIS, B. A. & CATZ, S. D. 2008. The Rab27a effectors JFC1/Slp1 and Munc13-4 regulate exocytosis of neutrophil granules. *Traffic*, 9, 2151-64.
- CARMAN, C. V. & SPRINGER, T. A. 2004. A transmigratory cup in leukocyte diapedesis both through individual vascular endothelial cells and between them. *J Cell Biol*, 167, 377-88.
- CATZ, S. D. 2013. Regulation of vesicular trafficking and leukocyte function by Rab27 GTPases and their effectors. *J Leukoc Biol*, 94, 613-22.

- CATZ, S. D. 2014. The role of Rab27a in the regulation of neutrophil function. *Cell Microbiol*, 16, 1301-10.
- CHAO, J. R., PARGANAS, E., BOYD, K., HONG, C. Y., OPFERMAN, J. T. & IHLE, J. N. 2008. Hax1-mediated processing of HtrA2 by Parl allows survival of lymphocytes and neurons. *Nature*, 452, 98-102.
- CHOI, J., OH, S., LEE, D., OH, H. J., PARK, J. Y., LEE, S. B. & LIM, D. S. 2009. Mst1-FoxO signaling protects Naive T lymphocytes from cellular oxidative stress in mice. *PLoS One*, 4, e8011.
- CHRISTOFIDOU-SOLOMIDOU, M., NAKADA, M. T., WILLIAMS, J., MULLER, W. A. & DELISSER, H. M. 1997. Neutrophil platelet endothelial cell adhesion molecule-1 participates in neutrophil recruitment at inflammatory sites and is down-regulated after leukocyte extravasation. *J Immunol*, 158, 4872-8.
- COLOM, B., BODKIN, J. V., BEYRAU, M., WOODFIN, A., ODY, C., ROURKE, C., CHAVAKIS, T., BROHI, K., IMHOF, B. A. & NOURSHARGH, S. 2015. Leukotriene B-Neutrophil Elastase Axis Drives Neutrophil Reverse Transendothelial Cell Migration In Vivo. *Immunity*, 42, 1075-1086.
- CREASY, C. L. & CHERNOFF, J. 1995. Cloning and characterization of a member of the MST subfamily of Ste20-like kinases. *Gene*, 167, 303-6.
- CREQUER, A., PICARD, C., PATIN, E., D'AMICO, A., ABHYANKAR, A., MUNZER, M., DEBRE, M., ZHANG, S. Y., DE SAINT-BASILE, G., FISCHER, A., ABEL, L., ORTH, G., CASANOVA, J. L. & JOUANGUY, E. 2012. Inherited MST1 deficiency underlies susceptibility to EV-HPV infections. *PLoS One*, 7, e44010.
- D'ELIOS, M. M., AMEDEI, A., CAPPON, A., DEL PRETE, G. & DE BERNARD, M. 2007. The neutrophil-activating protein of *Helicobacter pylori* (HP-NAP) as an immune modulating agent. *FEMS Immunol Med Microbiol*, 50, 157-64.
- DALE, D. C., PERSON, R. E., BOLYARD, A. A., APRIKYAN, A. G., BOS, C., BONILLA, M. A., BOXER, L. A., KANNOURAKIS, G., ZEIDLER, C., WELTE, K., BENSON, K. F. & HORWITZ, M. 2000. Mutations in the gene encoding neutrophil elastase in congenital and cyclic neutropenia. *Blood*, 96, 2317-22.
- DANG, T. S., WILLET, J. D., GRIFFIN, H. R., MORGAN, N. V., O'BOYLE, G., ARKWRIGHT, P. D., HUGHES, S. M., ABINUN, M., TEE, L. J., BARGE, D., ENGELHARDT, K. R., JACKSON, M., CANT, A. J., MAHER, E. R., KOREF, M. S., REYNARD, L. N., ALI, S. & HAMBLETON, S. 2016. Defective Leukocyte Adhesion and Chemotaxis Contributes to Combined Immunodeficiency in Humans with Autosomal Recessive MST1 Deficiency. *J Clin Immunol*.
- DANGERFIELD, J., LARBI, K. Y., HUANG, M. T., DEWAR, A. & NOURSHARGH, S. 2002. PECAM-1 (CD31) homophilic interaction up-regulates alpha6beta1 on transmigrated neutrophils in vivo and plays a functional role in the ability of alpha6 integrins to mediate leukocyte migration through the perivascular basement membrane. *J Exp Med*, 196, 1201-11.
- DANGERFIELD, J. P., WANG, S. & NOURSHARGH, S. 2005. Blockade of alpha6 integrin inhibits IL-1beta- but not TNF-alpha-induced neutrophil transmigration in vivo. *J Leukoc Biol*, 77, 159-65.
- DE SOUZA, P. M., KANKAANRANTA, H., MICHAEL, A., BARNES, P. J., GIEMBYCZ, M. A. & LINDSAY, M. A. 2002. Caspase-catalyzed cleavage and activation of Mst1 correlates with eosinophil but not neutrophil apoptosis. *Blood*, 99, 3432-8.
- DONG, Q. G., BERNASCONI, S., LOSTAGLIO, S., DE CALMANOVICI, R. W., MARTIN-PADURA, I., BREVIARIO, F., GARLANDA, C., RAMPONI, S., MANTOVANI, A. &

- VECCHI, A. 1997. A general strategy for isolation of endothelial cells from murine tissues. Characterization of two endothelial cell lines from the murine lung and subcutaneous sponge implants. *Arterioscler Thromb Vasc Biol*, 17, 1599-604.
- DONG, Y., DU, X., YE, J., HAN, M., XU, T., ZHUANG, Y. & TAO, W. 2009. A cell-intrinsic role for Mst1 in regulating thymocyte egress. *J Immunol*, 183, 3865-72.
- DU, X., SHI, H., LI, J., DONG, Y., LIANG, J., YE, J., KONG, S., ZHANG, S., ZHONG, T., YUAN, Z., XU, T., ZHUANG, Y., ZHENG, B., GENG, J. G. & TAO, W. 2014. Mst1/Mst2 regulate development and function of regulatory T cells through modulation of Foxo1/Foxo3 stability in autoimmune disease. *J Immunol*, 192, 1525-35.
- DU, X., YU, A. & TAO, W. 2015. The non-canonical Hippo/Mst pathway in lymphocyte development and functions. *Acta Biochim Biophys Sin (Shanghai)*, 47, 60-4.
- FABBRI, M., DI MEGLIO, S., GAGLIANI, M. C., CONSONNI, E., MOLTENI, R., BENDER, J. R., TACCHETTI, C. & PARDI, R. 2005. Dynamic partitioning into lipid rafts controls the endo-exocytic cycle of the alphaL/beta2 integrin, LFA-1, during leukocyte chemotaxis. *Mol Biol Cell*, 16, 5793-803.
- FAUST, N., VARAS, F., KELLY, L. M., HECK, S. & GRAF, T. 2000. Insertion of enhanced green fluorescent protein into the lysozyme gene creates mice with green fluorescent granulocytes and macrophages. *Blood*, 96, 719-26.
- FROMMHOLD, D., KAMPHUES, A., HEPPEL, I., PRUENSTER, M., LUKIC, I. K., SOCHER, I., ZABLOTSKAYA, V., BUSCHMANN, K., LANGE-SPERANDIO, B., SCHYMEINSKY, J., RYSCHICH, E., POESCHL, J., KUPATT, C., NAWROTH, P. P., MOSER, M., WALZOG, B., BIERHAUS, A. & SPERANDIO, M. 2010. RAGE and ICAM-1 cooperate in mediating leukocyte recruitment during acute inflammation in vivo. *Blood*, 116, 841-9.
- FROMMHOLD, D., LUDWIG, A., BIXEL, M. G., ZARBOCK, A., BABUSHKINA, I., WEISSINGER, M., CAUWENBERGHS, S., ELLIES, L. G., MARTH, J. D., BECK-SICKINGER, A. G., SIXT, M., LANGE-SPERANDIO, B., ZERNECKE, A., BRANDT, E., WEBER, C., VESTWEBER, D., LEY, K. & SPERANDIO, M. 2008. Sialyltransferase ST3Gal-IV controls CXCR2-mediated firm leukocyte arrest during inflammation. *J Exp Med*, 205, 1435-46.
- GENG, J., SUN, X., WANG, P., ZHANG, S., WANG, X., WU, H., HONG, L., XIE, C., LI, X., ZHAO, H., LIU, Q., JIANG, M., CHEN, Q., ZHANG, J., LI, Y., SONG, S., WANG, H. R., ZHOU, R., JOHNSON, R. L., CHIEN, K. Y., LIN, S. C., HAN, J., AVRUCH, J., CHEN, L. & ZHOU, D. 2015. Kinases Mst1 and Mst2 positively regulate phagocytic induction of reactive oxygen species and bactericidal activity. *Nat Immunol*, 16, 1142-52.
- HALACLI, S. O., AYVAZ, D. C., SUN-TAN, C., ERMAN, B., UZ, E., YILMAZ, D. Y., OZGUL, K., TEZCAN, I. & SANAL, O. 2015. STK4 (MST1) deficiency in two siblings with autoimmune cytopenias: A novel mutation. *Clin Immunol*, 161, 316-23.
- HALAI, K., WHITEFORD, J., MA, B., NOURSHARGH, S. & WOODFIN, A. 2014. ICAM-2 facilitates luminal interactions between neutrophils and endothelial cells in vivo. *J Cell Sci*, 127, 620-9.
- HALDER, G. & JOHNSON, R. L. 2011. Hippo signaling: growth control and beyond. *Development*, 138, 9-22.

- HALLMANN, R., ZHANG, X., DI RUSSO, J., LI, L., SONG, J., HANNOCKS, M. J. & SOROKIN, L. 2015. The regulation of immune cell trafficking by the extracellular matrix. *Curr Opin Cell Biol*, 36, 54-61.
- HARFI, H. A., BRISMAR, J., HAINAU, B. & SABBAH, R. 1992. Partial albinism, immunodeficiency, and progressive white matter disease: a new primary immunodeficiency. *Allergy Proc*, 13, 321-8.
- HARTWELL, L. H., MORTIMER, R. K., CULOTTI, J. & CULOTTI, M. 1973. Genetic Control of the Cell Division Cycle in Yeast: V. Genetic Analysis of cdc Mutants. *Genetics*, 74, 267-86.
- HERRERO-TURRION, M. J., CALAFAT, J., JANSSEN, H., FUKUDA, M. & MOLLINEDO, F. 2008. Rab27a regulates exocytosis of tertiary and specific granules in human neutrophils. *J Immunol*, 181, 3793-803.
- HORWITZ, M., BENSON, K. F., PERSON, R. E., APRIKYAN, A. G. & DALE, D. C. 1999. Mutations in ELA2, encoding neutrophil elastase, define a 21-day biological clock in cyclic haematopoiesis. *Nat Genet*, 23, 433-6.
- HORWITZ, M. S., DUAN, Z., KORKMAZ, B., LEE, H. H., MEALIFFE, M. E. & SALIPANTE, S. J. 2007. Neutrophil elastase in cyclic and severe congenital neutropenia. *Blood*, 109, 1817-24.
- HUBER, A. R. & WEISS, S. J. 1989. Disruption of the subendothelial basement membrane during neutrophil diapedesis in an in vitro construct of a blood vessel wall. *J Clin Invest*, 83, 1122-36.
- HYUN, Y. M., SUMAGIN, R., SARANGI, P. P., LOMAKINA, E., OVERSTREET, M. G., BAKER, C. M., FOWELL, D. J., WAUGH, R. E., SARELIUS, I. H. & KIM, M. 2012. Uropod elongation is a common final step in leukocyte extravasation through inflamed vessels. *J Exp Med*, 209, 1349-62.
- JOHNSON, J. L., BRZEZINSKA, A. A., TOLMACHOVA, T., MUNAFO, D. B., ELLIS, B. A., SEABRA, M. C., HONG, H. & CATZ, S. D. 2010. Rab27a and Rab27b regulate neutrophil azurophilic granule exocytosis and NADPH oxidase activity by independent mechanisms. *Traffic*, 11, 533-47.
- JOHNSON, J. L., HONG, H., MONFREGOLA, J. & CATZ, S. D. 2011a. Increased survival and reduced neutrophil infiltration of the liver in Rab27a- but not Munc13-4-deficient mice in lipopolysaccharide-induced systemic inflammation. *Infect Immun*, 79, 3607-18.
- JOHNSON, J. L., HONG, H., MONFREGOLA, J., KIOSSES, W. B. & CATZ, S. D. 2011b. Munc13-4 restricts motility of Rab27a-expressing vesicles to facilitate lipopolysaccharide-induced priming of exocytosis in neutrophils. *J Biol Chem*, 286, 5647-56.
- JOHNSON, J. L., MONFREGOLA, J., NAPOLITANO, G., KIOSSES, W. B. & CATZ, S. D. 2012. Vesicular trafficking through cortical actin during exocytosis is regulated by the Rab27a effector JFC1/Slp1 and the RhoA-GTPase-activating protein Gem-interacting protein. *Mol Biol Cell*, 23, 1902-16.
- JOHNSON, R. & HALDER, G. 2014. The two faces of Hippo: targeting the Hippo pathway for regenerative medicine and cancer treatment. *Nat Rev Drug Discov*, 13, 63-79.
- JUNG, U. & LEY, K. 1997. Regulation of E-selectin, P-selectin, and intercellular adhesion molecule 1 expression in mouse cremaster muscle vasculature. *Microcirculation*, 4, 311-9.

- KATAGIRI, K., IMAMURA, M. & KINASHI, T. 2006. Spatiotemporal regulation of the kinase Mst1 by binding protein RAPL is critical for lymphocyte polarity and adhesion. *Nat Immunol*, 7, 919-28.
- KATAGIRI, K., KATAKAI, T., EBISUNO, Y., UEDA, Y., OKADA, T. & KINASHI, T. 2009. Mst1 controls lymphocyte trafficking and interstitial motility within lymph nodes. *EMBO J*, 28, 1319-31.
- KATAGIRI, K., MAEDA, A., SHIMONAKA, M. & KINASHI, T. 2003. RAPL, a Rap1-binding molecule that mediates Rap1-induced adhesion through spatial regulation of LFA-1. *Nat Immunol*, 4, 741-8.
- KATAGIRI, K., UEDA, Y., TOMIYAMA, T., YASUDA, K., TODA, Y., IKEHARA, S., NAKAYAMA, K. I. & KINASHI, T. 2011. Deficiency of Rap1-binding protein RAPL causes lymphoproliferative disorders through mislocalization of p27kip1. *Immunity*, 34, 24-38.
- KENNE, E., SOEHNLEIN, O., GENOVE, G., ROTZIUS, P., ERIKSSON, E. E. & LINDBOM, L. 2010. Immune cell recruitment to inflammatory loci is impaired in mice deficient in basement membrane protein laminin alpha4. *J Leukoc Biol*, 88, 523-8.
- KLEIN, C. 2011. Genetic defects in severe congenital neutropenia: emerging insights into life and death of human neutrophil granulocytes. *Annu Rev Immunol*, 29, 399-413.
- KLEIN, C., GRUDZIEN, M., APPASWAMY, G., GERMESHAUSEN, M., SANDROCK, I., SCHAFFER, A. A., RATHINAM, C., BOZTUG, K., SCHWINZER, B., REZAEI, N., BOHN, G., MELIN, M., CARLSSON, G., FADEEL, B., DAHL, N., PALMBLAD, J., HENTER, J. I., ZEIDLER, C., GRIMBACHER, B. & WELTE, K. 2007. HAX1 deficiency causes autosomal recessive severe congenital neutropenia (Kostmann disease). *Nat Genet*, 39, 86-92.
- KLEIN, C., PHILIPPE, N., LE DEIST, F., FRAITAG, S., PROST, C., DURANDY, A., FISCHER, A. & GRISCELLI, C. 1994. Partial albinism with immunodeficiency (Griscelli syndrome). *J Pediatr*, 125, 886-95.
- KODAKA, M. & HATA, Y. 2015. The mammalian Hippo pathway: regulation and function of YAP1 and TAZ. *Cell Mol Life Sci*, 72, 285-306.
- KOLACZKOWSKA, E. & KUBES, P. 2013. Neutrophil recruitment and function in health and inflammation. *Nat Rev Immunol*, 13, 159-75.
- KUSTERS, J. G., VAN VLIET, A. H. & KUIPERS, E. J. 2006. Pathogenesis of *Helicobacter pylori* infection. *Clin Microbiol Rev*, 19, 449-90.
- LACY, P. & EITZEN, G. 2008. Control of granule exocytosis in neutrophils. *Front Biosci*, 13, 5559-70.
- LAMMERMAN, T., AFONSO, P. V., ANGERMANN, B. R., WANG, J. M., KASTENMULLER, W., PARENT, C. A. & GERMAIN, R. N. 2013. Neutrophil swarms require LTB4 and integrins at sites of cell death in vivo. *Nature*, 498, 371-5.
- LAMMERMAN, T., BADER, B. L., MONKLEY, S. J., WORBS, T., WEDLICH-SOLDNER, R., HIRSCH, K., KELLER, M., FORSTER, R., CRITCHLEY, D. R., FASSLER, R. & SIXT, M. 2008. Rapid leukocyte migration by integrin-independent flowing and squeezing. *Nature*, 453, 51-5.
- LE CABEC, V., COWLAND, J. B., CALAFAT, J. & BORREGAARD, N. 1996. Targeting of proteins to granule subsets is determined by timing and not by sorting: The

- specific granule protein NGAL is localized to azurophil granules when expressed in HL-60 cells. *Proc Natl Acad Sci U S A*, 93, 6454-7.
- LEFORT, C. T. & LEY, K. 2012. Neutrophil arrest by LFA-1 activation. *Front Immunol*, 3, 157.
- LEFORT, C. T., ROSSAINT, J., MOSER, M., PETRICH, B. G., ZARBOCK, A., MONKLEY, S. J., CRITCHLEY, D. R., GINSBERG, M. H., FASSLER, R. & LEY, K. 2012. Distinct roles for talin-1 and kindlin-3 in LFA-1 extension and affinity regulation. *Blood*, 119, 4275-82.
- LERMAN, Y. V., LIM, K., HYUN, Y. M., FALKNER, K. L., YANG, H., PIETROPAOLI, A. P., SONNENBERG, A., SARANGI, P. P. & KIM, M. 2014. Sepsis lethality via exacerbated tissue infiltration and TLR-induced cytokine production by neutrophils is integrin $\alpha 3 \beta 1$ -dependent. *Blood*, 124, 3515-23.
- LEY, K., BULLARD, D. C., ARBONES, M. L., BOSSE, R., VESTWEBER, D., TEDDER, T. F. & BEAUDET, A. L. 1995. Sequential contribution of L- and P-selectin to leukocyte rolling in vivo. *J Exp Med*, 181, 669-75.
- LU, L., LI, Y., KIM, S. M., BOSSUYT, W., LIU, P., QIU, Q., WANG, Y., HALDER, G., FINEGOLD, M. J., LEE, J. S. & JOHNSON, R. L. 2010. Hippo signaling is a potent in vivo growth and tumor suppressor pathway in the mammalian liver. *Proc Natl Acad Sci U S A*, 107, 1437-42.
- LUCAS, E. P., KHANAL, I., GASPAR, P., FLETCHER, G. C., POLESELLO, C., TAPON, N. & THOMPSON, B. J. 2013. The Hippo pathway polarizes the actin cytoskeleton during collective migration of *Drosophila* border cells. *J Cell Biol*, 201, 875-85.
- MAMDOUH, Z., CHEN, X., PIERINI, L. M., MAXFIELD, F. R. & MULLER, W. A. 2003. Targeted recycling of PECAM from endothelial surface-connected compartments during diapedesis. *Nature*, 421, 748-53.
- MAMDOUH, Z., MIKHAILOV, A. & MULLER, W. A. 2009. Transcellular migration of leukocytes is mediated by the endothelial lateral border recycling compartment. *J Exp Med*, 206, 2795-808.
- MAYADAS, T. N., CULLERE, X. & LOWELL, C. A. 2014. The multifaceted functions of neutrophils. *Annu Rev Pathol*, 9, 181-218.
- MAYADAS, T. N., JOHNSON, R. C., RAYBURN, H., HYNES, R. O. & WAGNER, D. D. 1993. Leukocyte rolling and extravasation are severely compromised in P selectin-deficient mice. *Cell*, 74, 541-54.
- MCEVER, R. P. 2015. Selectins: initiators of leucocyte adhesion and signalling at the vascular wall. *Cardiovasc Res*, 107, 331-9.
- MIYANAGA, A., MASUDA, M., TSUTA, K., KAWASAKI, K., NAKAMURA, Y., SAKUMA, T., ASAMURA, H., GEMMA, A. & YAMADA, T. 2015. Hippo pathway gene mutations in malignant mesothelioma: revealed by RNA and targeted exon sequencing. *J Thorac Oncol*, 10, 844-51.
- MOCSAI, A., LIGETI, E., LOWELL, C. A. & BERTON, G. 1999. Adhesion-dependent degranulation of neutrophils requires the Src family kinases Fgr and Hck. *J Immunol*, 162, 1120-6.
- MONFREGOLA, J., JOHNSON, J. L., MEIJLER, M. M., NAPOLITANO, G. & CATZ, S. D. 2012. MUNC13-4 protein regulates the oxidative response and is essential for phagosomal maturation and bacterial killing in neutrophils. *J Biol Chem*, 287, 44603-18.

- MONTECUCCO, C. & RAPPUOLI, R. 2001. Living dangerously: how *Helicobacter pylori* survives in the human stomach. *Nat Rev Mol Cell Biol*, 2, 457-66.
- MOU, F., PRASKOVA, M., XIA, F., VAN BUREN, D., HOCK, H., AVRUCH, J. & ZHOU, D. 2012. The Mst1 and Mst2 kinases control activation of rho family GTPases and thymic egress of mature thymocytes. *J Exp Med*, 209, 741-59.
- MULLER, W. A. 2015. The regulation of transendothelial migration: new knowledge and new questions. *Cardiovasc Res*, 107, 310-20.
- MULLER, W. A. 2016. Localized signals that regulate transendothelial migration. *Curr Opin Immunol*, 38, 24-9.
- MUNAFO, D. B., JOHNSON, J. L., ELLIS, B. A., RUTSCHMANN, S., BEUTLER, B. & CATZ, S. D. 2007. Rab27a is a key component of the secretory machinery of azurophilic granules in granulocytes. *Biochem J*, 402, 229-39.
- NEHME, N. T., PACHLOPNIK SCHMID, J., DEBEURME, F., ANDRE-SCHMUTZ, I., LIM, A., NITSCHKE, P., RIEUX-LAUCAT, F., LUTZ, P., PICARD, C., MAHLAOU, N., FISCHER, A. & DE SAINT BASILE, G. 2012. MST1 mutations in autosomal recessive primary immunodeficiency characterized by defective naive T-cell survival. *Blood*, 119, 3458-68.
- NIMMO, E. R., PRENDERGAST, J. G., ALDHOUS, M. C., KENNEDY, N. A., HENDERSON, P., DRUMMOND, H. E., RAMSAHOYE, B. H., WILSON, D. C., SEMPLE, C. A. & SATSANGI, J. 2012. Genome-wide methylation profiling in Crohn's disease identifies altered epigenetic regulation of key host defense mechanisms including the Th17 pathway. *Inflamm Bowel Dis*, 18, 889-99.
- NISHIKIMI, A., ISHIHARA, S., OZAWA, M., ETOH, K., FUKUDA, M., KINASHI, T. & KATAGIRI, K. 2014. Rab13 acts downstream of the kinase Mst1 to deliver the integrin LFA-1 to the cell surface for lymphocyte trafficking. *Sci Signal*, 7, ra72.
- NOURSHARGH, S. & ALON, R. 2014. Leukocyte migration into inflamed tissues. *Immunity*, 41, 694-707.
- NOURSHARGH, S., HORDIJK, P. L. & SIXT, M. 2010. Breaching multiple barriers: leukocyte motility through venular walls and the interstitium. *Nat Rev Mol Cell Biol*, 11, 366-78.
- NUSSBAUM, C., GLONING, A., PRUENSTER, M., FROMMHOLD, D., BIERSCHEK, S., GENZEL-BOROVICZENY, O., VON ANDRIAN, U. H., QUACKENBUSH, E. & SPERANDIO, M. 2013. Neutrophil and endothelial adhesive function during human fetal ontogeny. *J Leukoc Biol*, 93, 175-84.
- OH, S., LEE, D., KIM, T., KIM, T. S., OH, H. J., HWANG, C. Y., KONG, Y. Y., KWON, K. S. & LIM, D. S. 2009. Crucial role for Mst1 and Mst2 kinases in early embryonic development of the mouse. *Mol Cell Biol*, 29, 6309-20.
- PHILLIPSON, M., HEIT, B., COLARUSSO, P., LIU, L., BALLANTYNE, C. M. & KUBES, P. 2006. Intraluminal crawling of neutrophils to emigration sites: a molecularly distinct process from adhesion in the recruitment cascade. *J Exp Med*, 203, 2569-75.
- PIVOT-PAJOT, C., VAROQUEAUX, F., DE SAINT BASILE, G. & BOURGOIN, S. G. 2008. Munc13-4 regulates granule secretion in human neutrophils. *J Immunol*, 180, 6786-97.
- POON, I. K., CHIU, Y. H., ARMSTRONG, A. J., KINCHEN, J. M., JUNCADILLA, I. J., BAYLISS, D. A. & RAVICHANDRAN, K. S. 2014. Unexpected link between an antibiotic, pannexin channels and apoptosis. *Nature*, 507, 329-34.

- PROEBSTL, D., VOISIN, M. B., WOODFIN, A., WHITEFORD, J., D'ACQUISTO, F., JONES, G. E., ROWE, D. & NOURSHARGH, S. 2012. Pericytes support neutrophil subendothelial cell crawling and breaching of venular walls in vivo. *J Exp Med*, 209, 1219-34.
- PRUENSTER, M., KURZ, A. R., CHUNG, K. J., CAO-EHLKER, X., BIEBER, S., NUSSBAUM, C. F., BIRSCHENK, S., EGGERSMANN, T. K., ROHWEDDER, I., HEINIG, K., IMMLER, R., MOSER, M., KOEDEL, U., GRAN, S., MCEVER, R. P., VESTWEBER, D., VERSCHOOR, A., LEANDERSON, T., CHAVAKIS, T., ROTH, J., VOGL, T. & SPERANDIO, M. 2015. Extracellular MRP8/14 is a regulator of beta2 integrin-dependent neutrophil slow rolling and adhesion. *Nat Commun*, 6, 6915.
- QIN, F., TIAN, J., ZHOU, D. & CHEN, L. 2013. Mst1 and Mst2 kinases: regulations and diseases. *Cell Biosci*, 3, 31.
- REHBERG, M., KROMBACH, F., POHL, U. & DIETZEL, S. 2011. Label-free 3D visualization of cellular and tissue structures in intact muscle with second and third harmonic generation microscopy. *PLoS One*, 6, e28237.
- REN, J., WEN, L., GAO, X., JIN, C., XUE, Y. & YAO, X. 2009. DOG 1.0: illustrator of protein domain structures. *Cell Res*, 19, 271-3.
- RORVIG, S., HONORE, C., LARSSON, L. I., OHLSSON, S., PEDERSEN, C. C., JACOBSEN, L. C., COWLAND, J. B., GARRED, P. & BORREGAARD, N. 2009. Ficolin-1 is present in a highly mobilizable subset of human neutrophil granules and associates with the cell surface after stimulation with fMLP. *J Leukoc Biol*, 86, 1439-49.
- ROWE, R. G. & WEISS, S. J. 2008. Breaching the basement membrane: who, when and how? *Trends Cell Biol*, 18, 560-74.
- SACHS, G., WEEKS, D. L., MELCHERS, K. & SCOTT, D. R. 2003. The gastric biology of *Helicobacter pylori*. *Annu Rev Physiol*, 65, 349-69.
- SALOJIN, K. V., HAMMAN, B. D., CHANG, W. C., JHAVER, K. G., AL-SHAMI, A., CRISOSTOMO, J., WILKINS, C., DIGEORGE-FOUSHEE, A. M., ALLEN, J., PATEL, N., GOPINATHAN, S., ZHOU, J., NOURALDEEN, A., JESSOP, T. C., BAGDANOFF, J. T., AUGERI, D. J., READ, R., VOGEL, P., SWAFFIELD, J., WILSON, A., PLATT, K. A., CARSON, K. G., MAIN, A., ZAMBROWICZ, B. P. & ORAVECZ, T. 2014. Genetic deletion of Mst1 alters T cell function and protects against autoimmunity. *PLoS One*, 9, e98151.
- SCHAFFER, A. A. & KLEIN, C. 2013. Animal models of human granulocyte diseases. *Hematol Oncol Clin North Am*, 27, 129-48, ix.
- SCHINDELIN, J., ARGANDA-CARRERAS, I., FRISE, E., KAYNIG, V., LONGAIR, M., PIETZSCH, T., PREIBISCH, S., RUEDEN, C., SAALFELD, S., SCHMID, B., TINEVEZ, J. Y., WHITE, D. J., HARTENSTEIN, V., ELICEIRI, K., TOMANCAK, P. & CARDONA, A. 2012. Fiji: an open-source platform for biological-image analysis. *Nat Methods*, 9, 676-82.
- SCHMIDT, S., MOSER, M. & SPERANDIO, M. 2013. The molecular basis of leukocyte recruitment and its deficiencies. *Mol Immunol*, 55, 49-58.
- SENGELOV, H., FOLLIN, P., KJELDSSEN, L., LOLLIKE, K., DAHLGREN, C. & BORREGAARD, N. 1995. Mobilization of granules and secretory vesicles during in vivo exudation of human neutrophils. *J Immunol*, 154, 4157-65.
- SENGELOV, H., KJELDSSEN, L. & BORREGAARD, N. 1993. Control of exocytosis in early neutrophil activation. *J Immunol*, 150, 1535-43.

- SHESHACHALAM, A., SRIVASTAVA, N., MITCHELL, T., LACY, P. & EITZEN, G. 2014. Granule protein processing and regulated secretion in neutrophils. *Front Immunol*, 5, 448.
- SIXT, M., ENGELHARDT, B., PAUSCH, F., HALLMANN, R., WENDLER, O. & SOROKIN, L. M. 2001. Endothelial cell laminin isoforms, laminins 8 and 10, play decisive roles in T cell recruitment across the blood-brain barrier in experimental autoimmune encephalomyelitis. *J Cell Biol*, 153, 933-46.
- SMITH, M. L., OLSON, T. S. & LEY, K. 2004. CXCR2- and E-selectin-induced neutrophil arrest during inflammation in vivo. *J Exp Med*, 200, 935-9.
- SOROKIN, L. 2010. The impact of the extracellular matrix on inflammation. *Nat Rev Immunol*, 10, 712-23.
- SOROKIN, L. M., PAUSCH, F., FRIESER, M., KROGER, S., OHAGE, E. & DEUTZMANN, R. 1997. Developmental regulation of the laminin alpha5 chain suggests a role in epithelial and endothelial cell maturation. *Dev Biol*, 189, 285-300.
- SUERBAUM, S. & MICHETTI, P. 2002. Helicobacter pylori infection. *N Engl J Med*, 347, 1175-86.
- THOMPSON, B. J. & SAHAI, E. 2015. MST kinases in development and disease. *J Cell Biol*, 210, 871-82.
- THOMPSON, R. D., NOBLE, K. E., LARBI, K. Y., DEWAR, A., DUNCAN, G. S., MAK, T. W. & NOURSHARGH, S. 2001. Platelet-endothelial cell adhesion molecule-1 (PECAM-1)-deficient mice demonstrate a transient and cytokine-specific role for PECAM-1 in leukocyte migration through the perivascular basement membrane. *Blood*, 97, 1854-60.
- TOMIYAMA, T., UEDA, Y., KATAKAI, T., KONDO, N., OKAZAKI, K. & KINASHI, T. 2013. Antigen-specific suppression and immunological synapse formation by regulatory T cells require the Mst1 kinase. *PLoS One*, 8, e73874.
- TOONEN, R. F. & VERHAGE, M. 2003. Vesicle trafficking: pleasure and pain from SM genes. *Trends Cell Biol*, 13, 177-86.
- TRAMBAS, C. M. & GRIFFITHS, G. M. 2003. Delivering the kiss of death. *Nat Immunol*, 4, 399-403.
- UEDA, Y., KATAGIRI, K., TOMIYAMA, T., YASUDA, K., HABIRO, K., KATAKAI, T., IKEHARA, S., MATSUMOTO, M. & KINASHI, T. 2012. Mst1 regulates integrin-dependent thymocyte trafficking and antigen recognition in the thymus. *Nat Commun*, 3, 1098.
- URIARTE, S. M., POWELL, D. W., LUERMAN, G. C., MERCHANT, M. L., CUMMINS, T. D., JOG, N. R., WARD, R. A. & MCLEISH, K. R. 2008. Comparison of proteins expressed on secretory vesicle membranes and plasma membranes of human neutrophils. *J Immunol*, 180, 5575-81.
- VAZQUEZ-MARTINEZ, R. & MALAGON, M. M. 2011. Rab proteins and the secretory pathway: the case of rab18 in neuroendocrine cells. *Front Endocrinol (Lausanne)*, 2, 1.
- VESTWEBER, D. 2015. How leukocytes cross the vascular endothelium. *Nat Rev Immunol*, 15, 692-704.
- VOISIN, M. B., PROBSTL, D. & NOURSHARGH, S. 2010. Venular basement membranes ubiquitously express matrix protein low-expression regions: characterization in multiple tissues and remodeling during inflammation. *Am J Pathol*, 176, 482-95.

- VOISIN, M. B., WOODFIN, A. & NOURSHARGH, S. 2009. Monocytes and neutrophils exhibit both distinct and common mechanisms in penetrating the vascular basement membrane in vivo. *Arterioscler Thromb Vasc Biol*, 29, 1193-9.
- WANG, S., DANGERFIELD, J. P., YOUNG, R. E. & NOURSHARGH, S. 2005. PECAM-1, alpha6 integrins and neutrophil elastase cooperate in mediating neutrophil transmigration. *J Cell Sci*, 118, 2067-76.
- WANG, S., VOISIN, M. B., LARBI, K. Y., DANGERFIELD, J., SCHEIERMANN, C., TRAN, M., MAXWELL, P. H., SOROKIN, L. & NOURSHARGH, S. 2006. Venular basement membranes contain specific matrix protein low expression regions that act as exit points for emigrating neutrophils. *J Exp Med*, 203, 1519-32.
- WATERMAN, M., XU, W., STEMPAK, J. M., MILGROM, R., BERNSTEIN, C. N., GRIFFITHS, A. M., GREENBERG, G. R., STEINHART, A. H. & SILVERBERG, M. S. 2011. Distinct and overlapping genetic loci in Crohn's disease and ulcerative colitis: correlations with pathogenesis. *Inflamm Bowel Dis*, 17, 1936-42.
- WATSON, R. L., BUCK, J., LEVIN, L. R., WINGER, R. C., WANG, J., ARASE, H. & MULLER, W. A. 2015. Endothelial CD99 signals through soluble adenylyl cyclase and PKA to regulate leukocyte transendothelial migration. *J Exp Med*, 212, 1021-41.
- WEGMANN, F., PETRI, B., KHANDOGA, A. G., MOSER, C., KHANDOGA, A., VOLKERY, S., LI, H., NASDALA, I., BRANDAU, O., FASSLER, R., BUTZ, S., KROMBACH, F. & VESTWEBER, D. 2006. ESAM supports neutrophil extravasation, activation of Rho, and VEGF-induced vascular permeability. *J Exp Med*, 203, 1671-7.
- WENINGER, W., BIRO, M. & JAIN, R. 2014. Leukocyte migration in the interstitial space of non-lymphoid organs. *Nat Rev Immunol*, 14, 232-46.
- WESSEL, F., WINDERLICH, M., HOLM, M., FRYE, M., RIVERA-GALDOS, R., VOCKEL, M., LINNEPE, R., IPE, U., STADTMANN, A., ZARBOCK, A., NOTTEBAUM, A. F. & VESTWEBER, D. 2014. Leukocyte extravasation and vascular permeability are each controlled in vivo by different tyrosine residues of VE-cadherin. *Nat Immunol*, 15, 223-30.
- WOLF, K., ALEXANDER, S., SCHACHT, V., COUSSENS, L. M., VON ANDRIAN, U. H., VAN RHEENEN, J., DERYUGINA, E. & FRIEDL, P. 2009. Collagen-based cell migration models in vitro and in vivo. *Semin Cell Dev Biol*, 20, 931-41.
- WOODFIN, A., REICHEL, C. A., KHANDOGA, A., CORADA, M., VOISIN, M. B., SCHEIERMANN, C., HASKARD, D. O., DEJANA, E., KROMBACH, F. & NOURSHARGH, S. 2007. JAM-A mediates neutrophil transmigration in a stimulus-specific manner in vivo: evidence for sequential roles for JAM-A and PECAM-1 in neutrophil transmigration. *Blood*, 110, 1848-56.
- WOODFIN, A., VOISIN, M. B., BEYRAU, M., COLOM, B., CAILLE, D., DIAPOULI, F. M., NASH, G. B., CHAVAKIS, T., ALBELDA, S. M., RAINGER, G. E., MEDA, P., IMHOF, B. A. & NOURSHARGH, S. 2011. The junctional adhesion molecule JAM-C regulates polarized transendothelial migration of neutrophils in vivo. *Nat Immunol*, 12, 761-9.
- WOODFIN, A., VOISIN, M. B., IMHOF, B. A., DEJANA, E., ENGELHARDT, B. & NOURSHARGH, S. 2009. Endothelial cell activation leads to neutrophil transmigration as supported by the sequential roles of ICAM-2, JAM-A, and PECAM-1. *Blood*, 113, 6246-57.

- WU, C., IVARS, F., ANDERSON, P., HALLMANN, R., VESTWEBER, D., NILSSON, P., ROBENEK, H., TRYGGVASON, K., SONG, J., KORPOS, E., LOSER, K., BEISSERT, S., GEORGES-LABOUESSE, E. & SOROKIN, L. M. 2009. Endothelial basement membrane laminin alpha5 selectively inhibits T lymphocyte extravasation into the brain. *Nat Med*, 15, 519-27.
- XU, X., JAEGER, E. R., WANG, X., LAGLER-FERREZ, E., BATALOV, S., MATHIS, N. L., WILTSHIRE, T., WALKER, J. R., COOKE, M. P., SAUER, K. & HUANG, Y. H. 2014. Mst1 directs Myosin IIa partitioning of low and higher affinity integrins during T cell migration. *PLoS One*, 9, e105561.
- YANG, W. H., NUSSBAUM, C., GREWAL, P. K., MARTH, J. D. & SPERANDIO, M. 2012. Coordinated roles of ST3Gal-VI and ST3Gal-IV sialyltransferases in the synthesis of selectin ligands. *Blood*, 120, 1015-26.
- YOUNG, R. E., VOISIN, M. B., WANG, S., DANGERFIELD, J. & NOURSHARGH, S. 2007. Role of neutrophil elastase in LTB4-induced neutrophil transmigration in vivo assessed with a specific inhibitor and neutrophil elastase deficient mice. *Br J Pharmacol*, 151, 628-37.
- YOUSIF, L. F., DI RUSSO, J. & SOROKIN, L. 2013. Laminin isoforms in endothelial and perivascular basement membranes. *Cell Adh Migr*, 7, 101-10.
- YU, F. X., ZHAO, B. & GUAN, K. L. 2015. Hippo Pathway in Organ Size Control, Tissue Homeostasis, and Cancer. *Cell*, 163, 811-28.
- ZHANG, Y., TANG, W., ZHANG, H., NIU, X., XU, Y., ZHANG, J., GAO, K., PAN, W., BOGGON, T. J., TOOMRE, D., MIN, W. & WU, D. 2013. A network of interactions enables CCM3 and STK24 to coordinate UNC13D-driven vesicle exocytosis in neutrophils. *Dev Cell*, 27, 215-26.
- ZHOU, D., CONRAD, C., XIA, F., PARK, J. S., PAYER, B., YIN, Y., LAUWERS, G. Y., THASLER, W., LEE, J. T., AVRUCH, J. & BARDEESY, N. 2009. Mst1 and Mst2 maintain hepatocyte quiescence and suppress hepatocellular carcinoma development through inactivation of the Yap1 oncogene. *Cancer Cell*, 16, 425-38.
- ZHOU, D., MEDOFF, B. D., CHEN, L., LI, L., ZHANG, X. F., PRASKOVA, M., LIU, M., LANDRY, A., BLUMBERG, R. S., BOUSSIOTIS, V. A., XAVIER, R. & AVRUCH, J. 2008. The Nore1B/Mst1 complex restrains antigen receptor-induced proliferation of naive T cells. *Proc Natl Acad Sci U S A*, 105, 20321-6.

8 ABBREVIATION LIST

AA	Amino acid
ANOVA	Analysis of variance
BB	Brucella Broth
BM	Basement membrane
BSA	Bovine serum albumin
CCM3	cerebral cavernos malformations 3
CD99L2	CD99 antigen-like protein 2
CTL	Cytotoxic T lymphocytes
CXCL	CXC chemokine ligand
CXCR	CXC chemokine receptor
DENND1C	DENN domain containing 1C
ESAM-1	Endothelial cell-selective adhesion molecule 1
ESL1	E-selectin ligand 1
FACS	Fluorescence activated cell sorting
fMLP	<i>N</i> -Formylmethionyl-leucyl-phenylalanine
FOV	Field of view
GlyCAM	Glycosylation-dependent cell adhesion molecule
GS2	Griscelli syndrome type 2
GTP	Guanosine triphosphate
Hpo	Hippo
ICAM1	Intercellular adhesion molecule 1
ICAM2	Intercellular adhesion molecule 2
ID	Inner diameter
IL-1 β	Interleukine-1 β
JAM	Junctional adhesion molecule
KRS2	Kinase responsive to stress 2
LAD	Leukocyte adhesion deficiency
LATS	Large tumor suppressor
LBRC	Lateral border recycling compartment
LBRC	Lateral border recycling compartment
LER	Low expression region
LFA-1	Lymphocyte function-associated antigen 1 (CD18/CD11a; α L β 2)
LTB4	Leukotriene B4
Mac1	Macrophage-1 antigen (CD11b/CD18, α M β 2)

MALT	Mucosa-associated lymphoid tissue
MFI	Mean fluorescence intensity
MMP	Matrix metalloproteases
MPO	myeloperoxidase
MST	Mammalian sterile 20-like kinase
MU	
NE	Neutrophil elastase
NET	Neutrophil extracellular traps
NK cells	Natural killer cells
ORCA	
PBS	Phosphate-buffered saline
PCR	Polymerase chain reaction
PECAM	Platelet endothelial cell adhesion molecule
PKA	
PSGL-1	P-selectin glycoprotein ligand 1
PVDF	Polyvinylidenfluorid
PVR	Poliovirus receptor
Rab	Ras-related in brain
RAPL	
RHOG	Ras homology Growth-related
RIPA	Radioimmunoprecipitation assay buffer
RNA	Ribonucleic acid
ROS	Reactive oxygen species
RT	Room temperature
SARAH	Sav/Rassf/Hpo
Slp1	Synaptotagmin-like protein 1
SNARE	Soluble N-ethylmaleimide-sensitive factor attachment protein receptor
SNP	Single nucleotide polymorphisms
STK	Serine/threonine protein kinase
TBS	Tris-buffered saline
TEM	Transendothelial migration
TNF- α	Tumornekrosefaktor- α
t-SNARE	Target SNARE
VAMP	vesicle-associated membrane protein 2
VCAM1	Vascular cell adhesion molecule 1
VE-cadherin	Vascular endothelial-cadherin
VE-PTP	Vascular endothelial protein tyrosine phosphatase
VLA-3	Very late antigen 3 ($\alpha 3\beta 1$, CD49c/CD29)

VLA-6	Very late antigen 6 ($\alpha 6\beta 1$, CD49f/CD29)
v-SNARE	Vesicle SNARE
WT	Wild type
YAP	Yes-associated protein
YSK1	Yeast Sps1/Ste20-related Kinase 1

9 ACKNOWLEDGMENTS

During my PhD study, I benefited from the knowledge, support, helpful discussions, advices and collaboration of many excellent researchers and colleagues around me in the Walter Brendel Center for Experimental Medicine and especially in the SFB914. This thesis would not have been possible without the help and support and I would like to express my sincere gratitude.

First of all, I would like to thank my supervisor Prof.Dr.med. Markus Sperandio for giving me the opportunity to study this intriguing project. I would like to thank him for his supervision, encouragement, enthusiasm and support during the entire period of my PhD study. Importantly, he gave me the freedom to follow my own ideas.

Second, I want to thank my thesis advisory committee, Prof.Dr.rer.nat. Kirsten Lauber, PD Dr.rer.nat. Markus Moser and PD Dr.rer.physiol. Melanie Laschinger for fruitful discussions and very helpful brainstorming.

Third, I am specially and truly thankful to Dr.rer.nat. Monika Prünster for her invaluable supervision and constant support throughout my entire PhD thesis. I really learned a lot from her in many aspects.

I would like to acknowledge the SFB914 and the associated IRTG for excellent professional training to broaden my horizon and for funding. A special 'thank you' goes to Dr.rer.nat. Verena Kochan, for helping me to manage the bureaucracy.

I especially have to thank both, Dr.rer.nat. Monika Prünster and Dr.rer.nat. Ina Rohwedder for incredible insightful brainstorming and intensive discussions about everything during my PhD study.

Thank you to all group members, Roland Immler M.Sc., Dr.rer.nat. Kristina Heinig, Dr.med. Andreas Margraf, Dr.med. Claudia Nussbaum and also the students, Johannes

R. Wiessner and Gabriel Gouveia for the support, advice and good atmosphere. I also want to extend my thanks to all the members of the Walter Brendel Center. It is a pleasure working with you.

Furthermore, I would like to thank Susanne Bierschenk and Nadine Schmidt for excellent technical assistance, administrative support and for their help with experiments.

I also want to thank PD Dr.rer.nat. Steffen Dietzel, for introducing and helping me with the multi photon laser scanning microscope.

Last but not least I want to thank my family. I'm especially grateful to my mother, Christina Fischer-Titz. Thank you for your support, without you I would have never gotten to this point. And to Michael Forsthuber, thank you for your never ending support, encouragement and patience.

10 APPENDIX

10.1 PUBLICATIONS

Publications

1. **Kurz AR**, Pruenster P, Rohwedder I, Schäfer K, Breithaupt U, Gouveia G, Nussbaum C, Immler R, Wiessner JR, Margraf A; Lim DS, Walzog B, Dietzel S, Moser M, Klein C, Vestweber D, Haas R, Sperandio M. MST1-dependent vesicle trafficking regulates neutrophil transmigration through the vascular basement membrane. *In revision for publication in Journal of Clinical Investigation*.
2. Kruse C, **Kurz AR**, Pálfi K, Humbert PO, Sperandio M, Brandes RP, Fork C, Michaelis UR. (2015) Polarity Protein Scrib Facilitates Endothelial Inflammatory Signaling. *Arterioscler Thromb Vasc Biol.* 35(9):1954-62.
3. Pruenster M, **Kurz AR**, Chung KJ, Cao-Ehlker X, Bieber S, Nussbaum CF, Bierschenk S, Eggersmann TK, Rohwedder I, Heinig K, Immler R, Moser M, Koedel U, Gran S, McEver RP, Vestweber D, Verschoor A, Leanderson T, Chavakis T, Roth J, Vogl T, Sperandio M. (2015) Extracellular MRP8/14 is a regulator of $\beta 2$ integrin-dependent neutrophil slow rolling and adhesion. *Nat Commun.* 6:6915
4. Zuchtriegel G, Uhl B, Hessenauer ME, **Kurz AR**, Rehberg M, Lauber K, Krombach F, Reichel CA. (2015) Spatiotemporal expression dynamics of selectins govern the sequential extravasation of neutrophils and monocytes in the acute inflammatory response. *Arterioscler Thromb Vasc Biol.* 35(4):899-910.
5. Sperandio M, Quackenbush EJ, Sushkova N, Altstätter J, Nussbaum C, Schmid S, Pruenster M, **Kurz AR**, Margraf A, Steppner A, Schweiger N, Borsig L, Boros I, Krajewski N, Genzel-Boroviczeny O, Jeschke U, Frommhold D, von Andrian UH. (2013) Ontogenetic regulation of leukocyte recruitment in mouse yolk sac vessels. *Blood.* 121(21):e118-28

Scientific Presentations

09/2015	Scientific Retreat of SFB914, Villa Vigoni, Italy (Oral Presentation)
11/2014	Scientific Retreat of IRTG914, Günzburg, Germany (Oral Presentation)
07/2014	Summer Symposium of SFB914 (Oral presentation)
09/2013	World Congress on Inflammation, Natal, Brazil (Poster Presentation)
04/2013	47th Annual ESCI Meeting, Phagocyte workshop (Oral Presentation)
03/2013	Scientific Retreat of SFB914, Obergurgl, Austria (Poster Presentation)
10/2012	Scientific Retreat of IRTG914, San Servolo, Italy (Oral Presentation)
02/2012	Scientific Retreat of SFB914, Ringberg, Germany (Poster Presentation)

10.2 MANUSCRIPT

MST1-dependent vesicle trafficking regulates neutrophil transmigration through the vascular basement membrane

Angela R M Kurz¹, Monika Pruenster¹, Ina Rohwedder¹, Kerstin Schäfer², Ute Breithaupt³, Gabriel Gouveia^{1,4}, Claudia Nussbaum^{1,5}, Roland Immler¹, Johannes R Wiessner¹, Andreas Margraf¹, Dae-Sik Lim⁶, Barbara Walzog¹, Steffen Dietzel¹, Markus Moser⁷, Christoph Klein⁵, Dietmar Vestweber², Rainer Haas³ and Markus Sperandio¹

¹Walter-Brendel Center of Experimental Medicine, Ludwig Maximilians University Munich, Munich, Germany

²Department of Vascular Cell Biology, Max Planck Institute for Molecular Biomedicine, Münster, Germany

³Max von Pettenkofer-Institute for Hygiene and Medical Microbiology, Ludwig Maximilians University Munich, Munich, Germany

⁴CAPES Foundation, Ministry of Education of Brazil, Brasilia, Brazil

⁵Dr. Von Hauner Children's Hospital, Ludwig Maximilians University Munich, Munich, Germany

⁶Department of Biological Sciences, Biomedical Research Center, Korea Advanced Institute of Science and Technology, Daejeon, Korea

⁷Department of Molecular Medicine, Max Planck Institute of Biochemistry, Martinsried, Germany

Abstract: 139 words

Length: 9029 words

Running title: MST1 and neutrophil transmigration

Abstract

Neutrophils need to penetrate the perivascular basement membrane for successful extravasation into inflamed tissue, a process only incompletely understood. Here, we show that mammalian sterile 20-like kinase 1 (MST1) is a critical regulator of neutrophil extravasation during inflammation. We observed that *Mst1*-deficient (*Mst1*^{-/-}) neutrophils persisted between the endothelium and the basement membrane of inflamed murine cremaster muscle venules, unable to migrate into the inflamed tissue. *Mst1*^{-/-} neutrophils also failed to extravasate from gastric submucosal vessels in a murine *Helicobacter pylori* infection model. Mechanistically, impaired extravasation of *Mst1*^{-/-} neutrophils was accompanied by defective translocation of VLA-3, VLA-6, and neutrophil elastase from intracellular vesicles to the neutrophil surface, a requirement for neutrophils to penetrate the basement membrane. Together, these findings highlight an unexpected role of MST1 in neutrophil extravasation and explain the severe immune defect observed in patients with MST1 deficiency.

Introduction

Recruitment of neutrophils from the intravascular compartment to sites of inflammation is a fundamental process during the innate immune response. The process follows a well-defined cascade of events, including neutrophil capture and rolling, firm adhesion, crawling, extravasation and migration into inflamed tissue (Nourshargh and Alon, 2014). Although most of the recruitment steps have been thoroughly studied in the past (Kolaczowska and Kubes, 2013), the precise mechanism of neutrophil transmigration across venular walls and penetration of the perivascular basement membrane (BM) remain elusive (Hallmann et al., 2015, Rowe and Weiss, 2008, Sorokin, 2010, Muller, 2016). Once neutrophils have migrated through the endothelial layer, they are primed for subsequent penetration of the endothelial BM (Bixel et al., 2010, Thompson et al., 2001, Wegmann et al., 2006) at sites that express low levels of laminin 511 (Sixt et al., 2001, Wu et al., 2009, Kenne et al., 2010) and potentially also low levels of collagen IV (Wang et al., 2006). So far, it is known that the surface expression of VLA-3 ($\alpha 3\beta 1$, CD49c/CD29) (Hyun et al., 2012) and VLA-6 ($\alpha 6\beta 1$, CD49f/CD29) (Dangerfield et al., 2005), extracellular matrix binding integrins on neutrophils, are required for migration into inflamed tissue. VLA-3 was shown to be necessary for neutrophil extravasation in TNF- α and fMLP-induced transmigration *in vivo* (Hyun et al., 2012), while studies using blocking antibodies suggest a role for VLA-6 in IL-1 β , but not TNF- α dependent neutrophil extravasation (Dangerfield et al., 2005). Migration through the BM was described to be further accompanied by the surface expression of the serine protease neutrophil elastase (NE) (Wang et al., 2005), although experiments using NE deficient mice *in vivo* could not confirm a role in the extravasation process (Young et al., 2007). Since VLA-3, VLA-6 and NE are stored in intracellular vesicles (Uriarte et al., 2008, Wang et al., 2005), they need to be translocated to the cell surface during transmigration.

Recently, three independent groups identified a novel human primary immunodeficiency disorder, caused by autosomal recessive loss of function mutation in the serine/threonine protein kinase 4 (*STK4*), which encodes MST1, the mammalian homolog of the *Drosophila melanogaster* kinase Hippo. Children with *STK4* deficiency display recurring bacterial, viral and fungal infections together with autoimmune disease. They also suffer from lymphopenia, which explains part of the clinical manifestations.

However, their impaired response to acute bacterial infections, also suggests a defect in myeloid cell function. (Abdollahpour et al., 2012, Crequer et al., 2012, Nehme et al., 2012)

Studies using *Mammalian Ste-20 like kinase 1 (Mst1)* deficient mice showed that the ubiquitously expressed serine/ threonine kinase MST1 is involved in lymphocyte trafficking by controlling exocytosis and localization of the β_2 integrin Lymphocyte Function-associated Antigen-1 (LFA-1, CD11a/CD18, $\alpha_L\beta_2$) to the plasma membrane. MST1 associates via RAPL with the cytoplasmic tail of the α_L subunit and leads to the translocation of LFA-1 containing vesicles in a DENND1C- Rab13 dependent manner (Nishikimi et al., 2014). The absence of MST1 in lymphocytes leads to adhesion as well as migration defects, resulting in impaired lymphocyte trafficking and a decreased number of peripheral lymphocytes (Katagiri et al., 2006, Katagiri et al., 2009). To investigate the role of MST1 for myeloid cell function, we evaluated neutrophil recruitment in *Mst1*^{-/-} mice under *in vivo* and *in vitro* conditions. We show that MST1 is dispensable for LFA-1 dependent neutrophil adhesion in mice and humans, but critical for neutrophil extravasation into the interstitial space through controlling translocation of VLA-3, VLA-6 and neutrophil elastase (NE) to the neutrophil surface. Hence, we identify MST1 deficiency as a neutrophil transmigration deficiency with a basement membrane penetration defect.

Results

MST1 is dispensable for neutrophil adhesion but critical for extravasation

In the past, conflicting results on the expression of MST1 in mouse neutrophils were published (De Souza et al., 2002). Therefore, we first confirmed the expression of MST1 in neutrophils from wild type (WT) and the absence of MST1 in *Mst1*^{-/-} neutrophils (**Figure 1A**). In addition, we also tested for MST2 and did not detect any MST2 expression neither in WT nor in *Mst1*^{-/-} neutrophils (**Figure 1A** and **Supplemental Figure 1A**). Next, we determined differential cell counts of peripheral blood and in accordance to previously published data (Choi et al., 2009) found decreased numbers of lymphocytes in *Mst1*^{-/-} mice compared to WT mice (**Figure 1B**). In contrast, neutrophil counts were not significantly altered in *Mst1*^{-/-} mice compared to WT mice.

Previous studies had shown that MST1 is crucial for β 2 integrin LFA-1 (α L β 2)-dependent T-cell adhesion (Katagiri et al., 2006). To test whether LFA-1 dependent adhesion is also affected in neutrophils lacking MST1, we compared neutrophil adhesion efficiency in TNF- α stimulated cremaster muscle venules of WT and *Mst1*^{-/-} mice using intravital microscopy. Unexpectedly, we observed no difference in neutrophil adhesion efficiency between WT and *Mst1*^{-/-} mice (**Figure 1C**). In addition, neutrophil rolling flux fraction and neutrophil rolling velocity, which is regulated by LFA-1, were not altered in *Mst1*^{-/-} mice compared to WT mice (**Supplemental Figure 1B** and **C**). We then performed *ex vivo* flow chamber assays using glass capillaries coated with various combinations of adhesion molecules and found no difference in the number of adherent leukocytes (**Figure 1D**). Furthermore, *Mst1*^{-/-} neutrophils displayed proper LFA-1 reorganization and accumulation at the uropod during postarrest modifications as observed in flow chambers using confocal microscopy (**Figure 1E** and **Supplemental Video 1A,B**). Neutrophil surface expression of LFA-1, Mac-1, CXCR2, CD44, PSGL1 and CD62L were similar in WT and *Mst1*^{-/-} mice (**Supplemental Figure 1D**). In addition, CXCL1 dependent LFA-1 activation in a soluble ICAM-1 binding assay were similar between neutrophils isolated from WT and *Mst1*^{-/-} mice (**Supplemental Figure 1E,F**).

Next, we investigated neutrophil adhesion from two human patients with *STK4* (also known as *MST1*) deficiency and their heterozygous parents (Abdollahpour et al., 2012). For this approach, we determined the number of adherent neutrophils/FOV in flow

chambers coated with E-selectin/ICAM-1/CXCL8. The number of adherent neutrophils/FOV of *STK4*^{-/-} patients was similar to adhesion observed for chambers perfused with neutrophils from their heterozygous (*STK4*^{+/-}) parents (**Figure 1F**).

We then went on and asked whether MST1 deficiency could have any impact on neutrophil extravasation in a TNF- α induced peritonitis model. In WT mice, i.p. injection of TNF- α dramatically increased the number of neutrophils in the peritoneum compared to NaCl control injection. In contrast, neutrophils from *Mst1*^{-/-} mice failed to transmigrate into the peritoneal cavity within 2h hours of TNF- α stimulation (**Figure 1G**).

Taken together, these *in vitro* and *in vivo* results demonstrate that, in contrast to T-cells, MST1 is dispensable for LFA-1 activation and clustering in neutrophils. Hence, neutrophil adhesion is unaffected in *Mst1*^{-/-} mice as well as in patients with *STK4* deficiency. However, we could detect a massive decrease in the number of extravasated neutrophils in the peritoneal lavage of *Mst1*^{-/-} mice compared to WT mice in the TNF- α induced peritonitis model suggesting a neutrophil recruitment defect downstream of intravascular adhesion.

Loss of MST1 in neutrophils results in decreased transmigration *in vivo*

Using multi-photon laser scanning microscopy we next investigated neutrophil transmigration 180 to 240 min after intrascrotal injection of TNF- α , together with a non-blocking antibody against PECAM1 (Woodfin et al., 2011), into *Ly22*^{GFP} (Faust et al., 2000) and *Mst1*^{-/-} x *Ly22*^{GFP} mice, where neutrophils are endogenously labeled with EGFP. We observed an increasing number of neutrophils in *Ly22*^{GFP} mice crossing postcapillary venules and migrating into the inflamed tissue (**Figure 2A**, upper panel and **Supplemental Video 2A**). In contrast, neutrophils from *Mst1*^{-/-} x *Ly22*^{GFP} mice remained close to the abluminal part of the vessel wall (**Figure 2A**, lower panel and **Supplemental Video 2B**). We then determined the duration of neutrophil transmigration into tissue and observed that transmigration of *Ly22*^{GFP} mice required 7.5 ± 0.8 min (median \pm SEM), which is similar to the time reported by others (Woodfin et al., 2011). In contrast, most neutrophils of *Mst1*^{-/-} x *Ly22*^{GFP} mice failed to transmigrate into tissue within the 20 min of observation (20 ± 0.8 min, median \pm SEM) (**Figure 2B**) and accumulated at the abluminal site of postcapillary venules (**Figure 2C**).

To test, whether further inflammatory stimulation could induce migration into the interstitial matrix, a laser injury near postcapillary venules was set 3 h after TNF- α stimulation. Neutrophils of *Lyz2^{GFP}* mice swarmed and accumulated at the site of laser injury within 30 min, as described by Lämmermann et al. (Lämmermann et al., 2013). Interestingly, neutrophils deficient in MST1 remained at the abluminal site of venules and were unable to interstitially migrate to the site of laser injury (**Figure 2D,E** and **Supplemental Video 3A,B**). However, absent interstitial migration was not due to an intrinsic migration defect of *Mst1^{-/-}* neutrophils as migration of bone marrow-derived neutrophils to fMLP or CXCL1 in a 3D collagen gel assay was not affected by the absence of MST1 (**Supplemental Figure 2A,B**), indicating that interstitial migration is independent of MST1.

MST1 deficient neutrophils fail to transmigrate to the site of infection in a *Helicobacter pylori* mouse infection model

Next, we evaluated the role of MST1 in a murine *Helicobacter pylori* (*H. pylori*) infection model. Previous work had shown that neutrophils play an important role in the pathogenesis of *H. pylori* infection (D'Elia et al., 2007). The bacterium induces a strong inflammatory response in the gastric mucosa, which is dependent on the *H. pylori* neutrophil-activating protein (HP-NAP). Furthermore, pro-inflammatory cytokines such as CXCL8 are secreted during the inflammatory process, recruiting additional neutrophils and monocytes to the site of inflammation (Montecucco and Rappuoli, 2001). We infected WT and *Mst1^{-/-}* mice with *H. pylori* orogastrically and sacrificed the mice 3 months later. As reported earlier (Suerbaum and Michetti, 2002), the majority of infiltrated neutrophils were found in the antrum region of the stomach (**Figure 3A** upper panel). In contrast, we only detected a very small number of neutrophils in the gastric epithelium of the antrum of *Mst1^{-/-}* mice (**Figure 3A** lower panel) demonstrating reduced neutrophil extravasation (**Figure 3B**). In line with this, the number of colony forming units (cfu) of *H. pylori* in the antrum showed a significant increase in *Mst1^{-/-}* mice compared to WT mice (**Figure 3C**), indicating a more successful colonization.

Finally, we immunostained tissue sections from the lower part of the mucosa, where neutrophils extravasate from postcapillary venules (**Figure 3D**). We did not observe any difference in the number of total neutrophils/FOV between WT and *Mst1^{-/-}* mice (**Figure**

3E). However, in WT mice neutrophils migrated from venules into the inflamed tissue, while, as expected, neutrophils from *Mst1*^{-/-} mice remained near the vessel wall (**Figure 3F**). Thus, MST1 is required for proper neutrophil extravasation from the submucosal vasculature into tissue during *H. pylori* infection.

MST1 is essential for neutrophils to penetrate the basement membrane

Next, we focused on the capacity of *Mst1*^{-/-} neutrophils to penetrate the perivascular BM. To this end, we performed whole mount stainings of TNF- α stimulated cremaster muscles using antibodies against laminin α 5 (LN α 5), endothelial cell-specific adhesion molecule 1 (ESAM1) to visualize the BM and endothelial cell contacts, and anti-MRP14 to identify neutrophils (**Figure 4A**). By means of confocal microscopy, neutrophils were classified into three groups according to their position during the extravasation from postcapillary venules. Neutrophils, embedded within the endothelial layer belonged to position I. Position II represented neutrophils located between the endothelium and BM and fully transmigrated neutrophils were classified as being in position III (**Figure 4B**) (Bixel et al., 2010). Neutrophils of WT and *Mst1*^{-/-} mice were present at similar percentages embedded within the endothelium (position I). However, significantly more *Mst1*^{-/-} neutrophils were located between the endothelium and the BM (position II) compared to WT neutrophils while significantly more WT than *Mst1*^{-/-} neutrophils were fully transmigrated (position III) (**Figure 4C**).

To gain further insights into the molecular mechanisms of MST1 dependent transmigration, we performed transwell assays where filters were coated with BSA (control), laminin, a key component of the BM, alone (Yousif et al., 2013), or with PECAM-1 and ICAM-1, while CXCL1 was used as chemoattractant. Laminin alone did not induce transmigration of neither WT nor *Mst1*^{-/-} neutrophils. A combination of laminin, PECAM-1 and ICAM-1 efficiently induced transmigration along a CXCL1 gradient, however only for WT but not for *Mst1*^{-/-} neutrophils (**Figure 4D**). In line with this, *Mst1*^{-/-} neutrophils failed to transmigrate as efficiently as WT neutrophils through filters containing a monolayer of mouse endothelial 1G11 cells in response to CXCL1 (**Figure 4E**). Importantly, we did not find differences in transmigrated WT and *Mst1*^{-/-} neutrophils in transwell assays without coating (**Figure 4F**), implying that MST1 is essential for neutrophils to penetrate the BM *in vivo* and *in vitro*.

MST1 is required for the translocation of VLA-3, VLA-6 and NE to the cell surface

It had been shown previously, that mobilization of VLA-3, VLA-6 and NE from intracellular stores to the plasma membrane is a crucial step for successful neutrophil transmigration (Hyun et al., 2012, Lerman et al., 2014, Wang et al., 2005). In order to evaluate the putative role of MST1 in the mobilization of VLA-3, VLA-6 and NE, neutrophils from WT or *Mst1*^{-/-} mice were seeded on slides coated with BSA or PECAM-1/ICAM-1/CXCL1 and immunostained with antibodies against VLA-3, VLA-6 or NE. Confocal microscopy showed that WT as well as *Mst1*^{-/-} neutrophils seeded on BSA displayed all three molecules - VLA-3, VLA-6 and NE (**Supplemental Figure 3D,G**) - within intracellular stores. Fluorescence intensity profiles (see Materials and Methods and **Supplemental Figure 3A**) of VLA-3, VLA-6 and NE were similar between WT and *Mst1*^{-/-} cells seeded on BSA (**Supplemental Figure 3B-D**). PECAM-1/ICAM-1/CXCL1 coating induced the translocation of VLA-3, VLA-6 and NE to the surface of interacting WT neutrophils, leading to a ring-like structure at the cell border (**Figure 5A-I**). In contrast, neutrophils derived from *Mst1*^{-/-} mice failed to efficiently mobilize any of the three proteins to the cell surface, resulting in less pronounced ring formation in *Mst1*^{-/-} neutrophils (**Figure 5A-I**). Of note, western blot analysis showed no difference in the total protein levels of VLA-3, VLA-6 and NE between WT and *Mst1*^{-/-} neutrophils (**Supplemental Figure 3E**).

In order to verify MST1-dependent mobilization *in vivo*, we investigated NE activity with an NE-fluorescent activatable substrate (NE680FAST) in postcapillary venules of unstimulated and TNF- α stimulated cremaster muscle whole mounts from WT and *Mst1*^{-/-} mice. In unstimulated venules of WT mice we were unable to detect any NE activity, while 2h after TNF- α stimulation NE activity could be observed (**Figure 5J**). TNF- α stimulated venules from *Mst1*^{-/-} mice showed decreased NE activity as compared to WT mice (**Figure 5J**). Importantly, the number of adherent cells was similar in WT and *Mst1*^{-/-} mice (**Supplemental Figure 3F**). Taken together, these *in vitro* and *in vivo* results demonstrate that MST1 is indispensable for efficient translocation of VLA-3, VLA-6 and NE to the surface of neutrophils.

MST1 translocates with Rab27a to the plasma membrane

Rab27a is a central regulator of vesicle trafficking in neutrophils (Catz, 2014, Sheshachalam et al., 2014). Therefore, we investigated Rab27a translocation to the plasma membrane in response to PECAM-1/ICAM-1/CXCL1-stimulation. Rab27a displayed an intracellular localization in WT and *Mst1*^{-/-} neutrophils when seeded on BSA (**Figure 6A** and **Supplemental Figure 4A**). In WT neutrophils, PECAM-1/ICAM-1/CXCL1-coating induced the translocation of Rab27a to the plasma membrane (**Figure 6A,B**) and led to ring formation of Rab27a in most of analyzed WT neutrophils (**Figure 6C**). In contrast, neutrophils derived from *Mst1*^{-/-} mice failed to translocate Rab27a to the plasma membrane in response to PECAM-1/ICAM-1/CXCL1 stimulation (**Figure 6A-C**). However, total protein levels of Rab27 were similar between WT and *Mst1*^{-/-} neutrophils (**Supplemental Figure 4B**).

Next, we investigated whether MST1 itself translocates to the plasma membrane upon ICAM-1/PECAM-1/CXCL1 stimulation. MST1 displayed intracellular localization in WT neutrophils seeded on BSA (**Figure 6D-F**). In response to ICAM-1/PECAM-1/CXCL1 stimulation, MST1 localized together with Rab27a at the plasma membrane (**Figure 6D-F**).

Taken together, these results demonstrate that Rab27a and MST1 translocate to the cellular membrane upon ICAM-1/PECAM-1/CXCL1 stimulation, implying a role of MST1 in Rab27a-dependent vesicle transport.

Discussion

In this study, we identify the serine/threonine kinase MST1 as the first signaling molecule indispensable for neutrophil basement membrane penetration into inflamed tissue.

Originally, MST1 (mammalian homolog of the *Drosophila* Hippo protein) was identified in *Drosophila melanogaster* as the central constituent of the Hippo pathway, controlling organ size and proliferation. Recently, MST1 has attracted more attention due to its role in cancer development (Yu et al., 2015) and the discovery that a mutation in human *STK4* (Mst1) leads to a primary immune deficiency. Patients with a deficiency in *STK4* present with recurring bacterial, fungal and viral infections, and display lymphopenia and intermittent neutropenia (Abdollahpour et al., 2012, Crequer et al., 2012, Nehme et al., 2012). Using *Mst1*^{-/-} mice, MST1 was shown to be required for LFA-1 dependent T-cell trafficking (Katagiri et al., 2009, Ueda et al., 2012) by regulating the transport and distribution of LFA-1 containing vesicles to the plasma membrane and subsequent LFA-1 clustering and adhesion of T-cells (Katagiri et al., 2006).

We demonstrate, that in contrast to T-cells (Katagiri et al., 2009), MST1 is dispensable for LFA-1-dependent neutrophil adhesion in mice and humans. Neutrophils from *Mst1*^{-/-} mice showed no defect in LFA-1 activation. In addition, clustering of LFA-1 as well as static adhesion on ICAM-1 coated surfaces was not altered in *Mst1*^{-/-} neutrophils compared to WT neutrophils. Murine *Mst1*^{-/-} neutrophils as well as neutrophils derived from two patients with *STK4* deficiency adhered to E-selectin/ICAM-1/CXCL1 coated flow chambers to the same extent as WT controls or their heterozygote parents, respectively. These results suggest that different mechanisms of LFA-1 regulation/activation exist between lymphocytes and neutrophils. This may be supported by data from Fabbri et al., reporting that Rab11, is required for the trafficking of LFA-1-containing vesicles in neutrophils (Fabbri et al., 2005). In T-cells, Rap13 is responsible for this step (Nishikimi et al., 2014).

Although *Mst1*^{-/-} neutrophils showed no defective adhesion in our studies, they failed to extravasate into the peritoneal cavity. In TNF- α stimulated cremaster muscles, *Mst1*^{-/-} neutrophils remained in close contact with the abluminal side of the vessel. Even after additional stimulation by inducing a laser injury next to the vessel, *Mst1*^{-/-} neutrophils persisted at the vessel wall and failed to migrate to the site of injury. After

crossing the endothelial cell layer, neutrophils have to penetrate the underlying BM (Hallmann et al., 2015, Sorokin, 2010, Wang et al., 2006). The BM of post-capillary venules is mainly composed of laminin 411 ($\alpha 4\beta 1\gamma 1$ laminin subunit), laminin 511 ($\alpha 5\beta 1\gamma 1$ laminin subunit) and type IV collagen (Sorokin, 2010). Although many studies have been performed on leukocyte adhesion and TEM, the mechanism by which neutrophils penetrate the BM is still poorly understood (Rowe and Weiss, 2008, Hallmann et al., 2015).

Previous studies showed that genetic, antibody or inhibitor-mediated blockade of PECAM-1 (Wang et al., 2005), VLA-3 (Hyun et al., 2012), VLA-6 (Dangerfield et al., 2002, Dangerfield et al., 2005, Wang et al., 2005) or NE (Wang et al., 2005) leads to an arrest of infiltrating neutrophils between the endothelial layer and the underlying BM. Extravasating neutrophils need to interact with ICAM-1 and PECAM-1 to induce the mobilization of vesicles containing VLA-6 and NE. This mobilization translocates VLA-6 and NE to the cellular surface, a prerequisite to pass the BM (Dangerfield et al., 2002, Wang et al., 2005). We found that MST1 is essential for the exocytosis of VLA-3, VLA-6 and NE as neutrophils from *Mst1*^{-/-} mice failed to translocate these proteins to the cell surface upon stimulation with PECAM-1/ ICAM-1/ CXCL1. In contrast to WT neutrophils, neutrophils from *Mst1*^{-/-} mice failed to pass through a PECAM-1, ICAM-1 and laminin-coated transwell filter in an *in vitro* transmigration assay.

As MST1 influences LFA-1 clustering in T-cells by regulating LFA-1 containing vesicle trafficking via Rab13 (Nishikimi et al., 2014), we hypothesized, that MST1 is similarly involved in the mobilization of the vesicles containing VLA-3, VLA-6 and NE to the plasma membrane in neutrophils. The GTPase Rab27a is a master regulator of exocytosis in neutrophils (Catz, 2014). Several studies indicate that Rab27a and its effectors JFC1 (synaptotagmin-like protein 1) and Munc13-4 regulate the secretion of azurophilic granules, containing NE and MPO (Brzezinska et al., 2008, Munafo et al., 2007). We discovered that Rab27a and MST1 itself translocate to the plasma membrane in response to PECAM-1/ ICAM-1/CXCL1. However, translocation of Rab27a is defective in *Mst1*^{-/-} neutrophils indicating that MST1 is involved in Rab27a dependent vesicle trafficking. Further studies may elucidate, whether Rab27a regulates only NE secretion or is furthermore involved in VLA-3 and VLA-6 translocation.

Taken together, we demonstrate that the serine/threonine-kinase MST1 is indispensable for neutrophil penetration of the basement membrane by regulating the mobilization of VLA-3, VLA-6 and NE from intracellular vesicles to the plasma membrane. These findings elucidate the importance of MST1 for early innate immune responses and also explain the phenotype of recurring infections found in patients suffering from *STK4* immune deficiency.

Methods

Study approval

Mst1^{-/-} mice were generated by Dae Sik Lim as described (Oh et al., 2009). *Lyz2*^{GFP} (Faust et al., 2000) were generously provided by Thomas Graf, Centre for Genomic Regulation, Barcelona, Spain. *Lyz2*^{GFP} x *Mst1*^{-/-} were generated by crossbreeding. C57BL/6 wild type (WT) mice were obtained from Janvier Labs. Animal studies were approved by the Regierung von Oberbayern, Germany, AZ 55.2-1-54-2531-149/10 and AZ 55.2-1-54-2532-34/14.

Human studies with purified neutrophils from parents (*STK4*^{+/-}) or *STK4*^{-/-} patients were approved by the ethical committee, LMU, Germany, AZ 66-14.

Western Blot

Isolated neutrophils were incubated in lysis buffer (1x PBS, 1% Triton X-100 (Applichem), 0.5% Na deoxycholate, 0.1% SDS supplemented with protease (Roche) and phosphatase inhibitors (Sigma)), homogenized in Laemmli sample buffer and boiled for 5min. Proteins were resolved by SDS–polyacrylamide gel electrophoresis (SDS–PAGE) and then electrophoretically transferred onto PVDF membranes, which were subsequently incubated with antibodies. The following antibodies were used: rabbit anti-MST1 antibody (Upstate), rabbit anti-MST2 antibody (Cell Signaling), rabbit anti-NE antibody (Abcam), mouse anti- VLA-3 antibody (42/CD49c, BD), rabbit anti- VLA-6 antibody (Thermo Scientific), sheep anti- Rab27a (R&D), mouse anti-GAPDH antibody (Calbiochem), goat anti-mouse HRP, goat anti-rabbit HRP or donkey anti-sheep HRP (Jackson ImmunoResearch). Bound antibodies were detected using enhanced chemiluminescence (Millipore Corporation).

Intravital microscopy of TNF- α stimulated mouse cremaster muscle venules

Intravital microscopy of mouse cremaster muscle venules was performed in WT and *Mst1*^{-/-} mice, as previously described (Pruenster et al., 2015). Briefly, 2 h after intrascrotal injection of TNF- α (R&D systems, 500 ng/mouse) a carotid artery catheter was placed for blood sampling (ProCyt Dx, IDEXX Laboratories). Thereafter, the cremaster muscle was exteriorized and rolling flux fraction (rolling cell/min divided by total neutrophil flux), rolling velocity and leukocyte adhesion efficiency (number of

adherent cells/mm divided by the systemic neutrophil count) determined by intravital microscopy (Olympus BX51WI microscope, water immersion objective 40x, 0.80 NA, Olympus; CCD camera, CF8/1, Kappa). Postcapillary venules ranged from 20-40 μm in diameter.

Murine *ex vivo* flow chamber system and LFA-1 clustering

To investigate adhesion under flow conditions, we used a previously described flow chamber system (Yang et al., 2012). Glass capillaries (Rect.Boro Capillaries 0.04 x 0.40 mm ID VitroCom, Mountain Lakes, USA) were coated with E-selectin (R&D systems, 20 $\mu\text{g/ml}$), ICAM-1 (R&D Systems, 15 $\mu\text{g/ml}$) and/ or CXCL1 (Peprtech, 15 $\mu\text{g/ml}$). Flow chambers were autoperfused with whole blood from WT or *Mst1*^{-/-} mice via a carotid artery catheter. One representative field of view was recorded by intravital microscopy (water immersion objective x20, 0.95 NA, Olympus).

In order to investigate LFA-1 clustering during neutrophil adhesion under flow conditions, flow chambers were perfused (2 $\mu\text{l/min}$) with whole blood from WT or *Mst1*^{-/-} mice, incubated with rat anti-LFA-1 Alexa Fluor 546 antibody (2D7, BioLegend). Adherent cells were imaged using confocal microscopy (Leica System SP5, 63x, 1.4 NA oil objective).

Human flow chamber system

In order to investigate adhesion of human neutrophils under flow conditions we used a previously described flow chamber system (Nussbaum et al., 2013). Glass capillaries (Rect.Boro Capillaries 0.2 x 2 mm ID VitroCom, Mountain Lakes, USA) were coated with combinations of E-selectin (R&D systems, 5 $\mu\text{g/ml}$), ICAM-1 (R&D Systems, 4 $\mu\text{g/ml}$) and CXCL8 (Peprtech, 5 $\mu\text{g/ml}$). Flow chambers were perfused (2 dyne/cm^2) with Ficoll purified neutrophils ($2 \times 10^5/\text{ml}$) from parents (*STK4*^{+/+}) or *STK4*^{-/-} patients.

Surface expression of LFA-1, Mac-1, CXCR2, CD44, PSGL1 and CD62L

Surface expression of αL (LFA-1, CD11a- APC, M17/4, eBioscience), αM (Mac-1, CD11b - Brilliant Violet 570, M1/70, BioLegend), CXCR2 (CD182- APC, 242216, R&D), CD44 (CD44- Brilliant Violet 570, IM7, BioLegend) , PSGL1 (CD162- PE, 2PH1, Pharmingen) und L-selectin (CD62L- FITC, MEL-14, BioLegend) of bone marrow derived Ly6G⁺ (Ly6G-Pacific Blue, 1A8, BioLegend) neutrophils from WT and *Mst1*^{-/-}

mice was compared using a Beckman Coulter GalliosTM flow cytometer and analyzed using Kaluza® Flow Analysis Software (Beckman Coulter).

Soluble ICAM-1 binding assay

Soluble ICAM-1 binding assay was performed as described previously (Pruenster et al., 2015). Briefly, bone marrow derived neutrophils were isolated from WT and *Mst1*^{-/-} mice using a Percoll gradient (Sigma). Cells were suspended in complete HBSS buffer (Hanks Balanced Salt Solution containing 0.1% Glucose, 1 mM CaCl₂ and MgCl₂, 0.25% BSA (GE healthcare) and 10 mM Hepes (Sigma), pH7.4). Cells were stimulated with 100 ng/ml rmCXCL1 (Peprtech) or an equal volume of HBSS buffer, in the presence of rmICAM-1 (ICAM-1 hFc chimera, R&D Systems, 20µg/ml), goat anti-human Fc gamma-biotin (polyclonal, eBioscience) and Streptavidin – PerCP-Cy5.5 (eBioscience) for 3 min at 37°C. Cells were fixed (FACS Lysing Solution, BD), stained with rat anti-mouse Ly6G-Pacific Blue antibody (1A8, BioLegend) and measured using flow cytometer.

TNF-α induced neutrophil extravasation into the peritoneal cavity

WT and *Mst1*^{-/-} mice were intraperitoneally injected with NaCl (control) or TNF-α (rmTNF-α, R&D Systems, 1 µg/mouse). Mice were sacrificed 2 h later, and peritoneal lavage was performed, cells were collected, stained with a rat anti- Ly6G (1A8, BioLegend) and the number of extravasated neutrophils was evaluated using rat anti-Ly6G antibody (1A8, BioLegend), Flow-CountTM Fluorospheres and flow cytometry.

Multi photon microscopy of the mouse cremaster muscle

Extravasation of neutrophils into inflamed mouse cremaster muscle of Lyz2^{GFP} and Lyz2^{GFP} x *Mst1*^{-/-} mice was investigated by multi photon microscopy (Woodfin et al., 2011). Briefly, TNF-α (R&D Systems, 500 ng) and a rat anti-PECAM-1 antibody Alexa Fluor 546 (390, BioLegend; 3 µg) were injected into the scrotum of mice. 1 h later, the cremaster muscle was prepared for intravital multi photon microscopy. Z-stacks were captured using a TrimScope (LaVision Bio Tec (Rehberg et al., 2011), upgraded with Hamamatsu H7422A-40 high sensitivity GaAsP photomultipliers; Olympus XLUMPlanFI, 20x, 0.95 W objective, 810 nm excitation, ultra-sensitive port (USP) 525/50, 580/60). Images (966 x 966 pixels, 300 x 300 µm, step size 4 µm) were acquired at intervals of

30 seconds. After acquisition, images were processed and analyzed using Imaris 7 (Bitplane). Transmigration time was defined from the point the cells started to transmigrate (excluding intraluminal crawling) until they completely detached from the abluminal vascular wall.

Laser induced injury using multi photon microscopy in the mouse cremaster muscle

A laser injury using high laser power by scanning an area of 50 x 50 μm 121 times in the center of 500 x 500 μm was set, 3 h after intrascrotal injection of rmTNF- α and anti PECAM1- Alexa Fluor 546 antibody. Images were acquired for 30 min as described above. The GFP intensity, which is proportional to the number of neutrophils at the site of injury, was analyzed using Fiji software.

Chemotaxis assay for neutrophils in 3D collagen gels

3D Chemotaxis was performed according to the manufacturer's instructions (Ibidi). Briefly, bone marrow derived neutrophils from WT and *Mst1*^{-/-} mice were isolated using a Percoll gradient and 3x10⁵ cells were seeded together with Collagen I into a channel of Ibidi μ - Slides Chemotaxis^{3D}. After 5 min of incubation at 37 °C, the reservoirs were filled with either complete HBSS-buffer alone or with rmCXCL1 (Peprotech, 100 ng/ml) or fMLP (Sigma, 10 μM). Images were acquired every 14 s for 30 min at 37 °C using an Axiovert 200M microscope. Images were analyzed using Fiji software.

***Helicobacter pylori* infection model**

WT or *Mst1*^{-/-} mice were infected with the *H. pylori* strain PMSS1wt orogastrically three times with 10⁹ bacteria or sterile Brucella Broth (BB) alone as a control. Animals were sacrificed after 6 weeks or 3 months. Stomachs were opened washed with PBS and divided into two equal halves. One half was homogenized and appropriate dilutions were spread on selective serum plates (GC agar Difco with horse serum (80 ml/l), IsoVitaleXTM (10 ml/l; BD, Germany), nalidixic acid (5 g/l), bacitracin (50 g/l), DENT (Oxoid). The number of cfu was calculated per gram of gastric tissue. The other half of the stomach was fixed in Tissue-Tek[®] O.C.TTM Compound (Sakura), stained with a primary rat anti-Ly6G antibody (BD Pharmingen) and detected using a goat anti-rat

Alexa Fluor 555 antibody (Invitrogen) together with DAPI (Sigma). Images were obtained using an Olympus fluorescence microscope (10x, 0.40 NA dry objective). In a second set of experiments, the sections were stained with a rat anti-PECAM-1 Alexa Fluor 488 antibody (clone 390, BioLegend) together with a rat anti-Ly6G antibody (BD Pharmingen) detected with a goat anti-rat Alexa Fluor 555 antibody (Invitrogen). DAPI was used for nuclear staining. Sections were imaged by confocal microscopy (Leica System SP5, 40x, 1.25 NA oil objective). The number of neutrophils was evaluated using Volocity software.

Analysis of neutrophil extravasation

TNF- α (R&D Systems, 500 ng/mouse) was applied to the scrotum of WT and *Mst1*^{-/-} mice. After 2 h the cremaster muscle was dissected and fixed with 4% PFA for 1 h, permeabilized and blocked for 2 h in 0.5% Triton X-100/ 2% ovalbumin /PBS, incubated with rat anti-laminin α 5 antibody 4G6 (Sorokin et al., 1997), rabbit anti- ESAM1 antibody (Wegmann et al., 2006) and goat anti-MRP14 antibody (S100A9, R&D Systems) overnight in 2% ovalbumin/ PBS at RT. After labeling with secondary antibodies (donkey anti-rat Alexa Fluor 488, donkey anti-goat Alexa Fluor 568, donkey anti-rabbit Alexa Fluor 647, Invitrogen) in 1% ovalbumin / PBS for 5 h at RT, the tissue was embedded on glass slides in Dako Fluorescence Mounting Medium. Images were acquired using a confocal microscope (Zeiss LSM 780, LSM 510) and analyzed with Imaris software.

Transwell assay

HBSS buffer, 10 ng/ml or 100 ng/ml CXCL1 were used as chemoattractant in the transwell system (5 μ m pore size). Isolated bone marrow neutrophils (EasySepTM mouse neutrophil enrichment kit; STEMCELL TECHNOLOGIES) were applied and allowed to migrate for 45 min at 37°C. Numbers of transmigrated neutrophils were evaluated using rat anti-Ly6G antibody (1A8, BioLegend), Flow-CountTM Fluorospheres and flow cytometry. In a second set of experiments, transwells (3 μ m pore size) were additionally coated with laminin 1 (life technologies, 15 μ g/ml) or 2% BSA (GE healthcare) as a control at 4 °C overnight. Laminin was additionally coated with PECAM-1 (R&D Systems, 2 μ g/ml) and ICAM-1 (R&D Systems, 8 μ g/ml) for 2 h at 37 °C. Using HBSS buffer alone (control) or HBSS buffer with 1 ng/ml CXCL1 as chemoattractant, isolated

bone-marrow neutrophils (2×10^5 cells/well) were allowed to migrate for 3 h at 37 °C (Wang et al., 2005). Numbers of transmigrated neutrophils were evaluated using rat anti-Ly6G antibody, Flow-Count™ Fluorospheres and flow cytometry. In a third set of experiments, murine endothelial 1G11 cells (generously provided by Annunciata Vecchi, Humanitas Research Hospital, Milan, Italy) were seeded on transwell inserts (5 µm pore size). Either HBSS buffer alone or HBSS buffer containing 100 ng/ml CXCL1 was added to the lower compartments. After 30 minutes of equilibration, isolated bone marrow neutrophils (2×10^5 cells/well) were allowed to migrate for 1 h at 37 °C. Numbers of transmigrated cells were evaluated using rat anti-Ly6G antibody and Flow-Count™ Fluorospheres with flow cytometry.

Mobilization of VLA-3, VLA-6, NE, MST1 and Rab27a in mouse neutrophils

Mobilization of neutrophil elastase (NE), $\alpha 3$ (VLA-3, CD49c) and $\alpha 6$ (VLA-3, CD49f) on PECAM-1, ICAM-1 and CXCL1 coated wells was performed as previously described (Wang et al., 2005). Briefly, slides were coated with either 2% BSA (control, GE healthcare) or PECAM-1 (2 µg/ml, R&D Systems), ICAM-1 (8 µg/ml, R&D Systems) and CXCL1 (10 µg/ml, Peprotech) overnight at 4 °C. Isolated bone marrow neutrophils from WT and *Mst1*^{-/-} mice were incubated on coated slides for 30 min at 37 °C. Cells were fixed with 4% PFA, blocked and permeabilized with PBS/ 0.1% Triton X-100/ 2% BSA and stained with a mouse anti-VLA-3 antibody (42/CD49c, BD), rat anti-VLA-6 antibody (GoH3, BioLegend), rabbit anti-NE antibody (polyclonal, Abcam), sheep anti-Rab27a antibody (R&D) and a rabbit anti-MST1 antibody (polyclonal, CellSignaling). Primary antibodies were detected using goat anti-mouse Alexa Fluor® 488, goat anti-rabbit Alexa Fluor® 546, donkey anti-sheep Alexa Fluor® 488 and goat anti-rat Alexa Fluor® 647 (Molecular Probes/ Invitrogen), respectively. Cells were embedded in PermaFluor (Thermo Scientific) and imaged by confocal microscopy (Leica System SP5, 63x, 1.4 NA oil objective). To investigate the translocation of VLA-3, VLA-6, NE, MST1 and Rab27a, fluorescence intensity profiles were obtained along a line through the cell as exemplified in **Supplementary Fig.3a**.

In vivo NE activity assay

NE680FAST (4 nmols per mouse, PerkinElmer) was injected i.v. TNF- α (rmTNF- α , R&D Systems, 500 ng/mouse) was applied to the scrotum of WT and *Mst1*^{-/-} mice 1 h later. 2 h after TNF- α injection, the cremaster muscle was dissected and fixed with 4% PFA, permeabilized and blocked with 0.5% Triton X-100/ 2% ovalbumin /PBS and stained with rat anti-PECAM-1 antibody Alexa Fluor 488 (MEC13.3, BioLegend) or rabbit anti-MRP14 antibody (gift of Thomas Vogl, University Münster, Germany) and detected with a goat anti-rabbit Alexa Fluor® 546 antibody (Invitrogen). Tissue was embedded on glass slides in PermaFluor (Thermo Scientific) and imaged by confocal microscopy (Leica System SP5, 40x, 1.4 NA oil objective).

Statistical analyses

All data were analyzed and plotted using Graph Pad Prism 6 Software (GraphPad Software Inc., San Diego, USA). For pairwise comparison of experimental groups a paired t-test, unpaired t-test or Mann-Whitney test was performed. For multiple comparisons, a two way analysis of variance (ANOVA) was used with either Sidak's multiple comparisons test or Tukey's multiple comparisons test (comparison of all experimental groups against each other). A p-value < 0.05 was considered as statistically significant.

Author contributions

A.R.M.K., M.P., I.R. designed, performed and analyzed experiments, interpreted data and wrote the manuscript; K.S., U.B., G.G. and C.N performed and analyzed experiments; B.W., R.I., J.R.W., A.M. analyzed experiments; D.S.L., S.D. provided reagents critical for the project; M.M., C.K., D.V., R.H. contributed to the design of the experiments and the interpretation of the data; M.S. designed experiments, interpreted data and wrote the manuscript.

Acknowledgments

We thank Susanne Bierschenk, Nadine Schmidt, Eva Loell and Jennifer Truong for excellent technical assistance. This work was supported by SFB914, projects A01 (MM), A02 (BW), A08 (CK), B01 (MS), and B05 (RH), the Care-for-Rare foundation (CK) and the EU-Project Tarkinaid FP7-Health.2011.1.4.5 #282095 (MS, BW).

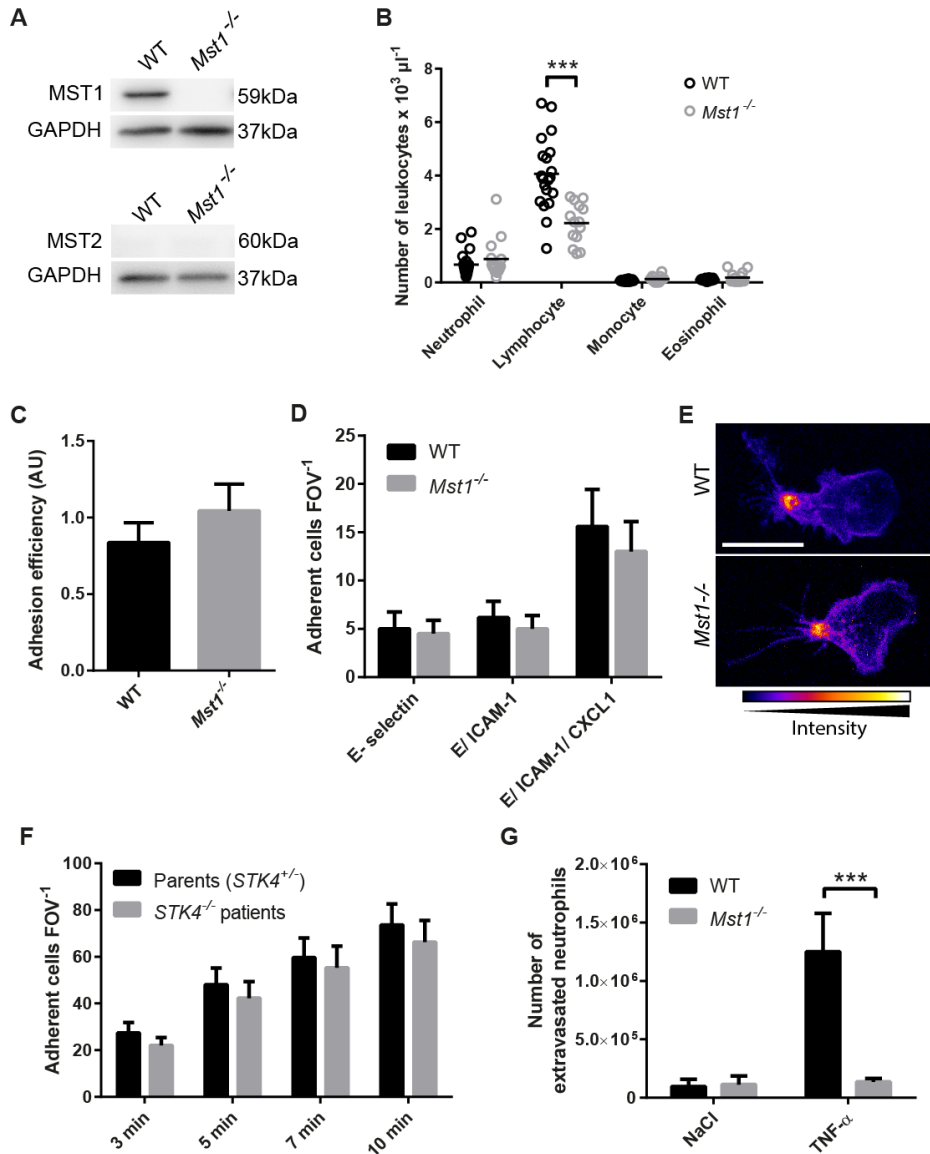


Figure 1 **MST1 is dispensable for neutrophil adhesion in humans and mice, but critical for neutrophil extravasation into inflamed peritoneum.** (A) MST1 and MST2 protein levels of WT and *Mst1*^{-/-} neutrophils. GAPDH served as loading control (n=3). (B) Differential blood counts of WT (n= 20) and *Mst1*^{-/-} mice (n= 14) (scatter blots with mean, *** p < 0.001, 2way ANOVA, Sidak's multiple comparisons test). (C) Neutrophil adhesion efficiency (arbitrary units) in cremaster muscle venules of WT and *Mst1*^{-/-} mice, 2 h after i.s. injection of TNF-α (n = 5, mean ± SEM, n.s., unpaired t-test). (D) Number of adherent leukocytes FOV⁻¹ in microflow chambers coated with E-selectin, E-selectin/ ICAM-1 or E-selectin/ ICAM-1/CXCL1 (n=3, mean ± SEM, n.s., 2way ANOVA, Sidak's multiple comparisons test). (E) LFA-1 clustering of WT or *Mst1*^{-/-} cells labeled with anti LFA-1 antibody conjugated with Alexa 546 (fluorescence intensity scale). Whole blood was perfused through microflow chambers coated with E-selectin, ICAM-1 and CXCL1 (Video S1A and S1B) (n= 3 mice, one representative picture is shown). Scale bar: 10μm. (F) Number of adherent neutrophils FOV⁻¹ from two patients with *STK4* deficiency and their heterozygous parents was calculated over time in flow chambers coated with E-selectin/ ICAM-1/ CXCL8 (n=2, chambers ≥ 2, mean ± SEM). (G) Total number of extravasated neutrophils in the peritoneal lavage 2 h after i.p. injection of NaCl or TNF-α (n=3, mean ± SEM, * p < 0.05, 2way ANOVA, Sidak's multiple comparisons test).

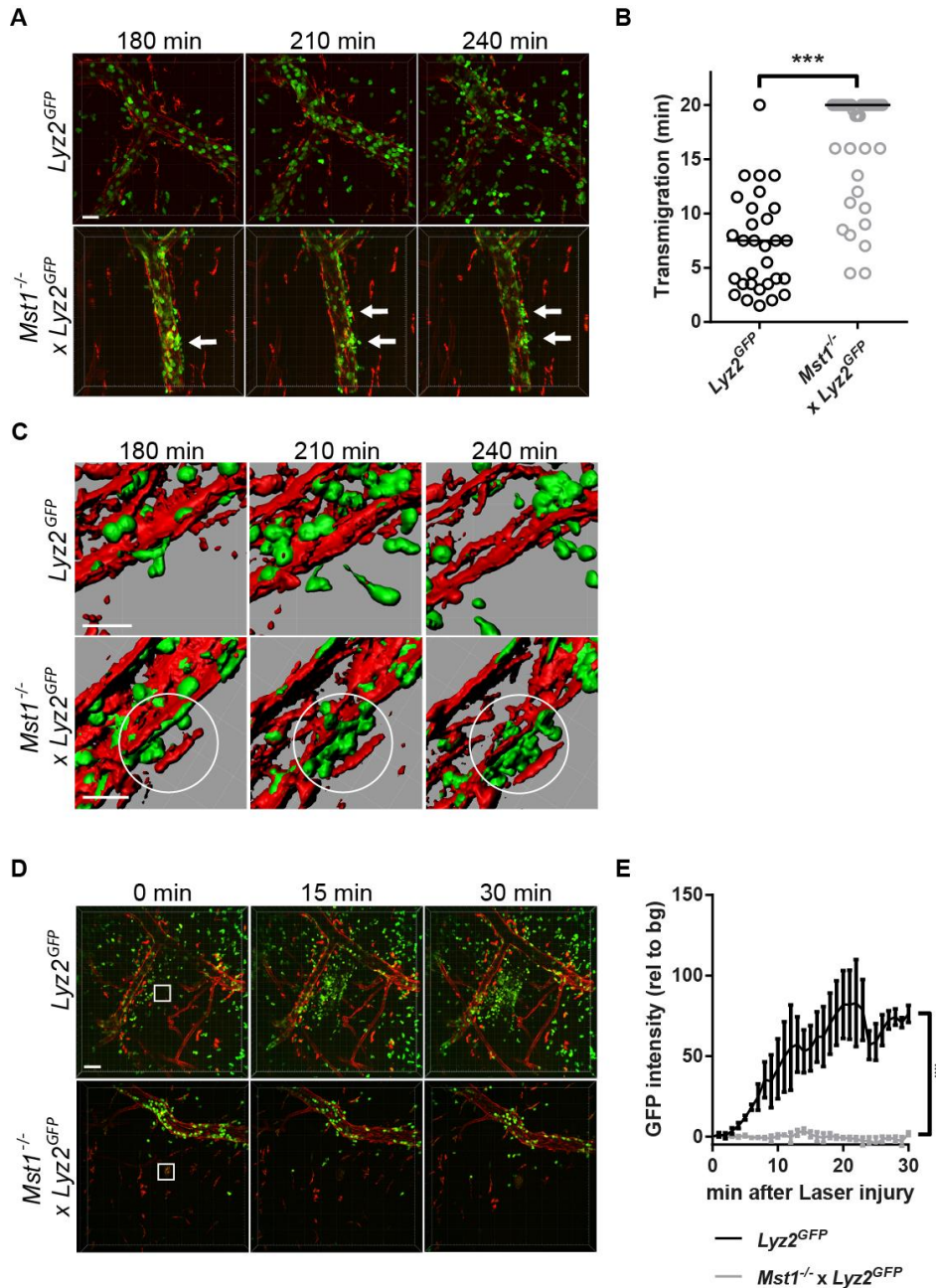


Figure 2 *Mst1^{-/-}* neutrophils fail to transmigrate into inflamed tissue. Neutrophils (green) and microvasculature (red, anti PECAM-1) of TNF- α stimulated mouse cremaster muscle. **(A)** Neutrophil transmigration in *Lyz2^{GFP}* (upper panels) and *Lyz2^{GFP} x Mst1^{-/-}* mice (lower panels, white arrows) at 180 min, 210 min and 240 min after i.s. injection of TNF- α . Images were obtained using intravital multi photon microscopy (n= 3). Scale bar: 30 μ m. **(B)** Transmigration time of *Lyz2^{GFP}* and *Lyz2^{GFP} x Mst1^{-/-}* neutrophils. Cut off was set at 20 min (n= 3 mice, scatter blot with median of > 30 analyzed transmigration events per group, *** p < 0.001, Mann Whitney test). **(C)** 3D reconstruction of neutrophil (green) transmigration with subendothelial accumulation of *Lyz2^{GFP} x Mst1^{-/-}* neutrophils (white circles) and complete extravasation of *Lyz2^{GFP}* neutrophils. Scale bar: 20 μ m. **(D)** Representative images of swarming neutrophils (green) and the microvasculature (PECAM-1, red) in the mouse cremaster muscle of *Lyz2^{GFP}* and *Lyz2^{GFP} x Mst1^{-/-}* mice after induction of a laser injury (white square). Scale bar: 50 μ m. **(E)** Intensity profile of the GFP signal in *Lyz2^{GFP}* and *Lyz2^{GFP} x Mst1^{-/-}* mice at the site of laser injury (n=3, mean \pm SEM, p < 0.05 after 12 min, * p < 0.05, ** p < 0.01, *** p < 0.001, 2way ANOVA, Sidak's multiple comparisons test).

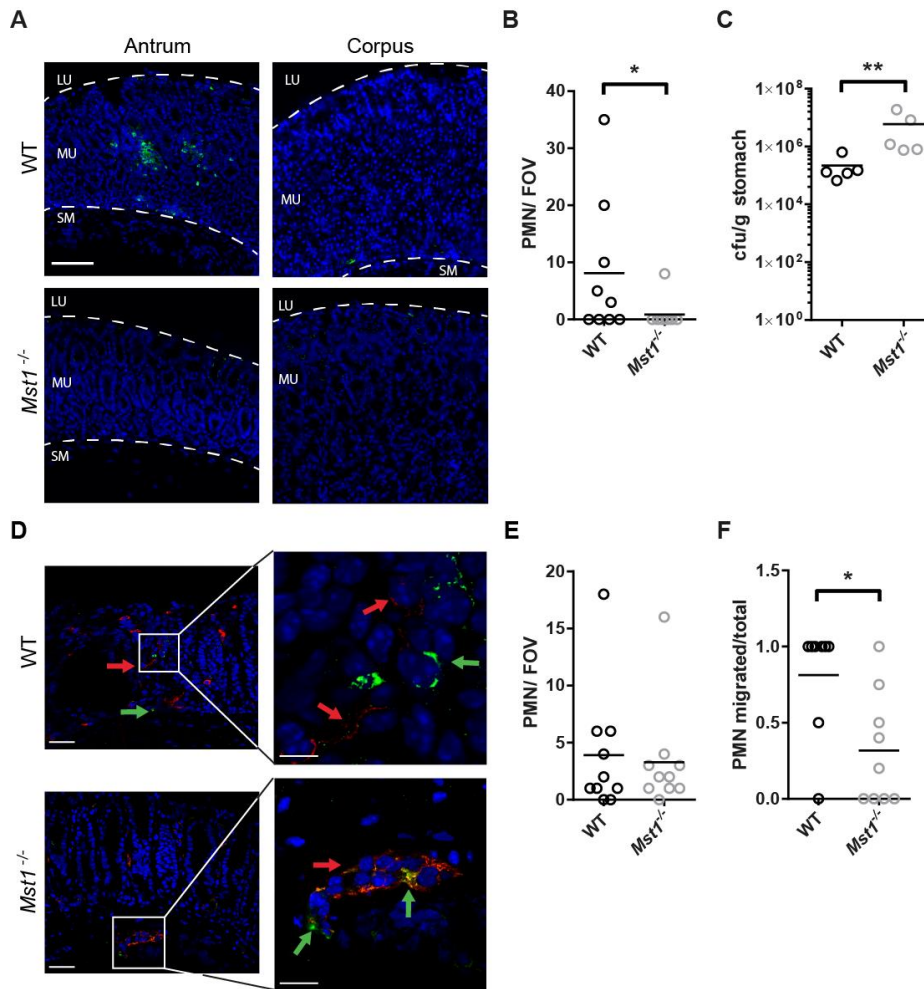


Figure 3 *Mst1*^{-/-} neutrophils fail to extravasate and migrate to the site of infection in a *H. pylori* mouse infection model. **(A)** Representative images are shown of the antrum and corpus from WT and *Mst1*^{-/-} mice 3 months after *H. pylori* infection. Lumen (LU), Mucosa (MU), Submucosa (SM). Neutrophils were identified with Ly6G antibody (green). Nuclei are visualized with DAPI (blue). Scale bar: 10 μ m. **(B)** Number of transmigrated neutrophils FOV⁻¹ in the antrum of WT and *Mst1*^{-/-} mice are displayed (n= 9 mice, scatter blot with mean, * p < 0.05, Mann-Whitney test). **(C)** The colony forming units (cfu) per gram stomach of WT and *Mst1*^{-/-} mice were evaluated 6 weeks after infection (n= 5 mice, scatter blot with mean, ** p < 0.01, Mann-Whitney test). **(D)** Immunostaining of the antrum of WT and *Mst1*^{-/-} mice for PECAM-1 (red) and Ly6G antibody (green). Nuclei are visualized with DAPI (blue). Scale bar: 40 μ m. Close-ups display high magnification of blood vessel rich areas. Red arrows indicate blood vessels, green arrows indicate neutrophils. Scale bar: 10 μ m (upper), 20 μ m (lower). **(E)** Number of neutrophils FOV⁻¹ from WT and *Mst1*^{-/-} mice (n= 10 mice, scatter blot with mean, n.s., Mann-Whitney test). **(F)** Ratio of extravasated neutrophils/total number of neutrophils is depicted from WT and *Mst1*^{-/-} mice (n= 10 mice, scatter blots with mean. * p < 0.05, Mann-Whitney test).

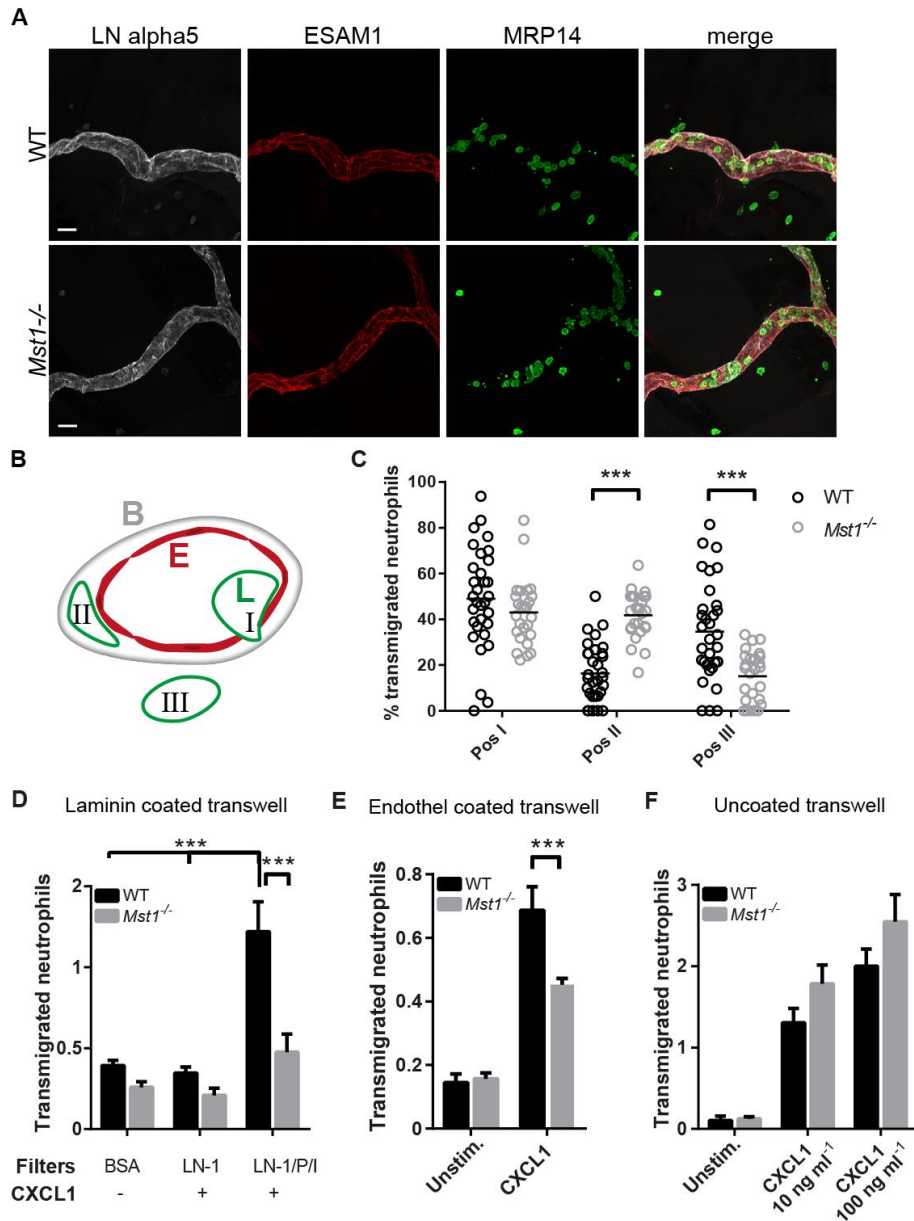


Figure 4 *Mst1*^{-/-} neutrophils fail to penetrate the basement membrane in vivo and in vitro. **(A)** Immunostaining of TNF- α stimulated cremaster muscle whole mounts from WT and *Mst1*^{-/-} mice for laminin α 5 (white, BM), ESAM1 (red, endothelial junctions) and MRP14 (green, neutrophils) (n=3). Scale bar: 20 μ m. **(B)** Illustration of a vessel cross section demonstrating the classification of transmigrating neutrophils respective to their position. Position I – neutrophils in intimate contact to the endothelium; Position II – neutrophils between the endothelium and the BM; Position III – fully transmigrated neutrophils. **(C)** Distribution pattern of transmigrating neutrophils respective to their positions (Pos. I-III) in WT and *Mst1*^{-/-} mice (n=3 mice, scatter blot with mean of >25 analyzed vessels per group, *** p < 0.001, 2way ANOVA, Sidak's multiple comparisons test). **(D-F)** Neutrophil transmigration in a transwell assay **(D)** with or without CXCL1 stimulation through BSA (control), laminin-1 (LN-1) and LN-1, PECAM-1 (P) and ICAM-1 (I) coated filters (n= 3 mice, mean \pm SEM, *** p < 0.001, ** p < 0.01, 2way ANOVA, Sidak's multiple comparisons test), **(E)** with or without CXCL1 stimulation through an endothelial monolayer of 1G11 cells (n= 3 mice, mean \pm SEM, *** p < 0.001, 2way ANOVA, Sidak's multiple comparisons test), **(F)** to HBSS, 10ng ml⁻¹ and 100ng ml⁻¹ CXCL1 (n= 3 mice, mean \pm SEM., 2way ANOVA, Sidak's multiple comparisons test).

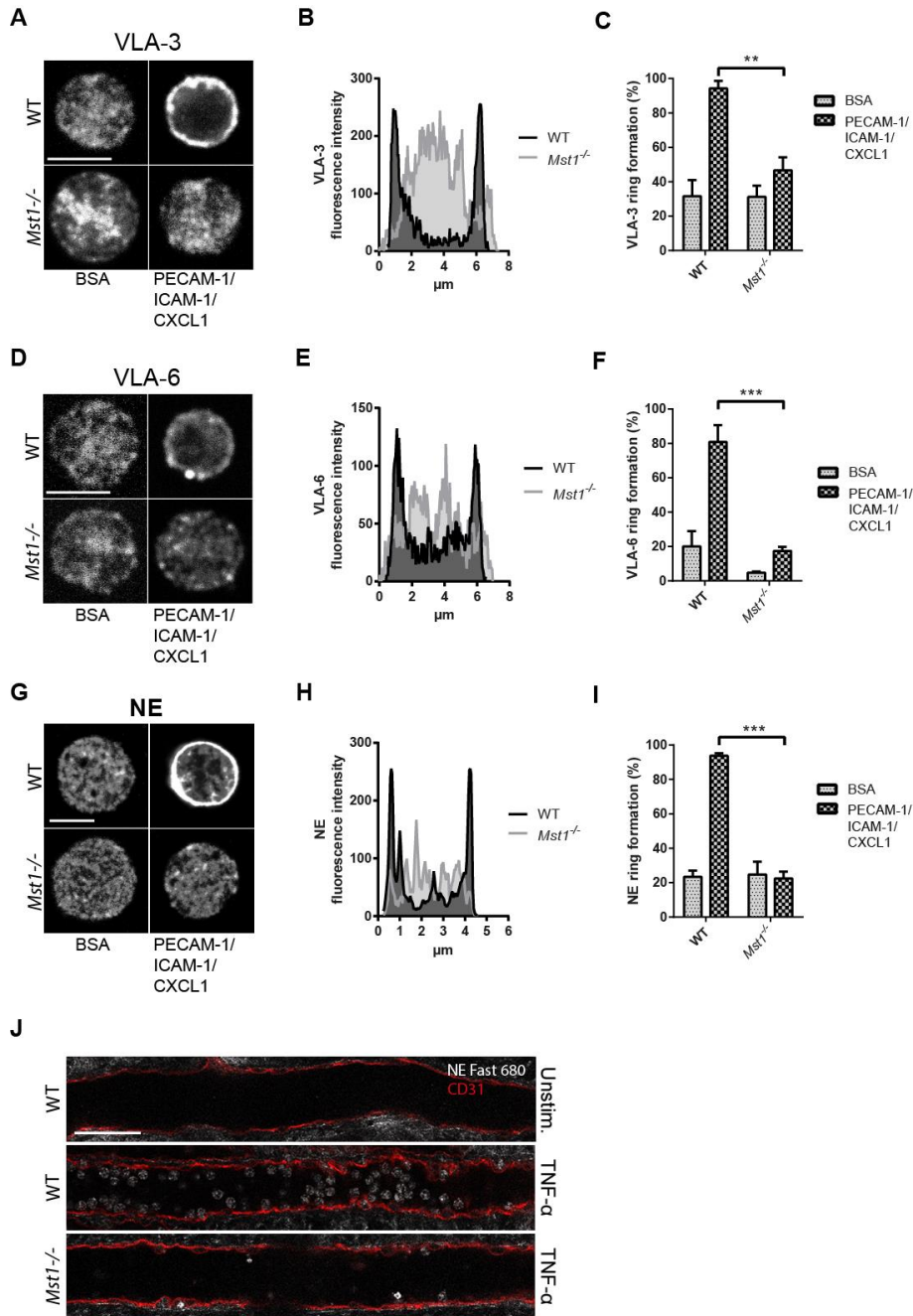


Figure 5 **MST1 is required for the mobilization of VLA-3, VLA-6 and NE to the plasma membrane.** Immunostaining of representative WT and Mst1^{-/-} neutrophil on BSA or PECAM-1/ ICAM-1/ CXCL1 coated wells for **(A)** VLA-3, **(D)** VLA-6 and **(G)** NE. Scale bar: 5 μm. Fluorescence intensity profiles along a line through the cell for **(B)** VLA-3, **(E)** VLA-6 and **(H)** NE of a representative WT (black line) and Mst1^{-/-} neutrophil (grey line) seeded on PECAM-1/ ICAM-1/ CXCL1 coated wells. Quantification of ring formation of **(C)** VLA-3, **(F)** VLA-6 and **(I)** NE (n = 3 mice, mean ± SEM of >50 analyzed neutrophils, *** p < 0.001, ** p < 0.01, 2way ANOVA, Sidak's multiple comparisons test or Tukey's multiple comparisons test). **(J)** NE activity (white) within venules in unstimulated and TNF-α stimulated cremaster muscle whole mounts from WT and Mst1^{-/-} mice imaged by confocal microscopy. Venules were visualized using a rat anti-mouse PECAM-1 antibody (red) (n=3 per group). Scale bar: 50 μm.

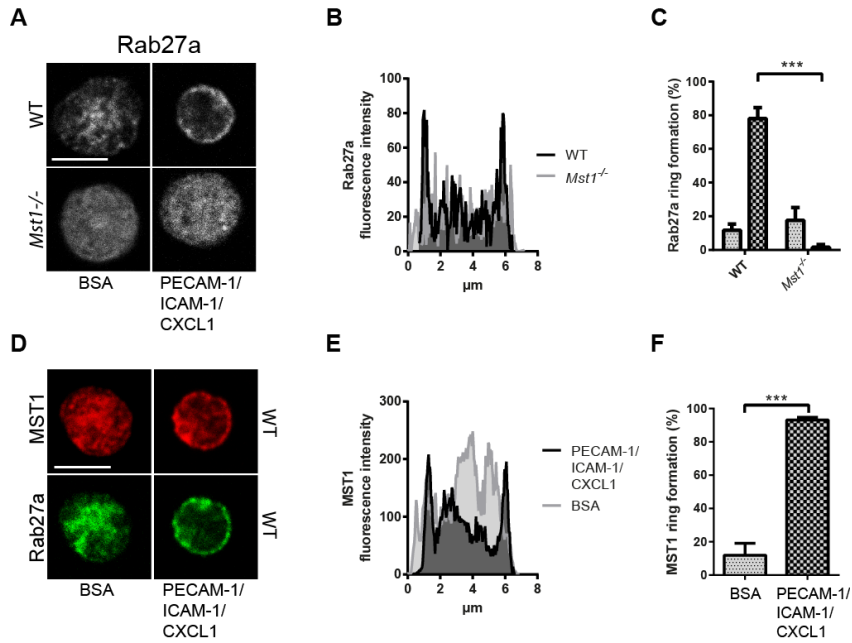
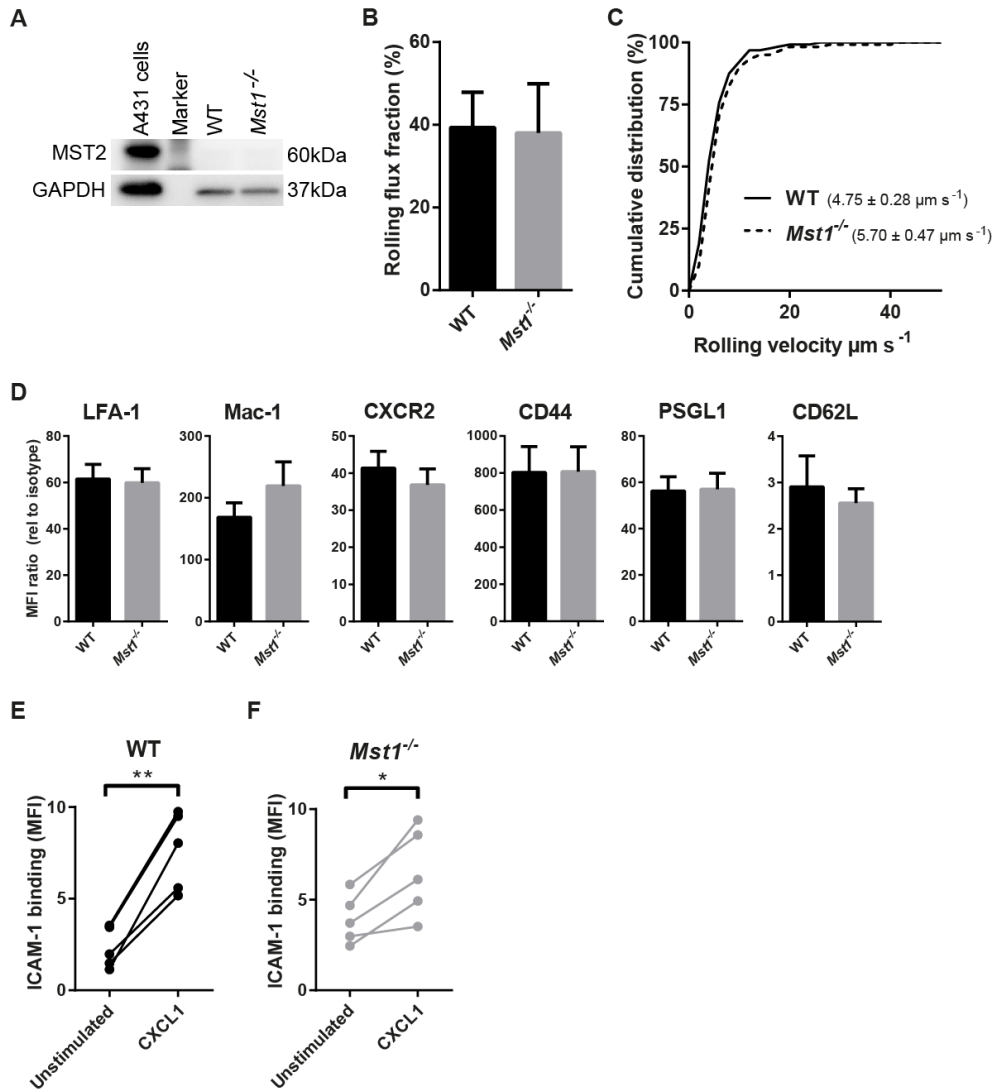
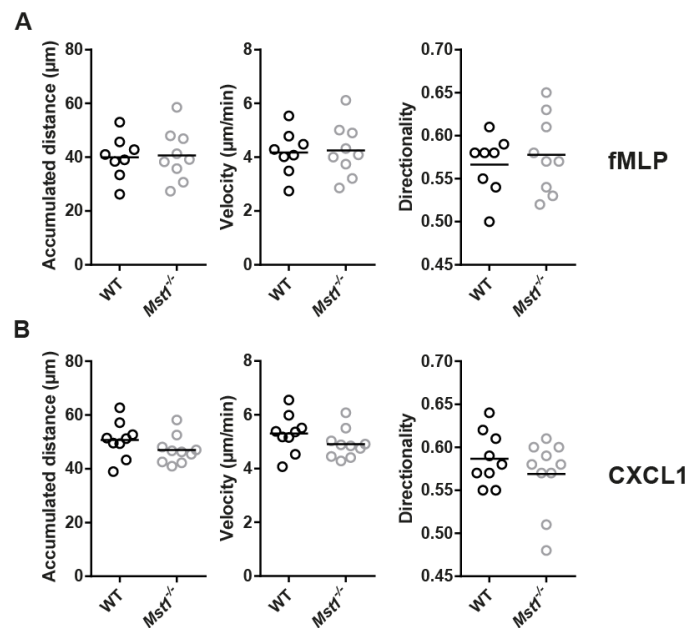


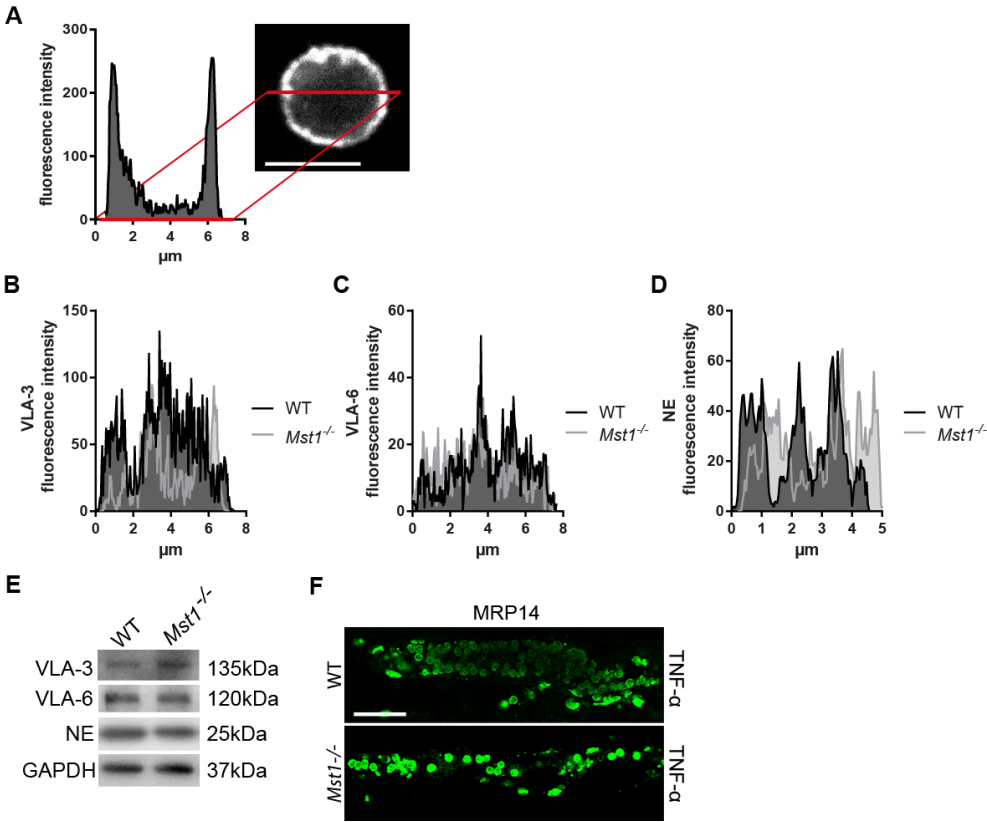
Figure 6 **Rab27a dependent vesicle transport to the plasma membrane is defective in *Mst1*^{-/-} mice** Immunostaining of WT and *Mst1*^{-/-} neutrophils seeded on BSA or PECAM-1/ ICAM-1/ CXCL1 coated wells for **(A)** Rab27a and **(D)** Rab27a (green) and MST1 (red). Scale bar: 5 μ m. Fluorescence intensity profiles assessed along a line through the cell for **(B)** Rab27a of representative WT (black line) and *Mst1*^{-/-} neutrophil (grey line) seeded on PECAM-1/ ICAM-1/ CXCL1 coated wells and **(E)** for MST1 of representative WT neutrophil seeded on BSA (grey line) or PECAM-1/ ICAM-1/ CXCL1 (black line) coated wells. Quantification of ring like expression of **(C)** Rab27a (n= 3 mice, mean \pm SEM of >50 analyzed neutrophils, *** p < 0.001, unpaired t-test) and **(F)** MST1 in response to BSA or PECAM-1/ ICAM-1/ CXCL1 stimulation (n=3 mice, mean \pm SEM of >50 analyzed neutrophils, *** p < 0.001, 2way ANOVA, Sidak's multiple comparisons test).



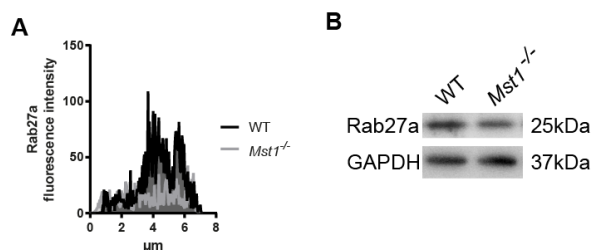
Supplemental Figure 1 Adhesion properties of WT and *Mst1*^{-/-} neutrophils. (A) MST2 protein levels of EGF-stimulated A431 cells, used as positive control, and of WT and *Mst1*^{-/-} neutrophils. GAPDH served as loading control (n=3). (B) Rolling flux fraction and (C) cumulative distribution of neutrophil rolling velocity in cremaster muscle venules of WT and *Mst1*^{-/-} mice 2 h after i.s. injection of TNF- α (n \leq 5, mean \pm SEM, n.s., unpaired t-test). (D) FACS analysis of WT and *Mst1*^{-/-} neutrophils for surface expression of LFA-1, Mac-1, CXCR2, CD44, PSGL-1, CD62L and corresponding isotype controls. The mean fluorescent intensity (MFI) was evaluated relative to the isotype control on Ly6G⁺ cells (neutrophils) (n= 3 mice, mean \pm SEM, n.s., unpaired t-test). (E,F) FACS analysis of ICAM-1 binding to (E) WT or (F) *Mst1*^{-/-} neutrophils with or without CXCL1 stimulation (n=5 * p < 0.05, ** p<0.01 paired t-test).



Supplemental Figure 2 Chemotactic migration of WT and Mst1^{-/-} neutrophils. (A,B) Chemotactic migration of WT and Mst1^{-/-} neutrophils seeded in 3D collagen gels towards a gradient of **(A)** fMLP or **(B)** CXCL1 for 30 min. Neutrophils were tracked using Fiji software (Schindelin et al., 2012). Accumulated distance, velocity and directionality of cells were evaluated (n= 3, scatter blots with mean, n.s., unpaired t-test).



Supplemental Figure 3 VLA-3, VLA-6 and NE – protein levels, distribution and NE activity. Fluorescence intensity profiles along a line cut through the center of the cell as exemplified in **(A)** for **(B)** VLA-3, **(C)** VLA-6 and **(D)** NE of a representative WT (black line) and *Mst1*^{-/-} neutrophil (grey line) seeded on BSA coated wells. Scale bar: 5 μm. **(E)** Total protein levels of VLA-3, VLA-6 and NE from neutrophils of WT and *Mst1*^{-/-} mice. GAPDH served as loading control (n=3 mice). **(F)** Immunostaining of MRP14 (green) in TNF-α stimulated cremaster muscle whole mounts from WT and *Mst1*^{-/-} mice (n=3 per group). Scale bar: 50 μm.



Supplemental Figure 4 Protein levels and distribution under unstimulated conditions of Rab27a. (A) Fluorescence intensity profile along a line cut through the center of the cell for Rab27a of a representative WT (black line) and *Mst1*^{-/-} neutrophil (grey line) seeded on BSA coated wells. **(B)** Total protein levels of Rab27a from neutrophils of WT and *Mst1*^{-/-} mice. GAPDH served as loading control (n=3 mice).

Supplemental Movie 1 LFA-1 clustering in WT and *Mst1*^{-/-} neutrophils. WHOLE BLOOD FROM (A) WT AND (B) *Mst1*^{-/-} mice was incubated with a non-blocking LFA-1 antibody AND PERFUSED THROUGH FLOW CHAMBERS COATED WITH E-SELECTIN, ICAM-1 AND CXCL1. Using confocal microscopy, interacting cells were recorded under flow conditions. Images were recorded for 195 s (one stack every 13 s). The movies were generated and converted using Fiji software.

Supplemental Movie 2 Intravital multi photon laser scanning microscopy of transmigrating neutrophils. Extravasation of neutrophils (green) was recorded from postcapillary venules (red) in a TNF- α stimulated mouse cremaster muscle of (A) *Lyz2*^{GFP} and (B) *Mst1*^{-/-} x *Lyz2*^{GFP} mice. Z-stacks of postcapillary venules were obtained every 30 seconds over a time period of 240 min. Sequences of z-stacks were processed and converted using Imaris 7 and Fiji software.

Supplemental Movie 3 Intravital multi photon laser scanning microscopy of laser injury. Four hours after intrascrotal injection of TNF- α in (A) *Lyz2*^{GFP} and (B) *Mst1*^{-/-} x *Lyz2*^{GFP} mice, a laser injury was induced near postcapillary cremaster muscle venules (red). Swarming of neutrophils (green) was then recorded to the sites of laser injury. Z-stacks of postcapillary venules (red) were obtained every 30 seconds over a time period of 30 min. Sequences of z-stacks were processed and converted using Imaris 7 and Fiji software.

AFFIDAVIT

Kurz, Angela R.M.

Surname, first name

Marchioninstrasse 27

Street

81377, Munich

Zip code, town

Germany

Country

I hereby declare, that the submitted thesis entitled

**MST1 kinase is critical for neutrophil transmigration through the
vascular basement membrane**

is my own work. I have only used the sources indicated and have not made unauthorised use of services of a third party. Where the work of others has been quoted or reproduced, the source is always given.

I further declare that the submitted thesis or parts thereof have not been presented as part of an examination degree to any other university.

Ort, Datum

Unterschrift, Doktorandin